Title
Pathway and organelle engineering for production of useful chemicals in yeast

Author
Grewal, Parbir

Publication Date
2020

Peer reviewed|Thesis/dissertation

Pathway and organelle engineering for production of useful chemicals in yeast

By

Parbir S. Grewal

A dissertation submitted in partial satisfaction of the

requirements for the degree of

Doctor of Philosophy

in

Chemical Engineering

in the

Graduate Division

of the

University of California, Berkeley

Committee in charge:

Professor John E. Dueber, Co-Chair
Professor Douglas S. Clark, Co-Chair
Professor Wenjun Zhang
Professor David F. Savage

Summer 2020

Pathway and organelle engineering for production of useful chemicals in yeast

Abstract

Pathway and organelle engineering for production of useful chemicals in yeast

by

Parbir S. Grewal

Doctor of Philosophy in Chemical Engineering

University of California, Berkeley

Professor John E. Dueber, Co-Chair
Professor Douglas S. Clark, Co-Chair

Researchers in the field of metabolic engineering aim to develop processes to produce useful chemicals, sustainably and responsibly, using biotechnology. These processes are often designed to replace products derived from fossil fuels, which are unsustainable and contribute to climate change, or plant-based products, which compete with food production for scarce land and are subject to supply uncertainty due to weather, crop disease, and climate change. Here, we present two research projects in metabolic engineering. First, we demonstrate microbial production of the red food dye betanin by engineering the betalain biosynthesis pathway into yeast. Betanin is currently manufactured through extraction from red beets specifically grown for dye production. We achieved betanin production levels of 17 mg/L, which is equivalent to the amount of betanin found in 10 g/L of beet extract. With further production improvements, this bioprocess may become cost-competitive with agricultural production and is likely to lead to a purer product. We also demonstrate the synthesis of a suite of non-natural betalain dyes achieved through feeding of diverse amines to a yeast production host, including several which have never been reported. In the second research project, we discover that an enzyme that limits production levels of a drug family is toxic to the yeast production host. This enzyme, norcoclaurine synthase, is critical to the production of benzylisoquinoline alkaloids, an important family of medicines that are extracted from plants like the opium poppy. We devised a novel subcellular compartmentalization strategy, sequestering norcoclaurine synthase in the peroxisome to alleviate cytotoxicity while maintaining access to the enzyme's substrates. By targeting norcoclaurine synthase for organellar compartmentalization, we achieved improved cell growth, final titer, and culture productivity. These projects highlight the potential of engineering complex plant pathways into microbial hosts for economical and sustainable chemical production.

Table of Contents

List of Figures

List of Tables

Acknowledgements

I have many, many people to acknowledge and quickly realized that one page was not enough, so I expanded to two pages and still completely filled them up. First, I want to thank my mom and dad for being the best caretakers, role models, and friends. You have been incredible parents, and although you probably don't realize it, you are also some of the coolest parents I know. Any child would be lucky to have you as parents. I also want to thank my brother for being an amazing friend and always having a cheery attitude whenever we talk.

Secondly, I want to acknowledge my advisor John Dueber. As with all meaningful relationships, we have had our ups and downs, but I feel lucky that I was part of your lab and had the opportunity to interact with and be mentored by you. You pushed me to do excellent work, taught me how to craft an elegant, big-picture story, and created a culture of entrepreneurial spirit. I hope that we will continue to be friends long into the future.

Third, I will acknowledge Dueber Lab members past and present, in somewhat chronological order. I am lucky that I overlapped briefly with two of the founding members of the lab, Mike Lee and Will DeLoache, and I thank them for creating invaluable lab infrastructure. Zach Russ, thank you for being helpful and fun and fixing everything during my early days in the lab. Luke Latimer, thanks for your broad and practical knowledge and willingness to chat. Tammy Hsu, thanks for being the first person to train me in the lab, for being my biggest and most valuable sounding board, and for putting up with marathon training. Thank you to my first lab partner Judy Savitskaya, my second lab partner Cyrus Modavi, and my third lab partner Jen Samson. Ryan Protzko, thanks for always being down to chat about both science and life. Thank you Shakked Halperin for being a role model of what it means to drive forward fearlessly. Thank you to the newest members of the peroxisome subgroup, Jordan Baker and Kay Siu, for in-depth work discussions, eclectic music preferences, and fun inside and outside of lab. Thanks to Juan Hurtado, Melanie Abrams, David Stanley, Qiong Zhang and Jake Flood for making the lab an enjoyable place to be. And finally, thank you to Harneet Rishi, my friend and longtime member of the Dueber Lab.

I would be remiss if I did not thank all the people whom I had the great pleasure to mentor during my time as a PhD student. Most importantly, thank you to my longest running undergrad Brian Choi who is an author on two papers with me and is at Princeton for grad school. Also, I enjoyed mentoring two other undergrads, Makoto Lalwani (also went to Princeton) and Phil Kim (enrolling at Stanford). Mentoring my first

SPSB team (Tristan Wasley, Leslie Leung, Alejandro Ramirez, Kimmy Ferry) with Tammy was a fun learning experience. Mentoring my second SPSB team (Kyle Zolkin, Maite Bradley Silva, Arjun Chandran, Frank Escalante, Parmita Das, Joshua Huang, plus Brian Choi) was a big job, excellent management training, and a fun time. I mentored one other undergrad (Edwin Monroy), several rotation students (Mandy Boontanrart, Andrew Ng, Matt Incha), and co-mentored other rotation students (Shohini Sen, Cody Krivacic, Jordan Baker, Sunnyjoy Dupuis). All were interesting and fun experiences.

With regard to lab support, I would like to thank Edward Rivera, Ariana Hirsh, and Marta Ortega for keeping things running smoothly in our building. I want to thank many members of Wenjun Zhang's lab for help over the years, particularly Nico Herman, Nick Harris, Will Skyrud, Antonio Del Rio Flores, Frederick Twigg, Jeffrey Li, Wenlong Cai, Nick Zill, and Will Porterfield.

I'd like to thank collaborators and scientific advisors I've had over the years. Collaborators include Vincent Martin, Mike Pyne, and Lauren Narcross from Concordia University, and Dawei Xu from Doug Clark's lab at UC Berkeley. I'd like to sincerely thank my chemical engineering advisor Doug Clark for giving me excellent exposure to his lab and my other dissertation committee members Wenjun Zhang and David Savage for feedback several times throughout my PhD. I'd like to thank members of Danielle Tullman-Ercek's lab for being my friends and science discussion buddies during the early years, particularly Kevin Metcalf and Chris Jakobson. Thank you to many members of the Center for Cellular Construction for interesting discussions as well as feedback on my peroxisome project. Thanks to the instructors I GSI'd with – Marjorie Went (twice), Shannon Ciston, Colin Cerratani, and David Graves. And I'd like to thank Adam Arkin for his thought provoking and interactive lectures during a class I took with him.

Finally, I'd like to thank many groups of friends who have supported and/or put up with me during my PhD. These include my wonderful housemates Andrew Crothers, Pete Dudenas, Matt Witman, Rebecca Pinals, Sarah Berlinger, Constance Visser Witman, Kyle Diederichsen, and Julie Rorrer. Other supportive members of my ChemE class, including Lisa Burdette, Monica Neugebauer, Dogan Gidon, Nico Giordano, Leslie Chan, Marc Casas, and Eddy Zaia. My SF friends, including Marisa Goo who knows what it's like to do a PhD, as well as Ani Rajan, Kristin Chan, Andrew Fong, Adrian Rami, Sid Singh, Lydia Beasley, and Matt Janicki. My long distance PhD classmate Do Soon Kim whom I have been lucky enough to see several times over the years. And finally, some of my Ohio friends – Andrew Wolf, Ted Wilson, Nate Shewmon, Megan Wilhelm, Bill Barrington and especially my best friend Alex Hauenstein, who put up with me submitting my first grad school paper while he was visiting.

Chapter 1. Introduction

1.1. Motivation

In the fields of biotechnology, metabolic engineering, and synthetic biology, scientists and engineers work to solve grand challenges using biology-based approaches[1]. These grand challenges include world hunger, the climate crisis, sustainability of the manufacturing sector, and global health and disease[1]. In many cases, the products which metabolic engineers aim to produce are inspired by the wide diversity of molecules produced by plants[2–6]. Moreover, industrial microbial production may be a more sustainable manufacturing method compared to plant-based production[7,8], and may allow for more rapid development of useful products that do not already exist in nature[6,9]. Advantages of industrial microbial production over plant-based production include decreased land use, increased stability of supply, and potential to produce non-natural analogues of existing natural products[5,10,11]. In some cases, plant-based production has already been replaced with synthetic chemical synthesis as with synthetic rubber and indigo dye[12,13]. Because these chemical processes rely on petrochemicals as precursors, biomanufacturing has the potential to be a sustainable alternative for production of valuable molecules currently derived through chemical synthesis.

With these broad goals as motivation, I present here two research projects in metabolic engineering. The first project covers the development of yeast strains capable of producing a class of food dyes and pigments, the betalains, which are currently extracted from plants. This biomanufacturing platform may also enable replacement of artificial, synthetically-derived food dyes. The second project covers the identification of a problem in the microbial production of a family of plant-derived drug molecules, the benzylisoquinoline alkaloids, and addresses this problem through a unique subcellular compartmentalization strategy. We hope that the insights gained from these research projects will aid in the development of sustainable bioprocesses in the 21st century.

1.2. Organization

In **Chapter 2**, I present the heterologous production of betalains. Betalains are a family of natural pigments found exclusively in the plant order *Caryophyllales*[14]. All members of this chemical family are biosynthesized through the common intermediate betalamic acid, which is capable of spontaneously condensing with various primary and secondary amines to produce betalains[15,16]. Of particular interest is the red-violet betanin, most

commonly obtained from *Beta vulgaris* (beet) as a natural food dye. We demonstrate the first complete microbial production of betanin in *Saccharomyces cerevisiae* from glucose, an early step towards a fermentation process enabling rapid, on-demand production of this natural dye. A titer of 17 mg/L was achieved, corresponding to a color intensity obtained from 10 g/L of beetroot extract. Further, we expanded the spectrum of betalain colors by condensing betalamic acid with various amines fed to an engineered strain of *S. cerevisiae*. Our work establishes a platform for microbial production of betalains of various colors as a potential alternative to land- and resource-intensive agricultural production.

In **Chapter 3**, I present examples of the utility of the peroxisome as an engineerable organelle to solve problems in biotechnology. Eukaryotic cells compartmentalize metabolic pathways in organelles to achieve optimal reaction conditions and avoid crosstalk with other factors in the cytosol[17,18]. We identified that norcoclaurine synthase (NCS), the enzyme which catalyzes the first committed reaction in benzylisoquinoline alkaloid (BIA) biosynthesis, is toxic when expressed cytosolically in *Saccharomyces cerevisiae* and, consequently, restricts (*S*)-reticuline production. We developed a compartmentalization strategy that alleviates NCS toxicity while promoting increased (*S*)-reticuline titer, achieved through efficient targeting of toxic NCS to the peroxisome while, crucially, taking advantage of the free flow of metabolite substrates and product across the peroxisome membrane. We identified that peroxisome protein capacity in *S. cerevisiae* becomes a limiting factor for further improvement of BIA production and demonstrate that expression of engineered transcription factors can mimic the oleate response for larger peroxisomes, further increasing BIA titer without the requirement for peroxisome induction with fatty acids. This work specifically addresses the challenges associated with toxic NCS expression and, more broadly, highlights the potential for engineering organelles with desired characteristics for metabolic engineering.

In **Chapter 4**, I provide concluding remarks, an outlook on biotechnology and synthetic biology, and future promising areas of research in metabolic engineering.

Chapter 2. Bioproduction of a betalain color palette in *Saccharomyces cerevisiae*

2.1. Introduction

Dyes improve the desirability of food and provide a visual cue of freshness[19]. A substantial fraction of the currently approved colorants on the market are chemically synthesized from petroleum[20,21]; however, there is growing demand for natural pigments as consumers become increasingly concerned with synthetic additives in their diet as well as the sustainability of product supply chains[19,20]. Plant cultivation for the extraction of natural dyes has been considered a promising solution; however, the seasonal nature of harvests and the use of arable lands for non-essential foodstuffs is not ideal[22,23]. Plant-cell culture systems have been proposed as an alternative production platform, but these systems will be difficult to scale and can lack genetic tractability[22,23]. Microbial metabolic engineering has the potential to address these concerns and limitations. Specifically, genetically tractable production hosts such as *Saccharomyces cerevisiae* (baker's yeast) can be engineered with heterologous biochemical pathways and rapidly optimized for high production titers[22].

One clade of useful natural pigments are the betalains, a set of tyrosine-derived compounds exclusively restricted to the *Caryophyllales* order of plants[14]. Betalains are divided into the yellow-orange betaxanthins and red-violet betacyanins; of the betalains, betanin is the most utilized in commercial applications[24]. Betanin has applications in a variety of short shelf-life foodstuffs, cosmetics, and pharmaceuticals owing to several favorable properties: high water solubility, robust stability and color intensity over a broad range of neutral and acidic conditions (pH 3-7), lack of intrinsic flavor, high extinction coefficient compared to most artificial red dyes, and stability to certain forms of pasteurization in high-sugar solutions[19,23,25]. Betanin is principally obtained via specialized cultivars of *Beta vulgaris* (beet) and sold in the form of "beetroot extract" (E number 162) at price points that can reach $100 per kg of extract[26].

As illustrated in **Figure 2-1**, all betalains share a common betalamic acid chromophore. This central molecule is formed from tyrosine via two enzymatic reactions. First, the monophenolase activity of various P450s (of the CYP76AD clade in *B. vulgaris*) generates L-3,4-dihydroxyphenylalanine (L-DOPA) from L-tyrosine[27]. Then, DOPA-4,5-dioxygenase (DOD) catalyzes the ring cleavage at the catechol moiety of L-DOPA allowing subsequent spontaneous cyclization with the alpha-amino group to form

betalamic acid[15]. Betalamic acid spontaneously undergoes a Schiff-base condensation with free primary or secondary amines via its reactive aldehyde group to produce betalains possessing yellow to violet color[16].

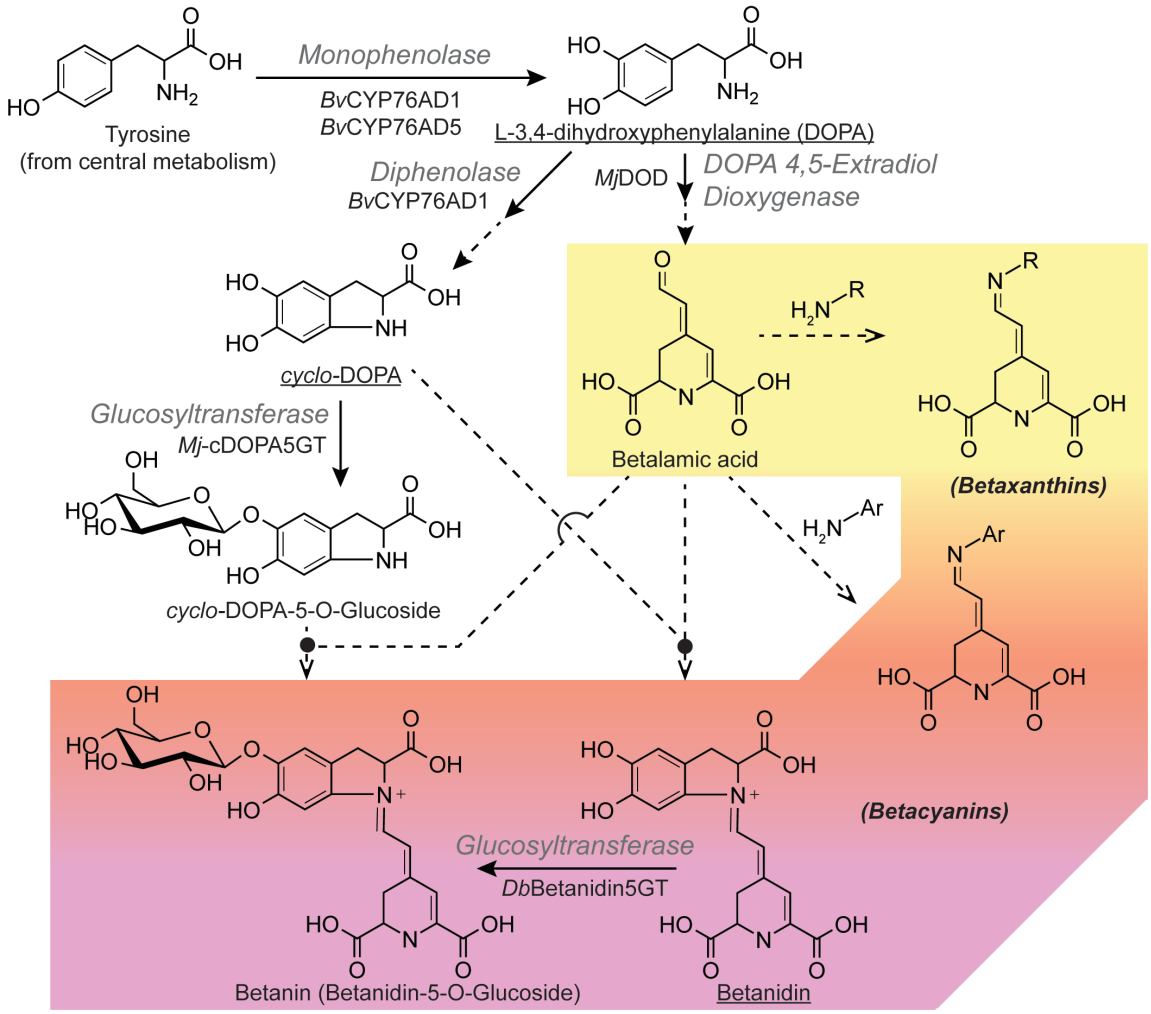

Figure 2-1. Betalain biosynthesis pathways. Diagram of the biosynthetic pathway with general enzymes activities in gray and the specific recombinant genes encoding these activities used in this work indicated in black. Solid lines are are enzymatic reactions and dashed lines indicate spontaneous reactions. Unstable compounds in absence of reducing agent have their names underlined. Abbreviations: R = any organic chemical; Ar = any organic aromatic chemical.

Biosynthesis of the red-violet betanin requires two additional enzymatic activities that supplement the betalamic acid pathway. The first step is an enzymatic oxidation of L-DOPA to form dopaquinone, which spontaneously cyclizes into *cyclo*-DOPA. In *B. vulgaris*, CYP76AD1 is the sole enzyme capable of providing this additional diphenolase activity necessary to produce *cyclo*-DOPA[28]. Next, the condensation of *cyclo*-DOPA with

betalamic acid results in the unstable, red-violet intermediate betanidin. A second enzymatic reaction, glucosylation, produces the dramatically more stable betanin (betanidin 5-O-beta-glucoside) pigment. Alternatively, the order of condensation and glucosylation can be reversed: *cyclo*-DOPA can be preemptively glucosylated prior to condensation with betalamic acid[24]. The reaction order differs among plant species. For example, *Mirabilis jalapa* (four o'clock flower) produces the *cyclo*-DOPA-5-O-glucoside[29], whereas *Dorotheanthus bellidiformis* (Livingstone daisy) utilizes a betanidin glucosyltransferase[30]. Although specially bred cultivars of *B. vulgaris* are currently the predominant source of betanin[24], the putative glucosyltransferase (*Bv*GT) for betanin biosynthesis in beets[31] has yet to be definitively confirmed by enzymatic assays.

In addition to the food dye betanin, applications of other betalains have been proposed. For example, the yellow betaxanthins have been proposed as replacements for artificial yellow dyes[32]. Betalains have also shown applicability as photocell sensitizers, spectrofluorometric probes, and medical diagnostic reagents[33–36]. One such chemical is the condensation product of betalamic acid with 7-amino-4-methylcoumarin that has reported utility as a live-cell imaging probe for *Plasmodium*-infected erythrocytes[34]. Such results highlight how derivatization with betalamic acid can be used to tune molecular properties and lead to value-added compounds. Although previously studied amines have yielded yellow, orange, and violet pigments upon condensation with betalamic acid[24,34,37,38], it is unclear what range of spectral and physical properties can be obtained from "designer" betalains.

To our knowledge, we herein provide the first description of betanin production from glucose in a heterologous microbial host. Additionally, we demonstrate that a heterologous system can be used to obtain novel betalain derivatives directly from yeast culture by feeding diverse amines. These results have implications for the fermentative production of natural colorants and further expand the spectrum of betalain colors obtainable via amine feeding.

2.2. Results

2.2.1. Microbial total synthesis of betanin from glucose

In order to create a *S. cerevisiae* strain capable of producing betanin from central metabolism, we took advantage of a previously codon optimized and engineered version of *B. vulgaris* CYP76AD1, which contains a W13L mutation for increased enzyme expression and activity[39]. We refer to this enzyme as CYP76AD1^{W13L}. For DOPA-4,5-

dioxygenase activity, we chose DOD enzyme from *M. jalapa* also optimized for *S. cerevisiae*[39]. Previous work has demonstrated that yeast heterologously expressing various orthologs of P450 and DOD enzymes can produce the betanin precursor molecules *cyclo*-DOPA and betanidin[27,28,40]. However, both of these compounds are unstable in the presence of oxygen due to the reactivity of their catechol moieties: *cyclo*-DOPA oxidizes and polymerizes into melanin, while betanidin decomposes into various orange-red and yellow byproducts[39,41,42]. These oxidation reactions can be blocked by the addition of a reducing agent such as ascorbic acid (ASC)[39,42]. Plants achieve a similar stabilization of the catechol moiety through the enzymatic addition of a glucose molecule, which serves as a biochemical protecting group inhibiting the oxidation pathway[43]. As illustrated in **Figure 2-1**, betanin is produced either through direct glucosylation of betanidin or through glucosylation of the precursor *cyclo*-DOPA followed by condensation with betalamic acid[29,30].

In the strain containing CYP76AD1^{W13L} and *Mj*DOD, we tested both the *cyclo*-DOPA glucosyltransferase from *M. jalapa* (*Mj*-cDOPA5GT) and betanidin glucosyltransferase from *D. bellidiformis* (*Db*Betanidin5GT) individually as well as co-expressed for their ability to produce betanin in *S. cerevisiae* (Fig. 2a). *Mj*-cDOPA5GT has been reported to regioselectively glucosylate only at the 5-hydroxyl position on *cyclo*-DOPA[29] and *Db*Betanidin5GT has been reported to regioselectively glucosylate at the corresponding position on betanidin[44]. Under the industrially-relevant condition of media lacking a reducing agent such as ASC, both glucosyltransferases were able to produce betanin in *S. cerevisiae*. Betanin production was confirmed by comparison of chromatography retention time, high resolution mass spectrometry, and MS/MS fragmentation pattern against a commercial standard (**Figure 2-2, Figure 2-3**). Expression of *Mj*-cDOPA5GT resulted in 16.8 ± 3.4 mg/L betanin, while expression of *Db*Betanidin5GT resulted in 10.4 ± 2.3 mg/L betanin (average ± one standard deviation). Co-expression of both glucosyltransferases produced 16.5 ± 2.4 mg/L betanin, thus not providing additional benefit over the expression of *Mj*-cDOPA5GT alone (**Figure 2-4a**).

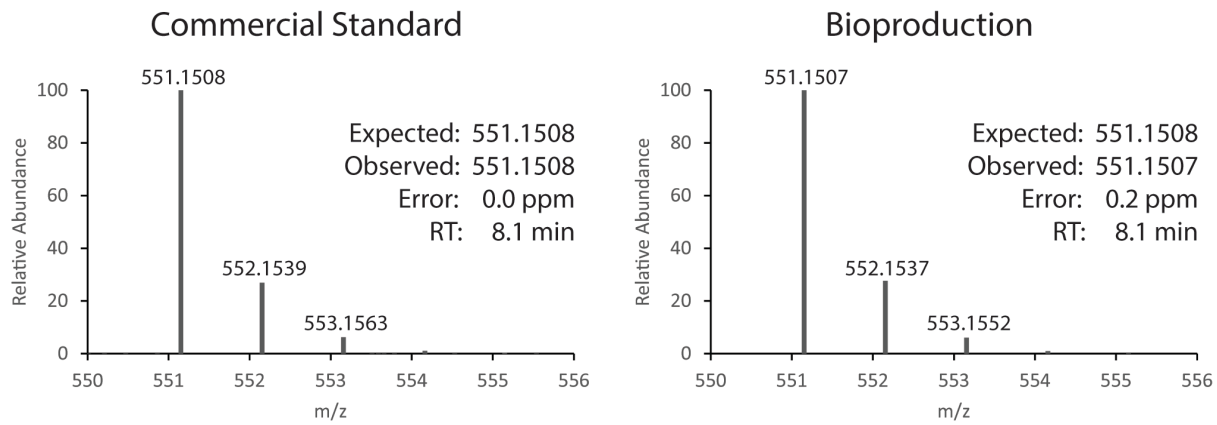

Figure 2-2. High resolution mass spectrometry of betanin in AdooQ beetroot extract and betanin produced by yeast culture. Mass spectrometry confirms yeast bioproduction of betanin by comparison to commercial standard and to theoretical m/z. **Abbreviations:** RT = Retention Time.

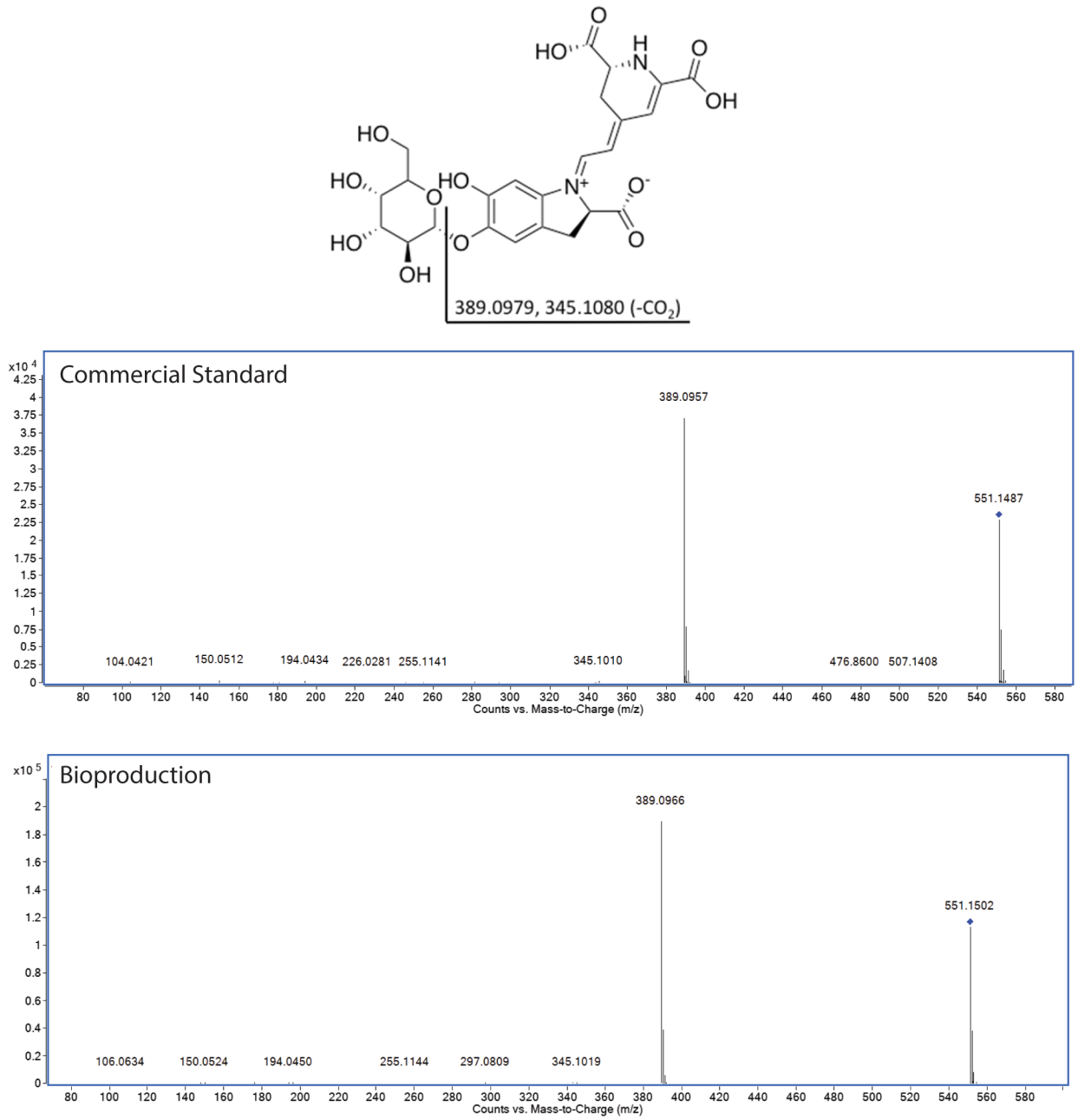

Figure 2-3. MS/MS of betanin in AdooQ beetroot extract and betanin produced by yeast culture. MS/MS fragmentation confirms yeast bioproduction of betanin by comparison to commercial standard. Precursor ion is indicated by a blue diamond.

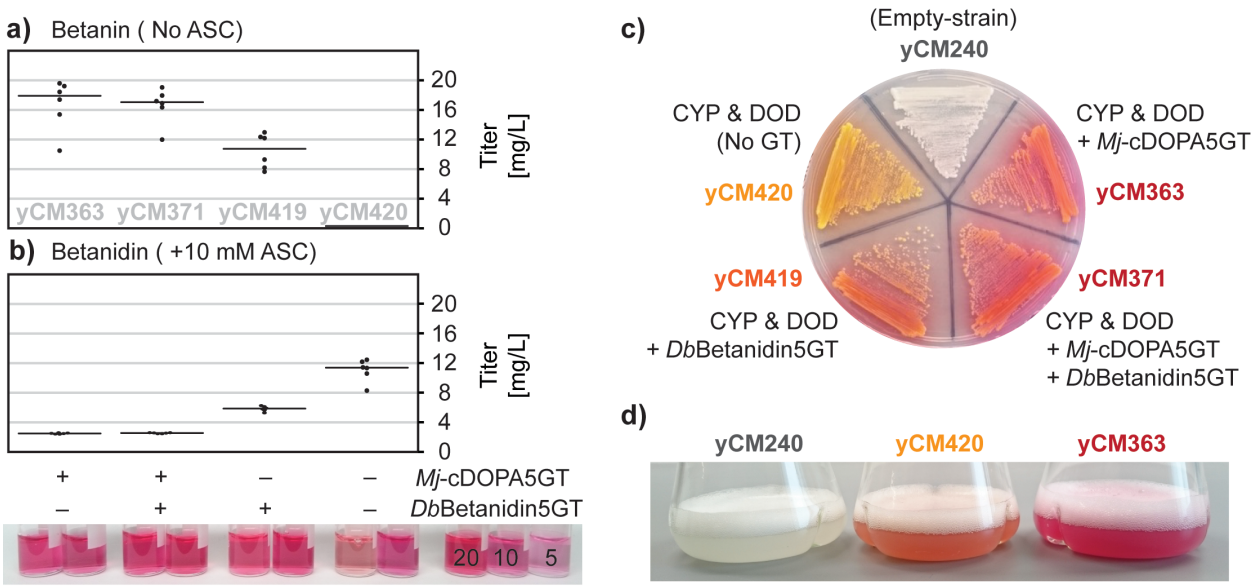

Figure 2-4. Production of betanin using various combinations of glucosyltransferases. Titer of **a**) betanin and **b**) betanidin in yeast determined by LCMS for six replicates, cultured in minimal media without and with 10 mM ascorbic acid (ASC), respectively. Data points represent individual measurements and lines indicate median values. Below, vials of supernatant from centrifuged cultures are staged with a dilution series of betanin beetroot extract. Numbers on vials refer to approximate concentrations of molecular betanin as previously calculated, in mg/L. Each pair represents the no ASC and +10 mM ASC supernatant, respectively. Note that solution color is derived from the total betacyanin (betanin + betanidin) content. **c**) Photograph of various betanin-producing and control strains. CYP denotes CYP76AD1^{W13L}. **d**) Photograph of betanidin and betanin production strains grown in flasks in minimal media.

Because the two glucosyltransferases act at different points in the pathway, it is difficult to definitively say whether the placement of the glucosylation reaction or differences in the glucosyltransferases' kinetic parameters account for the observed betanin titers. Glucosylation of *cyclo*-DOPA would prevent oxidation of this earlier intermediate while also bypassing the production of unstable betanidin intermediate. However, the higher accumulation of betanidin in the *Db*Betanidin5GT expressing strain compared to the *Mj*-cDOPA5GT strain under the ASC supplemented conditions (**Figure 2-4b**) suggests *Db*Betanidin5GT might be a less effective enzyme. Moreover, the data suggest that glucosylation is a more effective stabilization strategy than addition of ASC because approximately 17 mg/L of betanin are produced upon expression of *Mj*-cDOPA5GT (in the absence of ASC), whereas only approximately 11 mg/L of betanidin are produced in the presence of ASC (when no glucosyltransferase is expressed).

In addition to oxidative loss of catechol-containing intermediates, a major fermentative challenge for betalain production is the oxygen demand of this pathway. Both the P450 and DOD reactions require oxygen. In order to investigate the effect of oxygenation, we tested the *Mj*-cDOPA5GT-containing strain in both non-baffled and baffled Erlenmeyer

flasks at a 50 mL culture volume. The observed betanin titers were, respectively, 4.8 ± 0.1 and 14.2 ± 1.5 mg/L (**Figure 2-5**) with comparable final cell densities, highlighting the importance of oxygenated culture conditions.

a)

	mg/L				
	Flask 1	**Flask 2**	**Flask 3**	***Avg.***	***St. Dev.***
Non-baffled	4.75	4.88	4.62	4.8	0.1
Baffled	13.32	15.96	13.41	14.2	1.5

b)

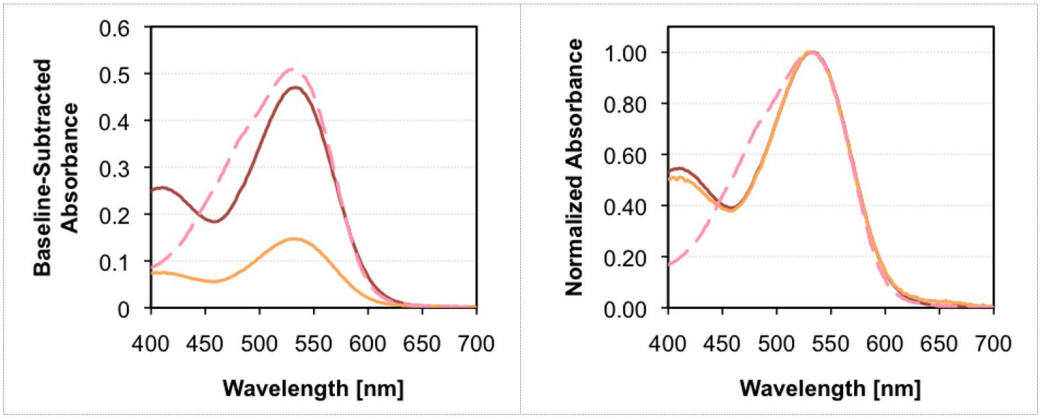

Figure 2-5. Betanin production from cultures grown in flasks. a) Quantification of the secreted betanin titer found within the supernatant fraction from the 50 mL cultures. All values are reported in milligrams per liter. **b**) Absorbance scan of AdooQ beetroot extract (prepared at ~17 mg/L molecular betanin, dashed pink line), non-baffled flask culture supernatant (orange line), and baffled flask culture supernatant (dark red line). The extra peak around 410-420 nm likely corresponds to betaxanthins formed with the amino acid supplements needed for auxotroph complementation.

S. cerevisiae's ability to export betanin is a key feature as it should simplify purification (**Figure 2-4**). Such efflux activity is particularly attractive when compared to the traditional maceration and extraction protocols utilized on beetroot[23]. This advantage in recovery remains even when yeast is compared to plant cell suspensions. In plants, betalains are primarily stored in the vacuole[45]. Stimulating the release of betanin from plant cells grown *in vitro* has required carefully applied stressors, often becoming a balancing act between cell viability and recovery yield[45]; in contrast, approximately two thirds of the yeast culture's pigmentation is found in the media without any requisite manipulation (**Figure 2-6**). We anticipate that identification and overexpression of the relevant plasma membrane transporters responsible for export could increase our overall titers.

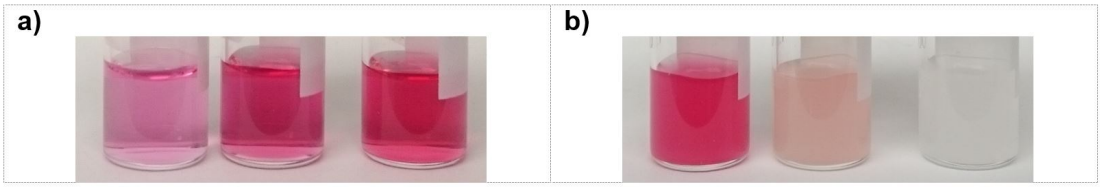

Figure 2-6. Betanin is secreted by yeast cells into the media. a) Non-baffled (left) and baffled (center) flask culture supernatant photographed alongside a vial of AdooQ beetroot extract (right, prepared at ~17 mg/L molecular betanin). **b**) Suspended culture (left) and suspended, washed cell pellet (center) from baffled flask fermentation juxtaposed against the suspended, washed cell pellet of a wild-type culture (right). Note that a fraction of the betanin produced remains trapped within the cell.

2.2.2. Probing of the betalain color palette using structurally diverse amines

Beyond betanin, we investigated the bioproduction of other betalains via yeast fermentation. Our inspiration was the *in vitro* work of Gandía-Herrero et al. (2010)[37] examining the effect of amine structure on betalain color, fluorescence, and antiradical activity. In particular, their research elucidated how different structural motifs found in the *cyclo*-DOPA moiety of betanin impact color. In our work, using purified *Mj*DOD enzyme, we tested the condensation of a set of structurally diverse aromatic amines with betalamic acid to determine what other color profiles could be generated *in vitro* (**Figure 2-7a, Figure 2-7b**). The selection of amines included metabolites naturally found in yeast, candidates for biosynthesis in future metabolic engineering efforts, and alternative unnatural structural motifs that extend beyond the limited assortment of aromatic amine compounds commonly found in nature. As a known test case, we used the amino acid leucine to produce the betaxanthin vulgaxanthin IV[24]. Beyond obtaining the expected yellow from the aliphatic leucine and oranges from aniline-like chemicals (para-aminobenzoic acid and anthranilic acid), we were also able to access the violet color space by producing previously unknown betalains. Previously, all reported violet betalains have been based on the formation of structurally rigid iminium ion adducts best illustrated by the nitrogen-carbon bond between the *cyclo*-DOPA and betalamic acid moieties in betanin[37]. The synthetic betaxanthins we have generated from condensates of 6-aminoindole (6AI) and o-dianisidine (oDA) with betalamic acid lack this fixed cation and instead contain the imine moiety prevalent in most betaxanthins.

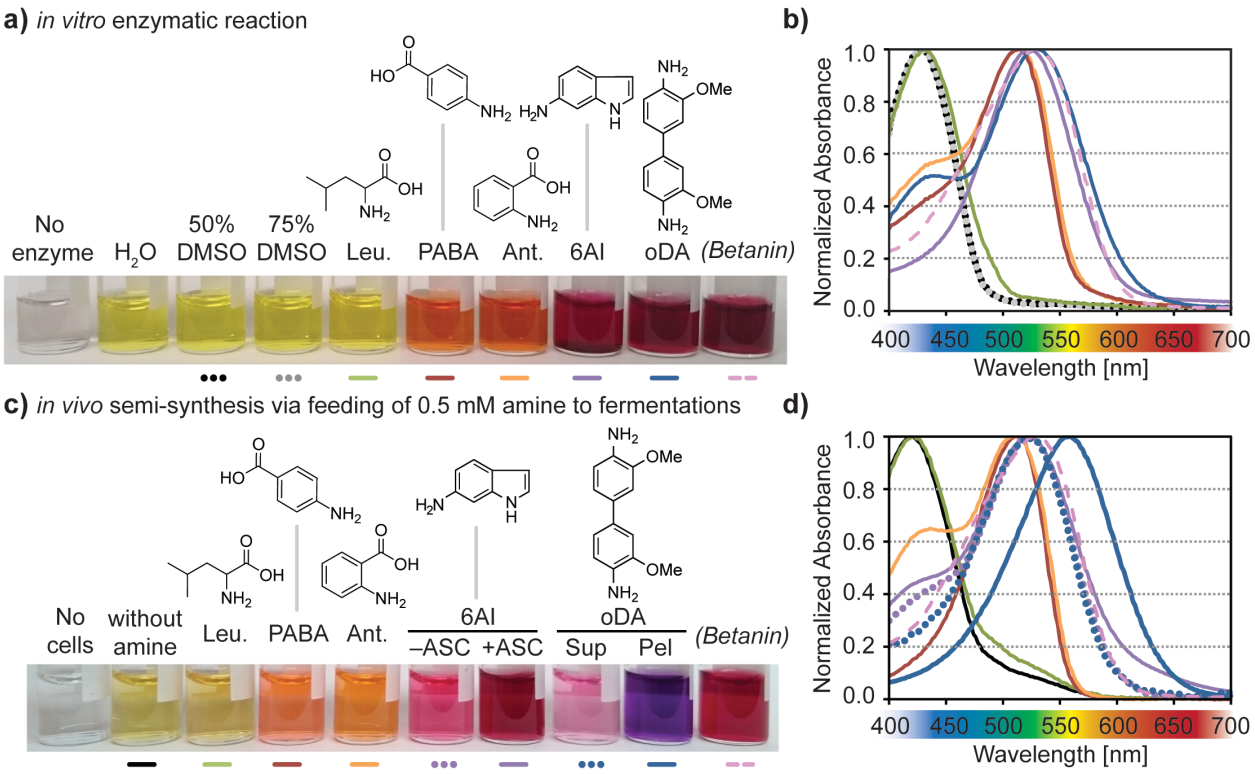

Figure 2-7. *In vitro* and *in vivo* condensations of betalamic acid using native metabolites and alternative substrates. a) Resulting solutions from *in vitro* reactions. The structure of each added amine is indicated above the abbreviation. The yellow color seen in the H_2O and DMSO controls is the result of betalamic acid itself as well as dopaxanthin by-product (L-DOPA serving as the amine for conjugation to betalamic acid). All samples were diluted to 0.44 mM betalain (assuming complete amine condensation). Betanin vials contain commercial beetroot extract used as a standard for comparison. **b**) Normalized absorbance curves of betalains generated from *in vitro* experiments, with corresponding colors indicated below each vial. **c**) Vials of supernatant from centrifuged cultures. -/+ refers to the absence or presence of 10 mM ascorbic acid in the case of 6AI. "Sup" refers to the recovered supernatant and "Pel" refers to the washed cell pellet liquor obtained in the case of oDA. All samples were diluted to 0.25 mM betalain (assuming complete amine condensation). **d**) Normalized absorbance curves of betalains generated from *in vivo* experiments, with corresponding colors indicated below each vial. Raw absorbance curves are provided in **Figure 2-8**. **Abbreviations:** Leu. = leucine; PABA = para-aminobenzoic acid; Ant. = anthranilic acid; 6AI = 6-aminoindole; oDA = o-dianisidine.

We next tested the ability to accomplish whole-cell semi-synthesis as a platform for potential industrial-scale production of betalain analogs. In order to accomplish high purity semi-synthesis, we created a prototrophic yeast strain heterologously expressing *Mj*DOD with *Bv*CYP76AD5. This strain enabled high purity betalain production for two reasons. First, prototrophy removes the need to supplement the media with high concentrations of amino acids that would function as substrates for a spectrum of undesired betaxanthin side-products. Second, the CYP76AD5's exclusive monophenolase activity[27] ensures that all produced L-DOPA is focused towards synthesis of betalamic acid. By adding 0.5 mM of each co-substrate amine to the yeast

growth medium in individual experiments, we were able to test our previous *in vitro* findings (**Figure 2-7a, Figure 2-7b**) in an *in vivo* context (**Figure 2-7c, Figure 2-7d**).

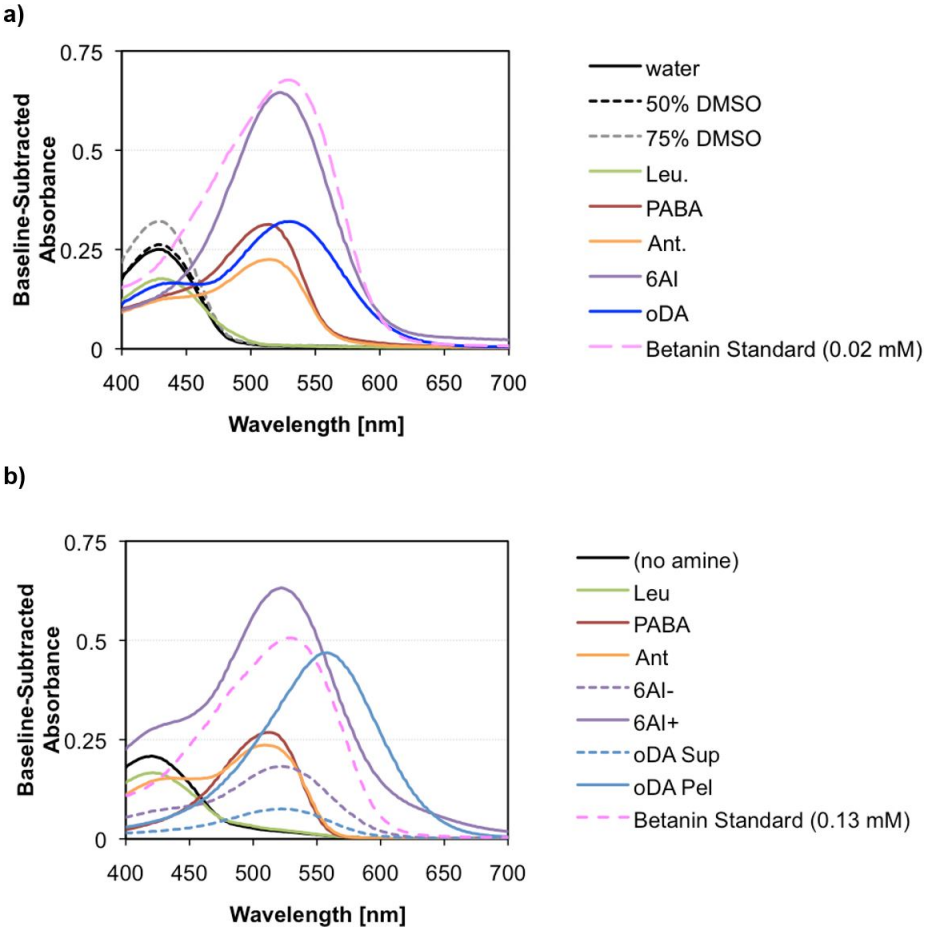

Figure 2-8. Absorbance curves from *in vitro* DOD reactions and *in vivo* bioconversions using various amines. a) *In vitro* DOD reaction raw absorbance values, after subtraction of the "no enzyme" control (not shown). Note that all reactions were diluted 10-fold in 1xPBS prior to absorbance measurement. **b**) *In vivo* bioconversion supernatant raw absorbance values, after subtraction of the "media-only" control (not shown). Note that all supernatant samples were diluted 4-fold in 1xPBS prior to absorbance measurement. **Abbreviations:** Leu. = leucine; PABA = para-aminobenzoic acid; Ant. = anthranilic acid; 6AI (-/+) = 6-aminoindole (without/with 10 mM ascorbic acid in media); oDA (Sup / Pel) = o-dianisidine (culture supernatant / liquid recovered from washing cells).

Amine feeding experiments with live cells were able to reproduce most of the colors found in the *in vitro* assays (**Figure 2-7**). However, two of the amine substrates – 6AI and oDA – showed unanticipated behavior during the *in vivo* assays. For 6AI, we were able to identify ascorbic acid as the determining variable. Similar to other recent protocols for *in vitro* reactions with DOD[46], we used ASC to stabilize the enzyme's Fe^{2+} cofactor; in contrast, our *in vivo* feeding was conducted in media without reducing agent. Supplementation of the 6AI bioconversion media with ASC recovered the color intensity

previously observed in the *in vitro* reactions as determined by visual inspection and upon comparison of the absorbance curves (**Figure 2-8**). Experiments with wild-type cells identified that cellular growth was inhibited at 0.5 mM 6AI. Feeding with 6AI also led to the formation of an unknown black precipitate, an undesired side-reaction that was effectively inhibited under reducing conditions (**Figure 2-9**).

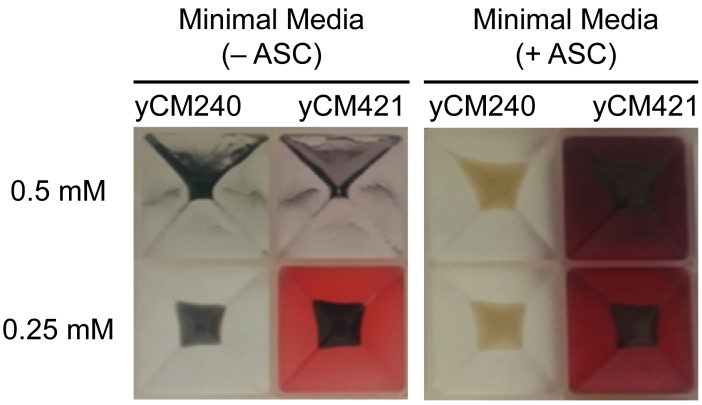

Figure 2-9. 6-Aminoindole (6AI) feeding experiments in minimal media without and with 10 mM ascorbic acid (ASC). Cells lacking (yCM240) and containing (yCM421) the betalamic acid production genes were grown at two different concentrations of 6AI using the same bioconversion protocol used in the main text prior to centrifugation. Note the absence of the dark precipitate in the yCM240 cultures in the +ASC condition.

The most surprising outcome was the production of a blue-violet color derived from oDA feeding. This coloration was not observed when the condensation was performed *in vitro*. When oDA was fed to strains producing betalamic acid, a blue product was observed as a precipitate that associated with the cell pellet after centrifugation. Recovery of this precipitate required a wash with a salt solution such as phosphate-buffered saline (PBS). We found that the precipitate was soluble in PBS, methanol, and ethanol but not in water. Feeding experiments conducted with yeast strains expressing different parts of the betalamic acid pathway confirmed that the blue precipitate was likely a betalain and not the result of an endogenous metabolite (**Figure 2-10**). When dissolved in PBS, this product exhibited maximum absorbance at approximately 560 nm (**Figure 2-7d**), making it the most red-shifted betalain reported to date. Additionally, betalamic acid producing yeast fed oDA initially displayed red pigmentation 12 hours after inoculation but became blue-violet over the next 12 hours (**Figure 2-11**). Therefore, we suspected that the red pigment, observed *in vitro* and *in vivo* in the supernatant (**Figure 2-7**), was the condensation product of oDA and one molecule of betalamic acid. Because oDA contains two amine groups, we suspected that the blue precipitate was the result of oDA condensing with two molecules of betalamic acid (a "double condensate"). Indeed, we had initially selected oDA for feeding experiments for its potential ability to conjugate to betalamic acid at both amine positions.

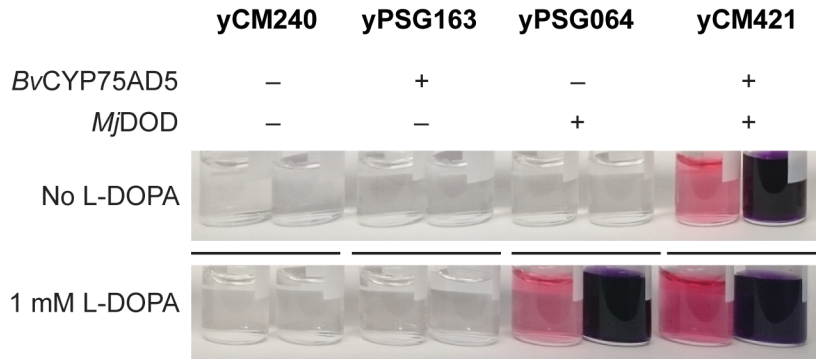

Figure 2-10. oDA-condensate requires L-DOPA and DOD activity. Feeding assay using strains lacking different parts of the betalamic acid biosynthesis pathway. Negative and positive signs indicate the absence or presence of the respective enzymes. Black bars between the two photographs delineate pairs of culture supernatant (left) and washed cell pellets (right) from each strain. All cells were grown in minimal media containing 0.5 mM oDA. **Abbreviations:** oDA = o-dianisidine; L-DOPA = L-3,4-dihydroxyphenylalanine.

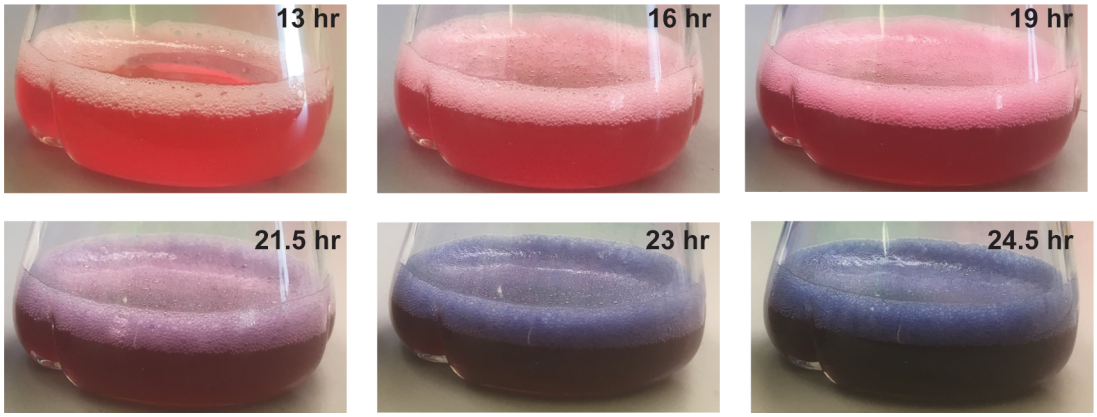

Figure 2-11. Formation of oDA single condensate and double condensate over time. 50 mL bioconversion reactions using 0.5 mM oDA. Red coloration is due to the single condensate, blue-violet coloration is due to the double condensate. Times are reported as number of hours after inoculation of yeast into minimal media containing oDA.

In order to favor production of the double condensate under the *in vitro* reaction conditions, we tested various ratios of L-DOPA to oDA with the hypothesis that a high ratio of betalamic acid to oDA would favor the condensation of oDA with two betalamic acid molecules. However, we were unable to detect production of the double condensate when the reaction was performed *in vitro*. This is likely due to the fact that L-DOPA itself is an amine that can react with betalamic acid. While we tested low concentrations of oDA to favor condensation with two molecules of betalamic acid, we were also favoring the reaction of betalamic acid with L-DOPA to produce dopaxanthin. In the case of *in vivo* production of betalamic acid from glucose, it is likely that L-DOPA does not accumulate to high concentrations as once it is produced by CYP76AD5, it is rapidly converted by

the more efficient DOD enzyme to betalamic acid[39]. Thus, dopaxanthin byproduct should be minimized and double condensate formation should be favored. This mechanism is consistent with our observation that the culture initially appears red 12 hours after inoculation (indicative of the single condensate) but changes to a blue-violet appearance over the next 12 hours (indicative of double condensate formation).

The *in vitro* and *in vivo* reaction products were characterized by high resolution mass spectrometry. Observed masses were within 0.5 ppm of the theoretical masses of the expected betalain products (**Figure 2-12**). Additionally, m/z values (**Figure 2-12**) and MS/MS fragmentation patterns (data available online[47]) for reactions performed *in vivo* are the same as those observed *in vitro* when fed PABA, Ant., or 6AI amines, further supporting the production of the expected betalains because the *in vitro* reactions contain only the reactants (L-DOPA and amine), DOD enzyme, $FeSO_4$, ascorbic acid, and PBS. When oDA was used as the amine, reactions performed both *in vitro* and *in vivo* resulted in a product with an m/z value consistent with the oDA single condensate. An additional product was observed *in vivo*, with an m/z value consistent with the oDA double condensate. The m/z of the double condensate was not observed in the supernatant upon centrifugation of the yeast culture (**Figure 2-13**); it was found only in the PBS wash of the cell pellet. The absorbance maxima determined for the single and double condensates when purified and subjected to HPLC UV-Vis analysis (**Figure 2-12**) were approximately 524 nm and 554 nm, respectively, which is consistent with the absorbance curves in **Figure 2-7d** obtained on culture supernatant and cell pellet wash. These results suggest that the observed blue-violet color obtained from a PBS wash of the cell pellet is the result of a mixture of the blue double condensate and the red-violet single condensate. Finally, the supernatants from the amine-fed yeast cultures were tested for stability at room temperature and ambient light conditions. The betalain pigments exhibited variable but significant loss of color one to six days after collection from yeast culture (**Figure 2-14**). Instability of betalains, and betaxanthins in particular, under ambient conditions is well-documented and they are considered more suitable for applications with short shelf-life or for products stored at cold temperatures[32]. Stability of the oDA double condensate was considerably increased at both 4°C and -20°C (**Figure 2-15**).

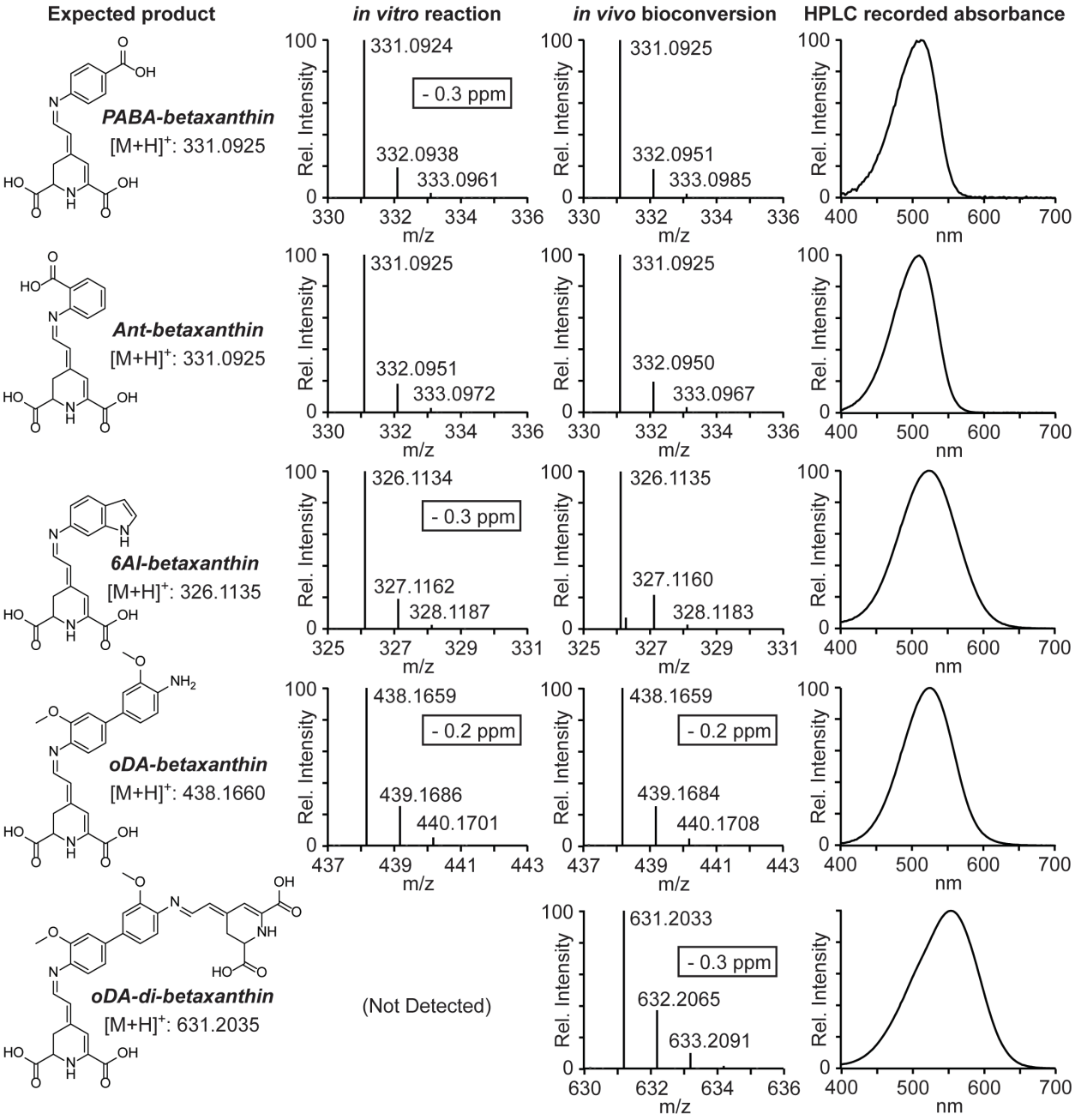

Figure 2-12. High resolution mass spectrometry and HPLC UV-Vis analysis of betalains. The predicted structures, theoretical m/z values, and betalain names using the generic amine-betaxanthin nomenclature[24] are shown on the left. High resolution mass spectra for *in vitro* and *in vivo* products are provided in the middle, with boxed values referring to differences between theoretical and observed masses in parts per million (ppm). Absorbance curves of the betalains recorded during HPLC analysis are shown on the right. oDA-di-betaxanthin was not detected in the *in vitro* reaction (**Figure 2-13**).

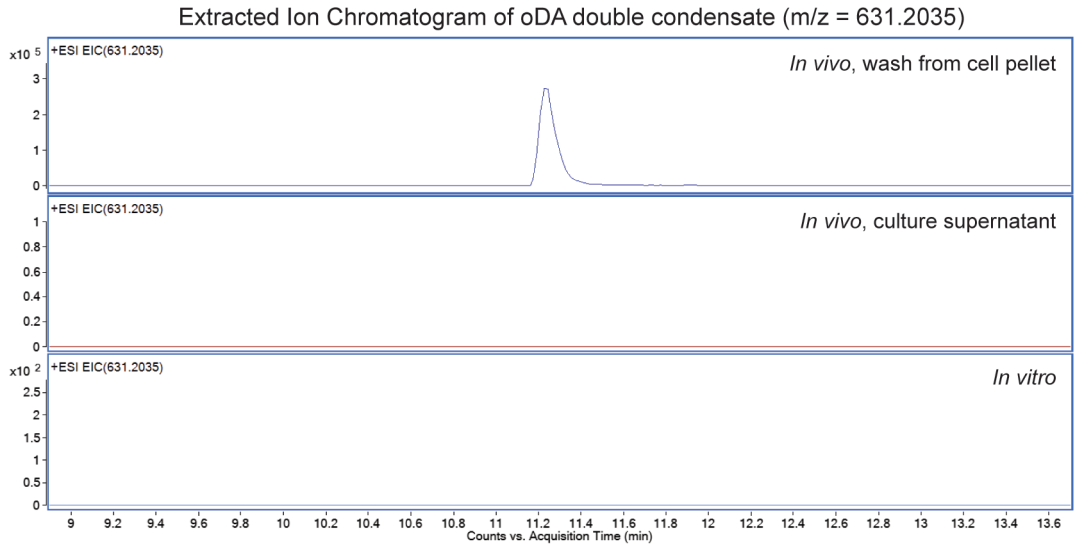

Figure 2-13. Extracted ion chromatogram of oDA double condensate. The oDA double condensate is observed in the wash from the cell pellet but is not observed in the culture supernatant or in the *in vitro* reaction with oDA.

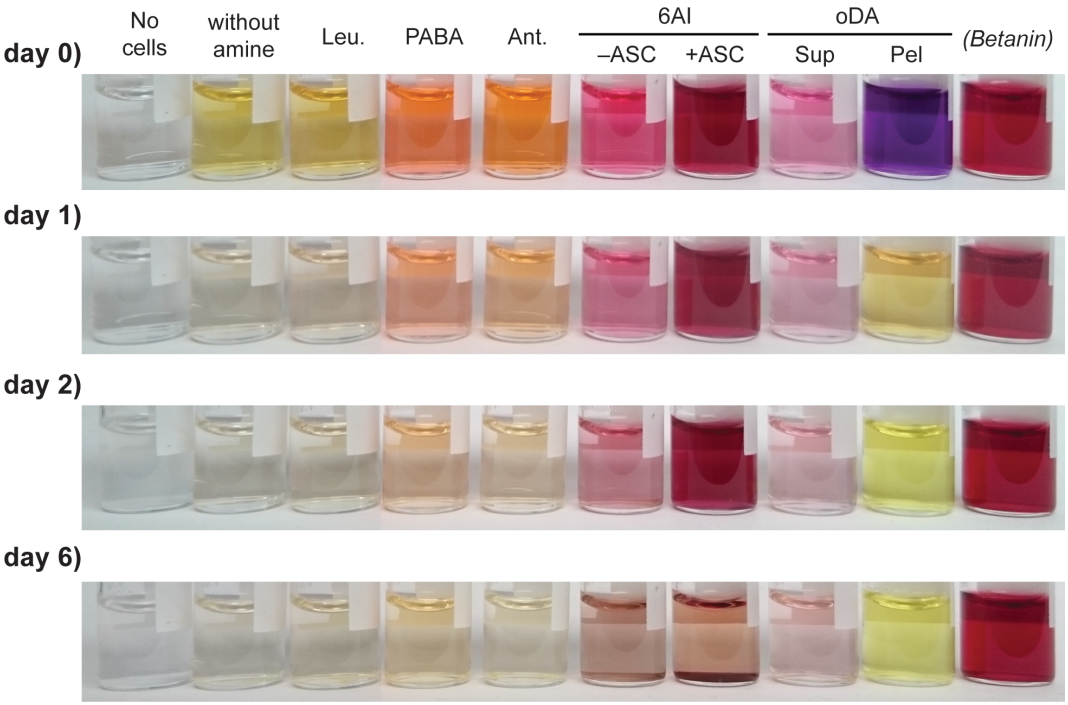

Figure 2-14. Room temperature stability of betalain pigments from amine-fed yeast culture supernatants. Samples were photographed at 0 (reproduction of **Figure 2-7c**), 1, 2, and 6 days after collection from cultures. Note the differential stabilities of the different betalain compounds. All samples were obtained from yeast culture supernatant other than the No cells condition, the oDA Pel which was obtained by PBS wash of the cell pellet, and the betanin sample which was AdooQ beetroot extract dissolved in minimal media.

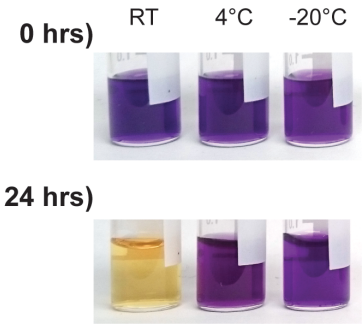

Figure 2-15. Effects of temperature on the color stability of the oDA-betaxanthin double condensate. Samples were obtained by wash of the cell pellet with 1xPBS (pH 7.4). **Abbreviations:** RT = room temperature.

2.3. Discussion

The completion of the betanin pathway in yeast and production of a demonstrative suite of both natural and semi-synthetic betalains highlights the potential of *S. cerevisiae* as a heterologous host for the production of betalamic acid derived pigments. For betanin, the ability to shift from plant production to microbial fermentation represents an opportunity to increase the overall market supply and provide a more consistent production level that is not vulnerable to the fluctuations that commonly afflict agricultural processes. Furthermore, a heterologous host could enable the production of alternative forms of betanin where the glucosyl group is further modified (e.g., 3-hydroxy-3-methyl-glutaryl-betanin or hylocerenin) that may have superior color stability[41] or other improved properties. Currently, our best strain can produce 17 mg of betanin per liter in 48 hours. This corresponds to the color intensity of approximately 10 grams per liter of purchased beetroot extract powder. In order to economically compete against beetroot for the production of natural betalains and provide the resource-saving advantages often attributed to microbial processes[22], considerable improvements will be required. To achieve these necessary production gains, we anticipate that metabolic engineering efforts should aim to further improve the P450 activity in *S. cerevisiae* as well as the supply of tyrosine[48,49].

A major challenge in industrial biosynthesis is ensuring that carbon is not lost to side reactions or degradation[22]. In betanin biosynthesis, unstable metabolites are protected from oxidation via glucosylation. Typically, glucosylation as a stabilization strategy is found as a final modification, best exemplified by the anthocyanin pigment pathway[50]. For betanin, this strategy is seen in the glucosylation of betanidin, which stabilizes the catechol domain and prevents oxidative decomposition. However, the glucosylation of

cyclo-DOPA presents an alternative route - the glucosylation and stabilization of an unstable intermediate further upstream in the biosynthetic pathway. In our heterologous system, the use of a *cyclo*-DOPA glucosyltransferase is more effective than expression of a betanidin glucosyltransferase. Whether *Beta vulgaris* utilizes a betanidin and/or *cyclo*-DOPA glucosyltransferase has not yet been determined, but it would be interesting to identify which strategy *B. vulgaris* favors given the commercial use of beetroot extract as a red food dye.

With regard to the larger betalain family, the work here expands the known spectral range and provides a facile bioproduction strategy. Previously, most synthesis methods were based on alkali-catalyzed hydrolysis of betanin (in beetroot extract) followed by re-acidification in the presence of excess amine[38]. More recent systems have included amine-functionalized solid-phase supports for direct condensation with betalamic acid obtained from base-hydrolysis of betanin[51]. Yeast feeding presents a direct synthesis route with minimal production of unintended betalains. Additionally, the biosynthesized betalains are found in the culture media, which simplifies downstream processing and purification. Future betalain variants could take advantage of tuned spectral properties (color, fluorescence) or decay half-lives. Decay half-life is of potential utility given that color depth or shade has been suggested as an accessible proxy "timer" for determining whether an item or formulation is no longer fit for use[52]. One particularly interesting avenue towards natural-product derived "unnatural" betalains would be through the rare 4-aminophenylalanine metabolite[53]. Previous work has shown that this amino acid can be converted into a phenylpropanoid pathway metabolite[54], opening the possibility of linking amino-analogs of flavonoids, stilbenes, and anthocyanins with betalamic acid.

Overall, this work enables future engineering of the unique family of pigments known as betalains by establishing a versatile biosynthetic platform in yeast. With this platform, it is possible to begin the process of pathway optimization that will be required for industrial viability. The results of pathway engineering here also speak to the evolutionary role of glucosyltransferases in enabling the accumulation of otherwise labile small molecules, using glucose as a biochemical protecting group to prevent metabolite oxidation. Lastly, through feeding structurally-diverse amines to yeast strains producing betalamic acid, we produced betalains with expanded spectral properties, including generation of violet and blue-violet molecules containing an uncharged imine group rather than the fixed iminium ion found in betanin.

2.4. Materials and Methods

Chemicals and Quantification. Amines used for *in vitro* and *in vivo* feeding were obtained from the following sources: L-DOPA (D9628, Sigma Aldrich), leucine (E811-100G, Amresco), para-aminobenzoic acid (100536-250G, Sigma Aldrich), anthranilic acid (A89855 Sigma Aldrich), 6-aminoindole (018336, Matrix Scientific), and o-dianisidine (01936, Chem-Impex International). Ascorbic acid was obtained from Gibco (13080-023) and iron(II) sulfate heptahydrate was obtained from Sigma Aldrich (215422).

Because pure betanin molecule is not commercially available, we used a >98% pure beetroot extract (A10132, AdooQ Bioscience) for the majority of experiments, in conjunction with beetroot extract diluted in dextrin (B0397, TCI). Using the Beer-Lambert law and a betanin extinction coefficient of 65,000 M^{-1} cm^{-1} at 536 nm[55,56], we determined that 1 g/L of AdooQ beetroot extract contained approximately 1.71 +/- 0.14 mg/L of molecular betanin. This conversion factor was used for the preparation of standards from the AdooQ extract for quantification of betanin titers.

For betanidin, we used the Beer-Lambert law with an extinction coefficient of 54,000 M^{-1} cm^{-1} at 538 nm[56] to quantify the amount of betanidin in the fermentation broth of strain yCM420 grown in media with ascorbic acid to prevent betanidin oxidation. We then generated a mass spectrometry calibration curve based on a serial dilution series starting from the yCM420 fermentation broth and used the calibration curve to quantify betanidin titers by mass spectrometry.

Spectroscopic quantification was accomplished using 1-cm optical pathlength plastic cuvettes on a Shimadzu UVmini-1240 spectrophotometer. All other absorbance measurements were obtained on a TECAN M1000 in a Costar 96-well plate (Corning 3904). Normalized absorbance curves were obtained by normalizing against their absorbance maxima after appropriate baseline subtraction. Samples were diluted in phosphate buffered saline (PBS, pH 7.4) as needed in order to obtain a linear signal.

Liquid chromatography/mass spectrometry (LCMS) was performed using a 1260 Infinity LC System connected to a 6120 Quadrupole Mass Spectrometer (Agilent Technologies). All culture supernatant samples, media control samples, and betanin standards were diluted ten-fold in water prior to injection, to achieve a linear calibration curve for betanin with all samples falling within the bounds of the calibration curve. Ten microliters of each ten-fold diluted sample were injected and sample separation was achieved using a Zorbax Eclipse Plus C18 guard column (4.6cm x 12.5cm, 5 μm packing, Agilent Technologies) connected to a Zorbax Eclipse Plus C18 column (4.6mm x 100mm, 3.5 μm packing, Agilent Technologies) at 20°C using a 0.5 mL/min flow rate. Water and acetonitrile mobile phases contained 0.1% formic acid as

the pH modifier. The elution gradient (water:acetonitrile volume ratio) was as follows: 98:2 (0-2 min), linear ramp from 98:2 - 5:95 (2-17 min), 5:95 (17-22 min), linear ramp from 5:95 - 98:2 (22-23 min), and 98:2 (23-28 min). Absorbance was measured using a diode array detector for UV-Vis analysis. MS was conducted in atmospheric pressure ionization-positive electrospray (API-ES positive) mode at 100-V fragmentor voltage with ion detection set to both full scanning mode (50 - 1200 m/z) and targeted detection of betanidin (389.1 m/z) and betanin (551.1 m/z).

Plasmid and Strain Construction. All plasmids were assembled using the Yeast Tool Kit system[57]. The final multigene assemblies utilized are described in **Table 2-1**.

Table 2-1. Plasmids used in betalains chapter.

Name	**Description**	**Source**
pDS0835	*Mj*DOD-GSx4-TEV-HISx6 (T7-vector)	This study
pZNR0521	LEU2 marker (LEU2 integration)	__
pWCD1934	HIS3 marker (HIS3 integration)	__
pML1371	URA3 marker (URA3 integration)	__
pCMC0756	pCCW12-*Mj*DOD-tADH1-pTDH3-*Bv*CYP76AD1^{W13L}-tTDH1-pTEF1-*Sc*ARO4^{K229L}-tENO2 (URA3 integration with URA3 marker)	This study
pCMC0759	pCCW12-*Mj*DOD-tADH1-pTDH3-*Bv*CYP76AD5-tTDH1-pTEF1-*Sc*ARO4^{K229L}-tENO2 (URA3 integration with URA3 marker)	This study
pPSG165	pPGK1-ARO4^{K229L}-tADH1-pTDH3-DOD-tTDH1 (URA3 integration with URA3 marker)	This study
pPSG331	pTDH3-Bv_CYP76AD5-tTDH1-pPGK1-ARO4^{K229L}-tPGK1 (URA3 integration with URA3 marker)	This study
pPSG0348	pTEF2-*Mj*cDOPA5GT-tSSA1 (LEU2 integration with LEU2 marker)	This study
pPSG0349	pTEF2-*Db*Betanidin5GT-tSSA1 (LEU2 integration with LEU2 marker)	This study
pPSG0350	pPGK1-*Db*Betanidin5GT-tENO2-pTEF2-*Mj*cDOPA5GT-tSSA1 (LEU2 integration with LEU2	This study

	marker)	

Strains of *Saccharomyces cerevisiae* were generated following the lithium acetate protocol[58] and confirmed by colony PCR for proper integrations. Strains are listed in **Table 2-2**.

Table 2-2. Yeast strains used in betalains chapter.

Name	**Genotype**	**Source**
BY4741	*MATα SUC2 gal2 mal2 mel flo1 flo8-1 hap1 ho bio1 bio6 his3Δ1 leu2Δ0 met15Δ0 ura3Δ0*	ATCC
yWCD230	[BY4741] *his3Δ0*	—
yCM208	[yWCD230] *his3Δ::pWCD1934 leu2Δ::pZNR0512 met15Δ::MET15*	This study
yCM240	[yCM208] *ura3Δ::pML1371*	This study
yCM363	[yWCD230] *leu2Δ::pPSG348 ura3Δ::pCMC0756*	This study
yCM371	[yWCD230] *leu2Δ::pPSG350 ura3Δ::pCMC0756*	This study
yCM419	[yWCD230] *leu2Δ::pPSG349 ura3Δ::pCMC0756*	This study
yCM420	[yWCD230] *leu2Δ::pZNR521 ura3Δ::pCMC0756*	This study
yCM421	[yCM208] *ura3Δ::pCMC0759*	This study
yPSG064	[BY4741] *ura3Δ::pPSG165*	This study
yPSG163	[BY4741] *ura3Δ::pPSG331*	This study

***In vitro* reactions using purified *Mj*DOD enzyme.** Stock solutions of 2 mM L-DOPA and 1 mM iron(II) sulfate with 10 mM ascorbic acid were prepared in PBS (pH 7.4). Stock solutions of amines were prepared at 20 mM in a 1:1 mixture of DMSO:water, except for leucine that was prepared at 20mM in water, and o-dianisidine that was prepared at 10 mM in a 3:1 mixture of DMSO:water. All stock solutions were made fresh and used within 24 hours.

DOPA-4,5-dioxygenase from *Mirabilis jalapa* (*Mj*DOD) was heterologously expressed in *E. coli* and purified to a final concentration of 50 μM. Specifically, the coding sequence for the *Mj*DOD enzyme was cloned into a pET-vector expression cassette including an

IPTG-inducible T7 promoter and C-terminal 6x-histidine affinity tag. *E. coli* BL21(DE3) cells carrying the plasmid were grown at 37°C in Terrific Broth media until an optical density at 600 nm of 3 was reached. After refrigeration at 4°C for 20 minutes the culture was induced by the addition of IPTG to a final concentration of 0.2 mM and incubated at 17°C for approximately 15 hours. Cells were harvested by centrifugation and stored at -20°C prior to purification. Frozen cell pellets were thawed and resuspended in Lysis Buffer (20 mM HEPES pH 7.6, 500 mM NaCl, 20 mM imidazole, 1 mM DTT) and lysed by sonication. The lysate was clarified by centrifugation and the resulting supernatant was subjected to NiNTA affinity purification using a 5 mL NiNTA FF column (GE) by FPLC. Eluted protein was mixed with TEV protease and allowed to incubate overnight at 4°C to remove the fusion tag, leaving a glycine-serine scar. Finally, the cleaved protein was further purified by size exclusion on a Superdex S200 column (GE) into a final buffer (20 mM Tris pH 7.6, 150 mM KCl, 1mM MgCl2, 1 mM DTT) and concentrated to 50 μM. Aliquots of the purified protein were stored at -80°C prior to use.

Enzyme reaction mixtures were prepared similar to Sasaki et al. (2009)[46] using 308 μL of L-DOPA stock solution, 308 μL of iron(II) sulfate / ascorbic acid solution, 70 μL of amine stock solution, and 14 μL of purified *Mj*DOD to achieve final concentrations of 0.88 mM L-DOPA, 0.44 mM iron(II) sulfate, 4.4 mM ascorbic acid, 2 mM amine, and 1 μM *Mj*DOD in 700 μL total volume. Reaction mixtures were incubated at 30°C for 16 hours to allow enzymatic conversion of L-DOPA to betalamic acid and further non-enzymatic condensation of betalamic acid with amines to form betaxanthins.

***In vivo* bioproduction and feeding assays.** Starter cultures of yeast strains were grown in synthetic complete media with the appropriate dropouts for auxotrophic selection. Saturated cultures after 48 hours were then back-diluted by a factor of fifty into 2 mL of minimal media (supplemented with missing auxotrophies) as reported previously[39] for a 48 hour bioproduction experiment. Ascorbic acid (10 mM) was added as indicated. The pilot work comparing glucosyltransferases was performed using 24-well blocks in a Multitron Standard shaker (Infors HT) set to 30℃ and 750 rpm. Flask scale production of betanin from yCM363 was conducted in a similar manner, with cultures instead back-diluted to 50 mL in both non-baffled and baffled Erlenmeyer flasks before incubation in a New Brunswick Scientific Innova 44 shaker set to 30℃ and 220 rpm.

Amine feeding experiments were conducted exactly as the pilot bioproduction experiments, except in media lacking all amino acids and supplemented to 0.5 mM amine using the same stock solutions utilized in the *in vitro* experiments.

Betalain purification and characterization. *In vitro* reactions were quenched by addition of two volumes of cold methanol, then stored at -20°C for at least ten minutes to precipitate protein. The quenched reactions were then centrifuged and an aliquot of the supernatant was removed for LCMS analysis.

In vivo bioconversions with yeast were centrifuged to remove cells. The supernatant was extracted with ethyl acetate and then chloroform to remove hydrophobic molecules. The betalain pigments remained with the aqueous phase through both extractions. The aqueous phase was then purified using a Sep-Pak Plus C18 cartridge (Waters) using the following procedure: the Sep-Pak cartridge was washed with 5 mL of ethanol and then 10 mL of water; the sample was applied and then washed with 10 mL of water to remove salts; finally, the sample was eluted with methanol. The eluted sample was then subjected to LCMS analysis.

High resolution LCMS was performed using a 6510 Accurate-Mass Q-TOF LCMS instrument (Agilent Technologies) and an Eclipse Plus C18 column (4.6mm x 100mm, 3.5 μm packing, Agilent Technologies). Analysis of betanin, PABA-betaxanthin, Ant-betaxanthin, and 6AI-betaxanthin was performed using a linear gradient of water:acetonitrile from 98:2 - 2:98 over 12 min with 0.1% formic acid at a flow rate of 0.5 mL/min. Analysis of oDA-betaxanthin single and double condensates was performed at a flow rate of 0.5 mL/min with 0.1% formic acid using a linear gradient of water:acetonitrile of either 90:10 - 50:50 over 12 min or 80:20 - 60:40 over 20 min. High resolution MS/MS analysis was conducted using targeted MS/MS with collision energy of 5-20 V.

Chapter 3. Repurposing the yeast peroxisome to compartmentalize a toxic enzyme enables improved (*S*)-reticuline production

3.1. Introduction

Cell factories, using production hosts ranging from bacterial, fungal, mammalian, and plant cells, are used to make important industrial products including pharmaceuticals, proteins, commodity chemicals, and biofuels[59–62]. As cellular engineering becomes increasingly sophisticated, incorporating longer and more complex heterologous metabolic pathways, the likelihood of crosstalk with native cellular functions in the host cell also increases. Consequently, there is greater risk for cytotoxicity and effects on host cell growth. Reduced growth has many negative consequences, including reduction in product titer due to fewer cells, decrease in production rate due to slower growth, and decrease in strain robustness because mutations that relieve toxicity are often ones that reduce or eliminate pathway flux.

Subcellular compartmentalization is an evolved strategy for coping with unproductive or harmful crosstalk[17,18,63,64]. In eukaryotes, lipid bilayer membrane-enclosed organelles are used to direct enzymatic activity toward specific substrates. In many cases, these activities would be unproductive in the cytosol. For example, vacuolar proteases have broad substrate specificity but their degradative activity is directed toward specific substrates due to their compartmentalization in the vacuole[65]. These degradation mechanisms are extremely precise. For instance, the Cvt pathway is known to degrade only three proteins, utilizing Atg19p to facilitate selective autophagy into the vacuole[66]. Additionally, many vacuolar proteases are imported as inactive forms called zymogens that are further processed once inside the vacuole into active forms, protecting proteins in the secretory pathway from degradation[67]. Compartments are also used to sequester toxic metabolites. For example, the parasite *Trypanosoma brucei* respecializes the peroxisome during the part of its life cycle in the human bloodstream from the β-oxidation of long-chain fatty acids to organelles known as glycosomes where the early steps of glycolysis are compartmentalized. While most organisms use allosteric feedback regulation of these glycolytic enzymes to prevent toxic accumulation of intermediates, *T. brucei* instead uses a compartmentalization strategy to enable increased flux while preventing toxic intermediate accumulation in the cytosol[68,69]. In the context of biomanufacturing and synthetic biology, compartmentalization may prove to be a

powerful strategy to isolate toxic heterologous components away from the host cell cytosol, thereby limiting cytotoxicity, improving growth, and increasing product titer.

Engineered compartmentalization has garnered considerable attention in recent years[17,70–74]. Many of the reports of engineered compartmentalization take advantage of the endogenous cofactor supply or substrate pool in a particular organelle. For example, the mitochondria has been used for its supplies of acetyl-CoA[75,76] and α-ketoisovalerate[77], the peroxisome for acyl-CoA[78,79], farnesyl diphosphate[80], and acetyl-CoA[74], and the vacuole for halide ions and *S*-adenosylmethionine[81]. Organelles have also been harnessed for the reactions that they natively perform. For example, the endoplasmic reticulum and Golgi in Chinese Hamster Ovary cells are used for the glycosylation of heterologous proteins[82], and recently the methanol assimilation pathway in the peroxisomes of *Pichia pastoris* was engineered into a carbon dioxide fixation pathway where six native peroxisome enzymes were utilized[73]. Advances in the development of synthetic compartments have also been reported, including the synthesis of prokaryotic encapsulin nanocompartments in eukaryotes[71,83], bacterially-derived proteinaceous gas vesicles in mammalian cells[84], and light-inducible phase-separated organelles in yeast[72].

In this work, we discovered that a titer-limiting enzyme in the industrially-valued benzylisoquinoline alkaloid (BIA) family of plant natural products is toxic when expressed in a yeast production host. The BIA family consists of ~2500 natural products exhibiting a variety of potential therapeutic bioactivities including antibacterial (berberine, sanguinarine), anticancer (noscapine), antispasmodic (papaverine), and analgesic (codeine, morphine)[5,85]. The first committed BIA molecule, (*S*)-norcoclaurine, is produced through the condensation of two tyrosine-derived substrates, dopamine and 4-hydroxyphenylacetaldehyde, by the enzyme norcoclaurine synthase (NCS)[86–88]. NCS is thought to be a gatekeeper enzyme that restricts entry into the BIA pathway[89,90]. Accordingly, high NCS activity is required for high production levels of BIAs in heterologous hosts. However, we found that our most active variant of NCS is toxic when expressed in the cytosol of *S. cerevisiae* and determined that the toxicity is caused by the NCS protein itself rather than by its catalytic function in the condensation of dopamine and 4-hydroxyphenylacetaldehyde to produce (*S*)-norcoclaurine.

We propose repurposing of the yeast peroxisome as the site for subcellular compartmentalization of toxic NCS enzyme. The peroxisome has several attributes that make it an ideal compartment for alleviating NCS toxicity without inhibiting flux through the BIA pathway. First, because peroxisomes in *S. cerevisiae* are used for the β-oxidation of fatty acids, they are not essential under typical industrial fermentation conditions where simple sugars are used as the carbon source[91]. Therefore, *S. cerevisiae* peroxisomes

can be repurposed for use in applications orthogonal to their evolved function without having major effects on native cellular processes and culture viability[74,92]. Second, heterologous protein can be targeted to the peroxisome by simply appending a small peptide tag to the C-terminus (peroxisomal targeting signal type 1, PTS1)[93,94] or N-terminus (PTS2)[95,96] of the protein of interest. In fact, our lab previously developed an enhanced targeting tag (ePTS1) that considerably increased the rate of protein import into the peroxisome[92]. Third, the peroxisome is thought to contain the highest concentration of protein in the eukaryotic cell[97,98] and can compartmentalize an impressive amount of heterologous cargo[92], more than has been demonstrated for other organelles[99]. Fourth, peroxisomes are permeable to many small molecules under approximately 500-700 Daltons, meaning that peroxisomally compartmentalized NCS would likely retain access to its substrates[92,100].

Here, we demonstrate that compartmentalization of toxic NCS in the peroxisome can both alleviate cytotoxicity and improve product titer. We utilize this compartment to selectively partition the toxic protein from other cytosolic factors while taking advantage of the ability of the peroxisome to allow small molecule substrates and products to freely diffuse into and out of the peroxisome lumen. Compartmentalization of toxic NCS enzyme improves production of (*S*)-norcoclaurine and the key branchpoint intermediate (*S*)-reticuline. More broadly, we provide a demonstration of the utility of the peroxisome as a two-way insulating compartment, one that can protect the host cell from toxicity associated with heterologous protein expression and, conversely, can protect heterologous protein from native cellular processes such as protein degradation. Although the peroxisome naturally has an impressive cargo capacity compared to other organelles, improved capacity is still desired for many engineering applications, including the compartmentalization of a toxic, activity-limiting metabolic enzyme as described here. We demonstrate initial progress toward this goal by using engineered transcription factors to mimic the peroxisome proliferation effect that is produced by long-chain fatty acid induction and utilize this strategy to further improve BIA titer.

3.2. Results

3.2.1. Expression of most active NCS variant causes cytotoxicity in yeast

While working to connect yeast central metabolism to the heterologous benzylisoquinoline alkaloid (BIA) pathway of plant-derived drug molecules, our group previously identified the norcoclaurine synthase (NCS) enzyme as a key rate-limiting step preventing high titer production of BIAs (**Figure 3-1a**)[39]. Since then, we have tested

several homologues (and truncated variants of these homologues for optimized expression) to identify enzyme sequences capable of producing higher levels of the NCS product, (*S*)-norcoclaurine, when expressed in yeast. In comparison to our original NCS derived from *Papaver somniferum*, heterologous expression of the NCS homologue from *Coptis japonica* resulted in a 3-fold higher (*S*)-norcoclaurine titer (**Figure 3-2**). Moreover, truncation of the N-terminus of the *Coptis japonica* homologue to remove residues upstream of the Bet v1 domain, the critical fold of NCS proteins[88], resulted in 20-fold higher titer than our original *Papaver somniferum* variant - the highest activity yet described in *S. cerevisiae*. For simplicity, we will refer to this truncated *Coptis japonica* homologue as tNCS. Previous studies have also reported improved titers upon truncation of NCS enzymes, with evidence suggesting that this effect is due to improved expression and/or stability of the protein[9,101,102].

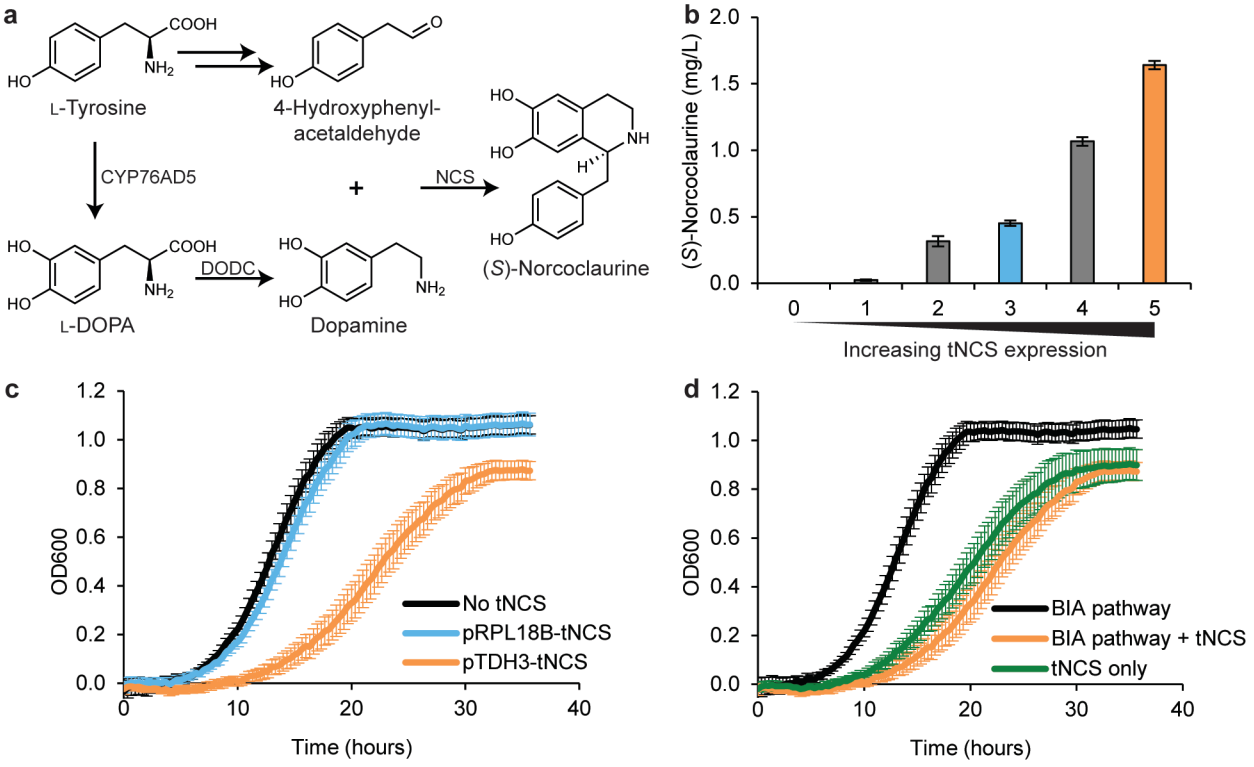

Figure 3-1. Cytosolic expression of truncated norcoclaurine synthase (tNCS) is toxic to *S. cerevisiae*. (**a**) Metabolic pathway for production of (*S*)-norcoclaurine from L-tyrosine using three heterologous enzymes: tyrosine hydroxylase (CYP76AD5), dopamine decarboxylase (DODC), and tNCS. 4-Hydroxyphenylacetaldehyde is produced endogenously by *S. cerevisiae*. (**b**) Higher expression of tNCS results in higher titer of (*S*)-norcoclaurine. The following well-characterized promoters were used to drive expression of tNCS on a CEN6/ARS4 plasmid: 1=pREV, 2=pRNR2, 3=pRPL18B, 4=pTEF1, 5=pTDH3. 0=No NCS. Error bars represent standard deviation of four biological replicates. (**c**) Higher expression of tNCS results in slower growth, with significant toxicity observed at pTDH3 expression level. Error bars represent standard deviation of eight biological replicates. (**d**) Significant toxicity is observed even in the absence of

upstream BIA pathway enzymes CYP76AD5 and DODC (green line). Error bars represent standard deviation of eight biological replicates.

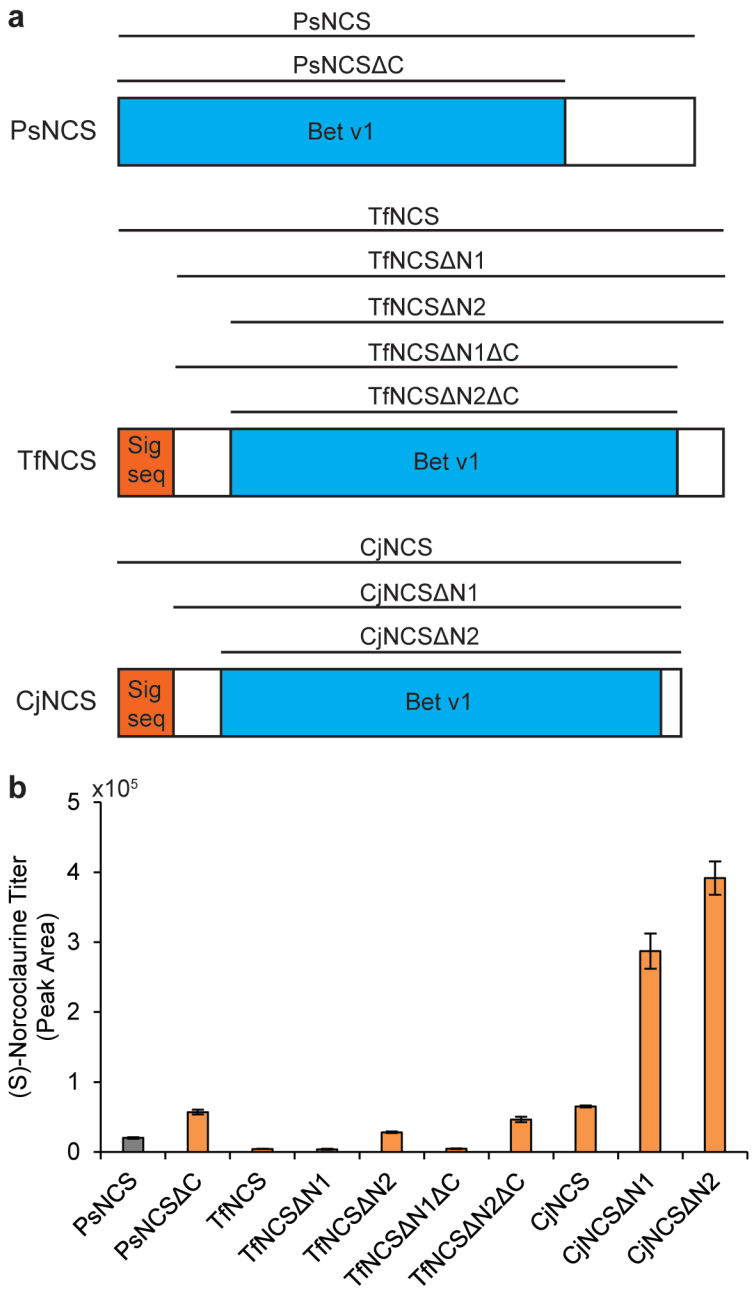

Figure 3-2. NCS homologues and truncated variants. (**a**) Truncation strategy for NCS homologues from *Papaver somniferum* (Ps), *Thalictrum flavum* (Tf), and *Coptis japonica* (Cj). Signal sequence (Sig seq) and Bet v1 domains were identified using the SMART domain analysis tool[103]. (**b**) (*S*)-Norcoclaurine production by each NCS variant at 72 hours. Gray bar shows our original NCS from *Papaver somniferum*[39]. Error bars represent standard deviation of three biological replicates.

(*S*)-Norcoclaurine titer was directly dependent on the expression level of tNCS, with stronger promoters and copy numbers resulting in higher (*S*)-norcoclaurine titers (**Figure 3-1b**). Copy number was increased compared to chromosomal integrations by using a CEN6/ARS4 yeast replicating plasmid (~2-5 copies per cell[104]). Additionally, transcription levels were controlled via a range of previously characterized yeast promoters[57,105]. Unexpectedly, we also observed that heterologous expression of tNCS resulted in a reduction in yeast growth rate in an expression-level dependent manner (**Figure 3-1c**). Moderate expression of tNCS (pRPL18B) had almost no effect on cell growth when compared to cells that do not express tNCS, whereas strong expression (pTDH3) considerably decreased both the growth rate and final cell density of the yeast culture.

Expression of tNCS in the cytosol resulted in toxicity yet the source of this toxicity was unclear. To determine whether this toxicity results from the metabolite intermediates or from the tNCS enzyme itself, we compared the expression of tNCS in yeast with and without the upstream BIA pathway. Without the upstream enzymes CYP76AD5 and DODC, yeast cannot produce dopamine, which is one of two substrates required for (*S*)-norcoclaurine biosynthesis. Even without the upstream BIA pathway, the strain exhibited a reduced growth rate indicating that toxicity is not due to excessively high levels of (*S*)-norcoclaurine production nor is it due to the reaction between dopamine and 4-hydroxyphenylacetaldehyde (**Figure 3-1d**). Based on this result, we concluded that the observed toxicity is not due to (*S*)-norcoclaurine biosynthesis but rather due to the tNCS protein itself, perhaps through an interaction with a native yeast factor, although the precise mechanism of this toxicity remains unknown.

3.2.2. Compartmentalizing toxic tNCS inside the yeast peroxisome improves cell growth and increases titer of BIA products

Although the mechanism of tNCS toxicity is unknown, we hypothesized that we could alleviate this toxicity via subcellular compartmentalization of the tNCS protein within the cell. We reasoned that an ideal compartment would sequester the toxic tNCS enzyme away from the cytosol while allowing the free flow of NCS's substrates and products into and out of the compartment. We identified the peroxisome as a promising candidate for subcellular compartmentalization because it can import fully-folded proteins[106], has a high capacity for imported heterologous protein[92,99], repurposing for compartmentalization of engineered protein should not have adverse effects on yeast viability[74,91], and the peroxisome is permeable to small molecules[92,100]. Previous work on peroxisomes *in vitro*[100], and our experiments on peroxisomes *in vivo*[92], have indicated a size exclusion threshold of approximately 500-700 daltons based on the permeability of particular substrates with different molecular weights. More precisely, the permeability

of small molecules across the peroxisome membrane is also affected by the molecule's shape or 'bulkiness,' including its hydrodynamic radius[92,107]. We predicted that substrates dopamine and 4-hydroxyphenylacetaldehyde as well as product (*S*)-norcoclaurine would be able to cross the peroxisomal membrane given the structure and small molecular weight of these molecules (153, 136, and 271 daltons, respectively). Therefore, if tNCS were compartmentalized within the peroxisome, it would retain access to its substrates and (*S*)-norcoclaurine product would diffuse out from the peroxisome into the cytosol (**Figure 3-3a**).

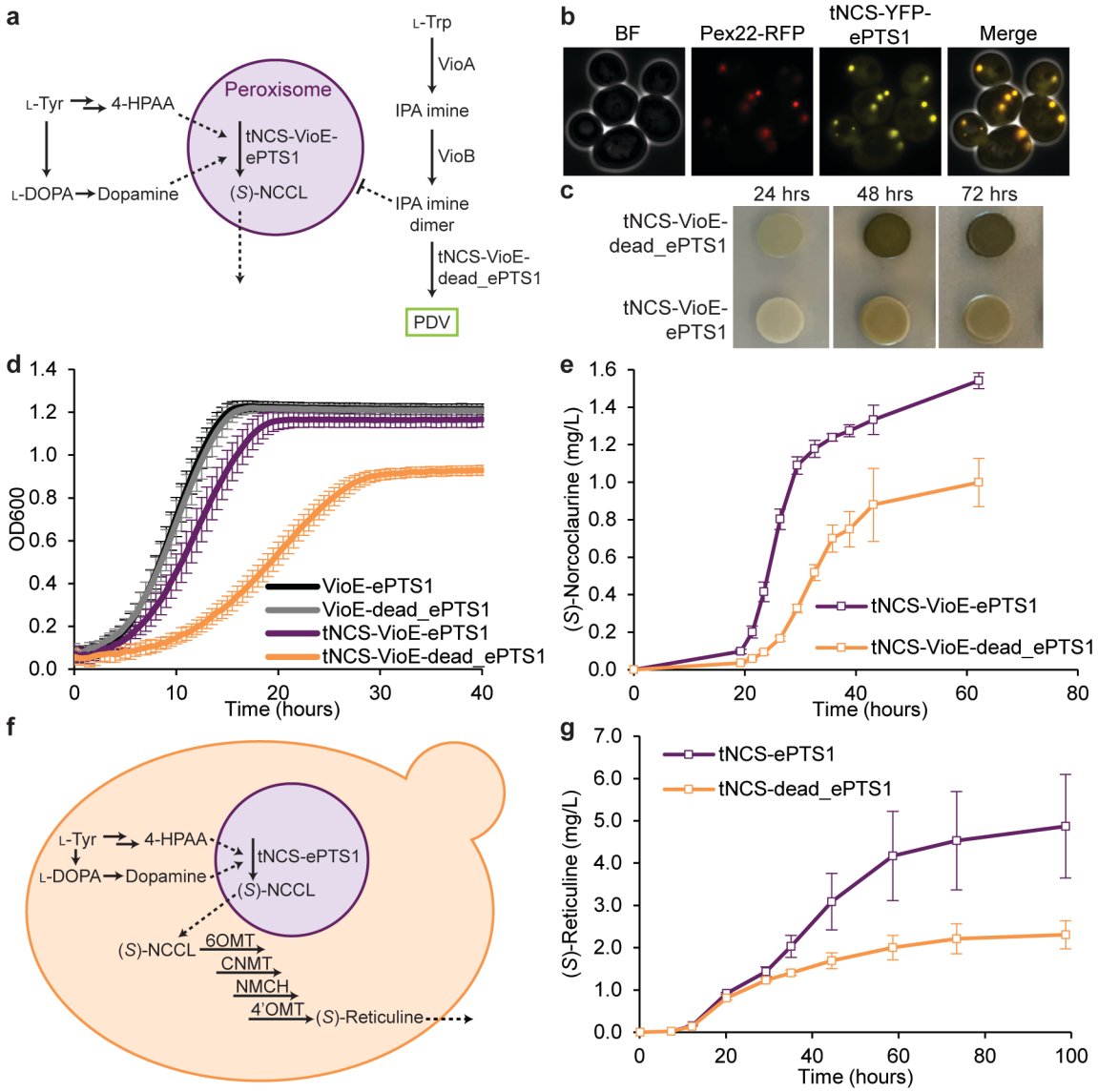

Figure 3-3. Compartmentalizing tNCS in the peroxisome alleviates cytotoxicity and increases BIA product titer. The tNCS-VioE fusion protein will be targeted to the peroxisome when tagged with ePTS1 but will remain in the cytosol when tagged with dead_ePTS1. NCS substrates 4-hydroxyphenylacetaldehyde (4-HPAA) and dopamine can pass freely across the peroxisomal membrane

to access tNCS and produce (*S*)-norcoclaurine ((*S*)-NCCL). The violacein pathway, which is used to assess peroxisomal compartmentalization, includes upstream enzymes VioA and VioB expressed in the cytosol. When VioE is also expressed in the cytosol (tNCS-VioE-dead_ePTS1), the green pigment prodeoxyviolacein (PDV) is produced. When VioE is targeted to the peroxisome (tNCS-VioE-ePTS1), less PDV is produced because the VioE substrate IPA imine dimer has low permeability across the peroxisomal membrane. (**b**) Microscopy showing co-localization of tNCS-YFP-ePTS1 with peroxisomal marker Pex22-RFP. (**c**) Agar plate spots showing compartmentalization efficiency of tNCS-VioE-ePTS1 in the peroxisome compared to tNCS-VioE-dead_ePTS1. tNCS-VioE-ePTS1 spots have less green color due to lower production of PDV pigment. (**d**) Expression of tNCS in the cytosol (tNCS-VioE-dead_ePTS1, orange line) results in poor growth, whereas compartmentalization in the peroxisome (tNCS-VioE-ePTS1, purple line) alleviates much of the toxicity when compared to control strains (VioE-ePTS1 and VioE-dead_ePTS1). Error bars represent standard deviation of twelve biological replicates. (**e**) Peroxisomal compartmentalization of tNCS (tNCS-VioE-ePTS1) results in higher (*S*)-norcoclaurine production compared to cytosolic expression of tNCS (tNCS-VioE-dead_ePTS1). Error bars represent standard deviation of four biological replicates. (**f**) Metabolic pathway for the production of (*S*)-reticuline in *S. cerevisiae* with tNCS-ePTS1 localized in the peroxisome but with free flow of substrates, 4-HPAA and dopamine, and product, (*S*)-norcoclaurine, across the peroxisomal membrane. All other enzymes are expressed in the cytosol. (*S*)-Reticuline is natively exported from the cell and measured in the media. (**g**) Compartmentalizing tNCS-ePTS1 in the peroxisome results in higher (*S*)-reticuline production compared to tNCS-dead_ePTS1 expression in the cytosol. Error bars represent standard deviation of four biological replicates.

Toxic tNCS was targeted to the peroxisome lumen using a C-terminal enhanced peroxisomal targeting signal type 1 (ePTS1). The canonical peroxisomal targeting signal consists of the amino acids SKL whereas the ePTS1 sequence includes a positively-charged amino acid linker, resulting in the C-terminal sequence LGRGRR-SKL. Compared to the canonical PTS1, use of the ePTS1 tag increases the rate of protein import into the peroxisome due to an increase in binding affinity between the tag and the cytosolic carrier protein Pex5p, which shuttles cargo to the protein import complex at the peroxisome membrane[92]. Toxic tNCS was fused to ePTS1 together with yellow fluorescent protein (YFP) to generate tNCS-YFP-ePTS1, and expressed in a yeast strain with a fluorescent peroxisomal marker consisting of the N-terminus of the peroxisomal membrane protein Pex22 fused to red fluorescent protein (RFP)[108]. Co-localization microscopy analysis of RFP and YFP signals demonstrated that ePTS1 can facilitate effective peroxisomal targeting of tNCS (**Figure 3-3b**).

As an orthogonal assessment of peroxisomal compartmentalization, we applied a pigment-producing enzyme sequestration assay[92] to tNCS. When three enzymes of the violacein pigment pathway, VioA, VioB, and VioE, are expressed in the cytosol, the green pigment prodeoxyviolacein (PDV) is produced. Upon fusion of ePTS1 to VioE, considerably less PDV is produced because the substrate for VioE, IPA imine dimer, has low permeability across the peroxisome membrane (**Figure 3-3a**). Accordingly, fusions between proteins of interest and VioE-ePTS1 can provide an assessment of how well these

tagged proteins are targeted to the peroxisome lumen, with better compartmentalized proteins resulting in yeast cultures with lower PDV pigment production.

The peroxisome is capable of compartmentalizing tNCS as assayed by the pigment-producing enzyme sequestration assay. We fused either our targeting tag (ePTS1) or a non-targeting tag (dead_ePTS1) to the C-terminus of tNCS-VioE to assay the efficiency of peroxisome compartmentalization. Dead_ePTS1 (LGRGRR-SKT) exchanges a threonine for the C-terminal leucine, resulting in a tag with low affinity for the cargo carrier Pex5p and, therefore, preventing import into the peroxisome[92,109]. tNCS constructs were expressed from a plasmid with a CEN6/ARS4 origin of replication and a strong pTDH3 promoter. By visually comparing the PDV pigment levels for peroxisomally targeted tNCS fused to VioE (tNCS-VioE-ePTS1) to cytosolic expression (tNCS-VioE-dead_ePTS1) at 24, 48, and 72 hours, we show that ePTS1 provides considerable compartmentalization of tNCS at these expression levels (strong pTDH3, CEN6/ARS4 copy number) (**Figure 3-3c**). PDV was quantified by extraction from liquid culture after three days of growth and tNCS-VioE targeted to the peroxisome showed a 40% reduction in PDV pigment production relative to tNCS-VioE in the cytosol.

Production host growth and (*S*)-norcoclaurine product titer were both improved when toxic tNCS enzyme was compartmentalized in the peroxisome. In addition to the violacein pathway, our strains contained the upstream BIA pathway (CYP76AD5, DODC) so that (*S*)-norcoclaurine titer could be directly measured from the same strains. The strain with peroxisomally-targeted tNCS achieved both higher final OD and growth rate (0.103 vs 0.058 h^{-1}) compared to the strain where tNCS was cytosolically expressed in small-scale growth experiments in microwell plates (**Figure 3-3d**). In fact, the peroxisomally-targeted tNCS-VioE-ePTS1 strain grew nearly as well as our two control strains lacking toxic tNCS expression: VioE-ePTS1 (growth rate 0.136 h^{-1}) and VioE-dead_ePTS1 (growth rate 0.129 h^{-1}). Encouraged by these results, we conducted shake flask fermentations to compare the cell growth and (*S*)-norcoclaurine titer of tNCS-VioE-ePTS1 and tNCS-VioE-dead_ePTS1. In addition to an improvement in growth as observed in the microwell experiment (**Figure 3-4**), we also observed a 54% increase in final titer and a 2.2-fold increase in maximum productivity (0.13 vs 0.06 mg/L/h) (**Figure 3-3e**).

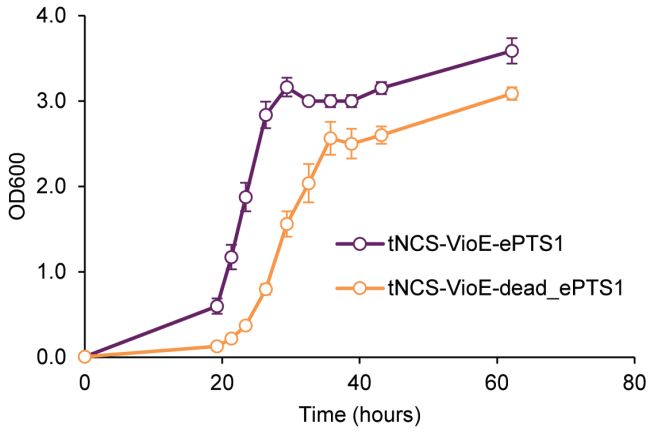

Figure 3-4. OD data from (*S*)-norcoclaurine shake flask fermentation experiment. tNCS-VioE-ePTS1 and -dead_ePTS1 constructs were expressed using the strong pTDH3 promoter on a CEN6/ARS4 plasmid. Error bars represent standard deviation of four biological replicates.

In order to demonstrate that the (*S*)-norcoclaurine product of peroxisomally targeted tNCS is not sequestered in the peroxisome, we showed that it was accessible to the downstream four enzyme pathway that converts (*S*)-norcoclaurine to (*S*)-reticuline in the cytosol (**Figure 3-3f**). (*S*)-Reticuline represents the last shared intermediate of the large and highly branched family of BIA natural products[85]. In order to synthesize (*S*)-reticuline, (*S*)-norcoclaurine must undergo two *O*-methylations, one *N*-methylation, and one hydroxylation, catalyzed by 6-*O*-methyltransferase (6OMT), coclaurine *N*-methyltransferase (CNMT), *N*-methylcoclaurine 3'-hydroxylase (NMCH), and 4'-*O*-methyltransferase (4'OMT)[85]. All four of these downstream enzymes were cytosolically expressed along with the upstream tyrosine hydroxylase CYP76AD5 and L-DOPA carboxylase DODC with NCS compartmentalized in either the peroxisome or cytosol. Compared to cytosolic expression (dead_ePTS1), peroxisomal targeting (ePTS1) resulted in both a modest growth rate improvement and a 34% increase in final OD (**Figure 3-5**). A corresponding titer improvement was also observed (**Figure 3-3g**), with a 2.1-fold increase in final titer and a 34% increase in maximum productivity (0.11 vs 0.08 mg/L/h). In general, (*S*)-reticuline titers were higher than (*S*)-norcoclaurine titers. Cell density was also higher for (*S*)-reticuline strains compared to (*S*)-norcoclaurine strains (**Figure 3-4** vs **Figure 3-5**). We attribute these differences to the inclusion of enzymes from the violacein pathway (VioA, VioB, and tNCS fused to VioE) in the (*S*)-norcoclaurine production strains, whereas the (*S*)-reticuline producing strains do not contain any of the violacein pathway enzymes.

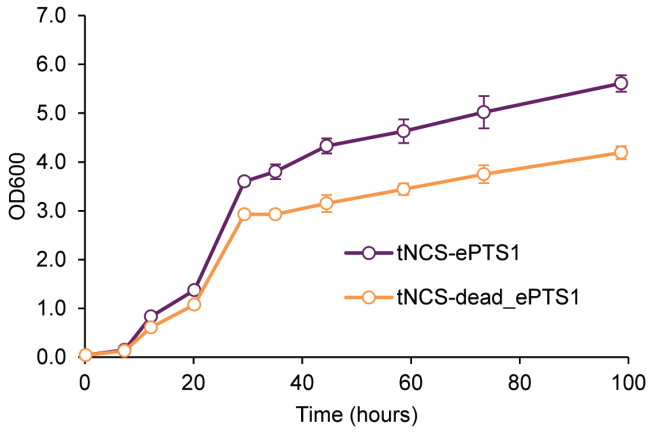

Figure 3-5. OD data from (*S*)-reticuline shake flask fermentation experiment. tNCS-ePTS1 and -dead_ePTS1 constructs, along with 6OMT, CNMT, NMCH, and 4'OMT, were expressed on a CEN6/ARS4 plasmid. Error bars represent standard deviation of four biological replicates.

3.2.3. Incomplete compartmentalization occurs at very high expression levels of tNCS

While compartmentalization of tNCS in the peroxisome is effective at the tested expression levels, we wanted to determine if the peroxisome is capable of compartmentalizing even higher expression levels of tNCS to achieve increased titers. To characterize the upper limits of enzyme targeting, we investigated peroxisome targeting when the plasmid copy number was increased from CEN6/ARS4 (2-5 copies per cell) to 2-micron (2μ) (15-50 copies per cell)[104,110]. At this very high expression level, peroxisomal compartmentalization was still effective but incomplete (**Figure 3-6**). At high 2μ expression level, much of the tNCS-YFP-ePTS1 protein was targeted to the peroxisome as visualized by microscopy using Pex22-RFP as a peroxisomal marker. However, more residual cytosolic tNCS-YFP-ePTS1 localization was observed at this higher expression level, indicated by increased cytosolic YFP signal compared to the previous CEN6/ARS4 expression (**Figure 3-6a** vs **Figure 3-3b**). At 2μ expression levels, incomplete compartmentalization and high toxicity were observed in the pigment-producing enzyme sequestration assay and in growth experiments. PDV pigment extraction after three days of growth showed a 39% reduction in PDV pigment production when tNCS-VioE was targeted to the peroxisome instead of the cytosol (**Figure 3-6b**). Toxicity due to high cytosolic expression of tNCS-VioE was apparent in the agar plate spots, evidenced by low cell density at 24 hours and abnormal spot morphology (wrinkled appearance) at 48 and 72 hours. Growth curves showed that cytosolic expression (tNCS-VioE-dead_ePTS1) was highly toxic, with hardly any measurable growth occurring before 20 hours, at which point the control strains lacking tNCS, VioE-ePTS1 and VioE-dead_ePTS1, had already reached a saturated cell density (**Figure 3-6c**). Peroxisomal

compartmentalization of tNCS (tNCS-VioE-ePTS1) was able to alleviate some of the toxicity, confirming that peroxisome targeting was still effective; however, final OD and growth rate were below that of the control strains, suggesting the peroxisome is not natively capable of completely compartmentalizing the toxic tNCS at these elevated expression levels.

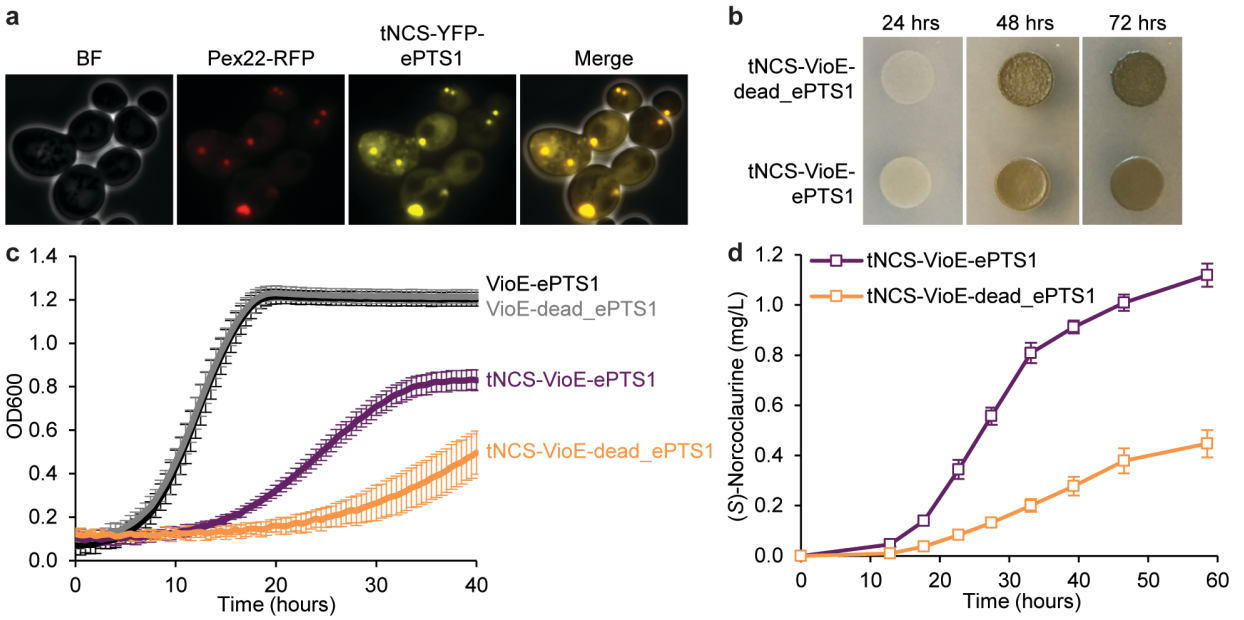

Figure 3-6. Peroxisomal targeting of toxic tNCS at a very high expression level improves growth and (*S*)-norcoclaurine titer, but compartmentalization is incomplete. (**a**) Microscopy showing co-localization of tNCS-YFP-ePTS1 (pTDH3 2μ expression level) with Pex22-RFP at peroxisomes and residual YFP signal in the cytosol (incomplete compartmentalization). (**b**) Agar plate spots showing compartmentalization efficiency of tNCS-VioE-ePTS1 in the peroxisome compared to tNCS-VioE-dead_ePTS1. Abnormal spot morphology for cytosolic expression (tNCS-VioE-dead_ePTS1) indicates incomplete compartmentalization and high toxicity. (**c**) Expression of tNCS in the cytosol (tNCS-VioE-dead_ePTS1) results in very poor growth (orange line) whereas peroxisomal expression (tNCS-VioE-ePTS1) partially alleviates toxicity at pTDH3 2μ expression level (purple line) when compared to growth of control strains (black and grey lines). Error bars represent standard deviation of twelve biological replicates. (**d**) Peroxisomal targeting of tNCS (tNCS-VioE-ePTS1) results in higher (*S*)-norcoclaurine production compared to cytosolic expression of tNCS (tNCS-VioE-dead_ePTS1). Error bars represent standard deviation of four biological replicates.

Production of (*S*)-norcoclaurine was greatly improved upon targeting of tNCS to the peroxisome compared to the cytosol at 2μ expression level. Final (*S*)-norcoclaurine titer is an impressive 2.5-fold higher for peroxisomal expression compared to cytosolic expression from a 2μ plasmid (**Figure 3-6d**), and maximum productivity is 3.2-fold higher (0.045 vs 0.014 mg/L/h). However, we observed that the final titer of peroxisomal expression from a 2μ plasmid is lower than that of peroxisomal CEN6/ARS4 expression (1.1 vs 1.5 mg/L). We attribute this lower titer to the poor growth caused by incomplete compartmentalization at the elevated expression level of the 2μ plasmid. Indeed, the final

OD and growth rate in flasks are 3.6 and 0.34 h^{-1}, respectively, for when tNCS is expressed from a CEN6/ARS4 plasmid while only 2.7 and 0.14 h^{-1} when expressed from a 2μ plasmid (**Figure 3-4** vs **Figure 3-7**).

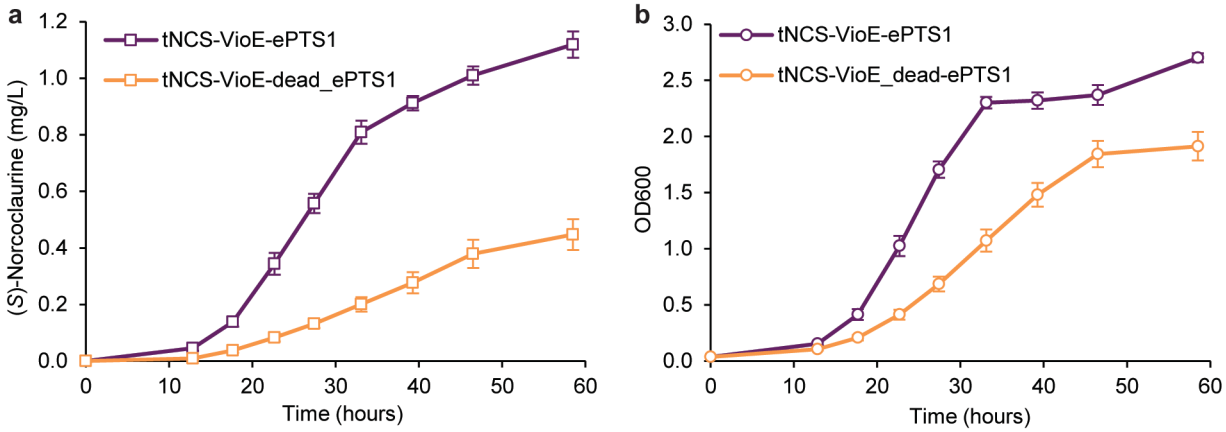

Figure 3-7. 2μ shake flask fermentation experiment. (**a**) (*S*)-Norcoclaurine titer. (**b**) OD600. tNCS-VioE-ePTS1 and -dead_ePTS1 constructs were expressed using the strong pTDH3 promoter on a 2μ plasmid. Error bars represent standard deviation of four biological replicates.

3.2.4. Developing strategies to improve compartmentalization capacity of peroxisome-targeted cargo

Protein capacity is limited in most organelles and, although the peroxisome can natively compartmentalize a comparably impressive amount[99], further increased capacity is desired for many applications, including the insulation of the toxic tNCS enzyme. In *Saccharomyces cerevisiae*, the natural function of peroxisomes is the β-oxidation of long-chain fatty acids[111]. In glucose-containing media, peroxisomes have an average diameter of 0.2 μm[112], but in media containing the C18 fatty acid oleate, peroxisomes are enlarged to diameters of 0.3-0.5 μm[113,114]. Glucose and other sugars repress the peroxisome induction effect, but growth on oleate as the sole carbon source is poor compared to growth on glucose[115]. Accordingly, induction media commonly uses an alternative carbon source such as glycerol in addition to oleate[116]. We found that yeast growth was also poor in this induction media (as has been reported for *S. cerevisiae* in glycerol[117]). To balance growth rate with the ability to induce higher peroxisome capacity, we developed a hybrid induction media that contained 0.5% glucose in addition to 10% glycerol and 0.1% oleate (compared to standard media containing 2% glucose). Given that glucose will be preferentially consumed over other carbon sources in *S. cerevisiae*, we reasoned that 0.5% glucose would support fast initial culture growth before being fully utilized. This initial

biomass would subsequently switch to consumption of glycerol, thereby permitting proliferation of large peroxisomes due to oleate induction.

Peroxisomes appeared brighter in YFP fluorescence when induced in oleate growth media and visualized by peroxisome-targeted YFP and microscopy (**Figure 3-8**). In order to capture and compare the relative differences in YFP fluorescence when cells were grown in different media, a fairly low exposure setting was used for all microscopy images to avoid overexposure of YFP signal in oleate media. As a result, YFP fluorescence of peroxisomes grown in only glucose look very dim in comparison, although YFP targeting was confirmed both using higher exposure settings during image capture and by post image processing. Both the standard oleate glycerol induction media and our hybrid induction media (glucose, glycerol, and oleate) showed brighter YFP peroxisome puncta compared to cells grown in glucose only, which we interpret as being consistent with oleate-induced peroxisome proliferation to accommodate increased targeting of fatty acid utilization enzymes. We then performed a (*S*)-norcoclaurine production experiment using toxic tNCS targeted to the peroxisome and expressed on the high copy 2μ plasmid, comparing standard glucose media to our hybrid induction media (**Figure 3-9**). Growth and final cell density were decreased in the hybrid induction media compared to standard glucose media. Consequently, final (*S*)-norcoclaurine titer was reduced 14% in the hybrid induction media; however, normalizing titer by OD showed a 21% higher production, indicating higher per cell productivity and suggesting that peroxisome induction could be a promising strategy for increasing protein cargo capacity if growth were further improved.

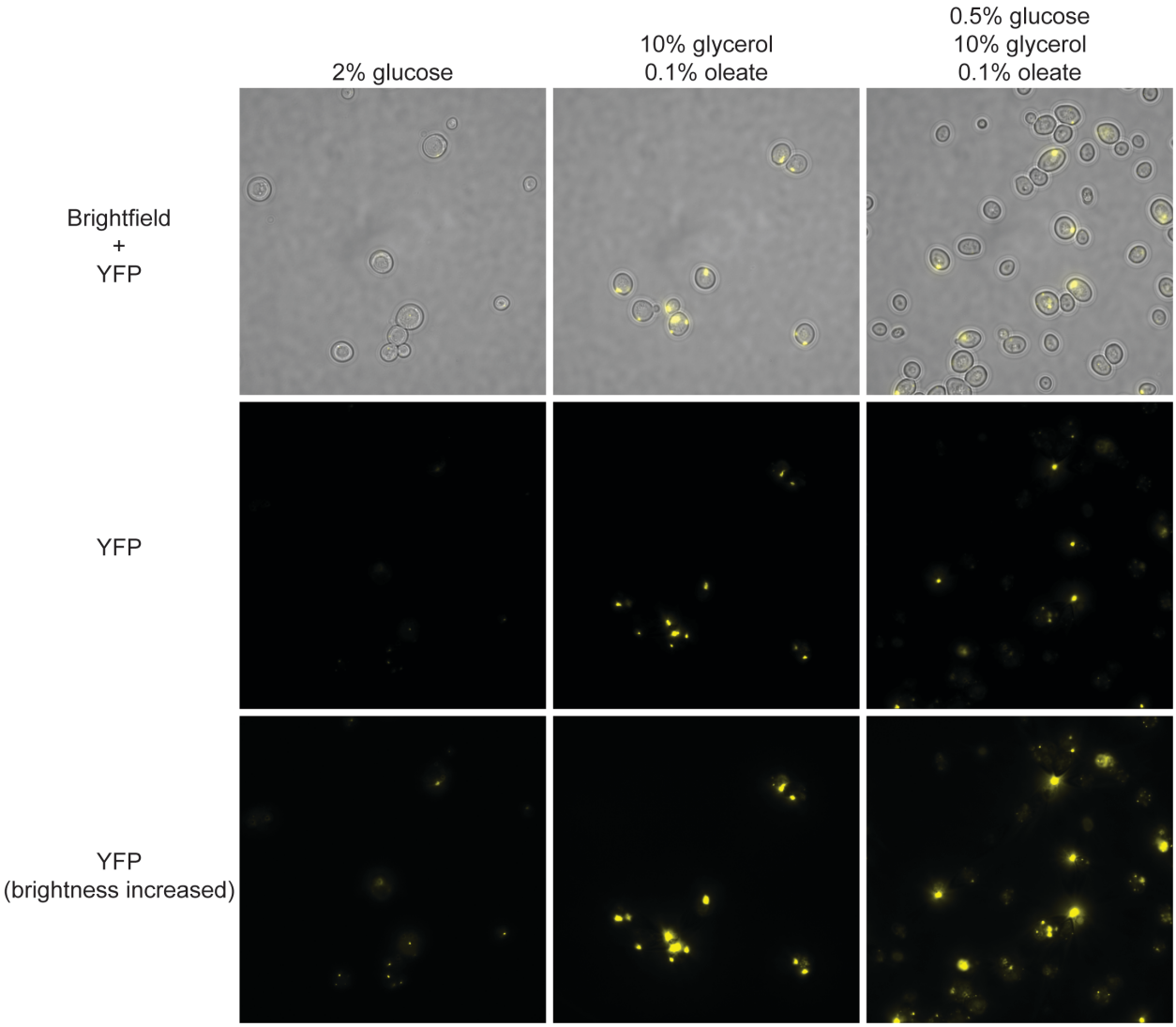

Figure 3-8. Oleate induction increases peroxisome size. Peroxisomes were visualized using a strain expressing VioE-YFP-ePTS1 on a CEN6/ARS4 plasmid. In glucose, small peroxisomes were observed whereas larger peroxisomes were observed when cells were grown in oleate-containing media. Large peroxisomes are known to be induced when cells utilize fatty acids, including oleate[113,114]. All images were taken with identical exposure settings. After image acquisition, YFP channel brightness was increased during image processing to allow visualization of peroxisomes in glucose media (3rd row).

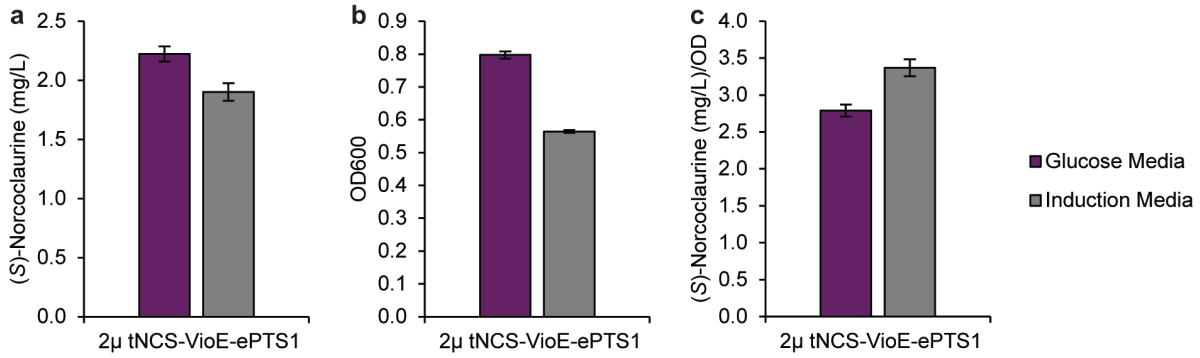

Figure 3-9. (*S*)-Norcoclaurine production using oleate induction media. (**a**) (*S*)-Norcoclaurine titer. (**b**) OD600. (**c**) Titer normalized by OD. Glucose media is yeast synthetic complete media, minus leucine and uracil, plus 2% glucose. Induction media is our hybrid media: synthetic complete media, minus leucine and uracil, plus 0.5% glucose, 10% glycerol, 0.4% Tween80, and 0.1% oleate. Measurements were taken at 160 hours to allow sufficient time for growth and production. Error bars represent standard deviation of four biological replicates.

To avoid the poor growth phenotype that results from use of glycerol as the main carbon source with oleate induction, we sought to engineer a strain with increased peroxisome capacity while grown on the favored glucose carbon source by constitutively expressing transcription factors involved in peroxisome proliferation. We focused on three transcription factors known to control peroxisome proliferation - ADR1, OAF1, and PIP2[118–120]. All three transcription factors are post-translationally repressed by glucose[121,122] and OAF1 is post-translationally induced by oleate[123]. We aimed to make ADR1, OAF1, and PIP2 constitutively active in standard growth media containing glucose as well as remove the requirement for oleate by engineering or deleting the regulatory domains of these transcription factors.

An engineered version of the ADR1 transcription factor was designed to enable constitutive activation in glucose media. ADR1 is known to be inactivated by phosphorylation at Ser-230 under high glucose concentrations[124]. ADR1 activation is achieved by Ser-230 dephosphorylation when glucose concentration is low. Mutation of Ser-230 to alanine has been shown to mimic the dephosphorylated, active state, leading to transcription of downstream genes even in the presence of glucose[125]. We applied this S230A mutation to generate ADR1c, a constitutively active version of ADR1.

Engineered versions of OAF1 and PIP2 transcription factors were designed through removal of regulatory domains to enable activation in glucose media without oleate. OAF1 and PIP2 are paralogs with similar domain architectures, both containing an N-terminal DNA binding domain, followed by regulatory domains, and ending with a C-terminal activation domain[122]. We hypothesized that removal of the regulatory domains

would enable constitutive activation in standard growth media by removing glucose repression and the need for oleate induction. For OAF1, we specifically tethered amino acids 1-100 (containing the DNA binding domain) via a flexible two amino acid glycine-serine linker to amino acids 807-1047 (containing the activation domain). Likewise, for PIP2 we tethered amino acids 1-56 (containing the DNA binding domain) to amino acids 833-996 (containing the activation domain) via a two amino acid glycine-serine linker. We called these engineered transcription factors OAF1c and PIP2c, respectively.

A fluorescence-based assay was devised to test peroxisome compartmentalization capacity upon expression of combinations of the three engineered transcription factors (ADR1c, OAF1c, PIP2c). The assay utilizes YFP fused to an N-terminal proteasome-based degradation signal, UbiY[57,126], and a C-terminal ePTS1 tag (**Figure 3-10a**). In this assay, Pex5p recognizes the ePTS1 tag and shuttles UbiY-YFP-ePTS1 cargo to the peroxisomal membrane for import where it would be protected from degradation. Residual UbiY-YFP-ePTS1 remaining in the cytosol is recognized and targeted to the proteasome for degradation. The fluorescent signal should, consequently, only reflect YFP localized in the peroxisome. Therefore, combinations of constitutively-active transcription factors resulting in improved cargo capacities will be reflected as increased YFP signal compared to the signal produced in a strain with no transcription factor overexpression.

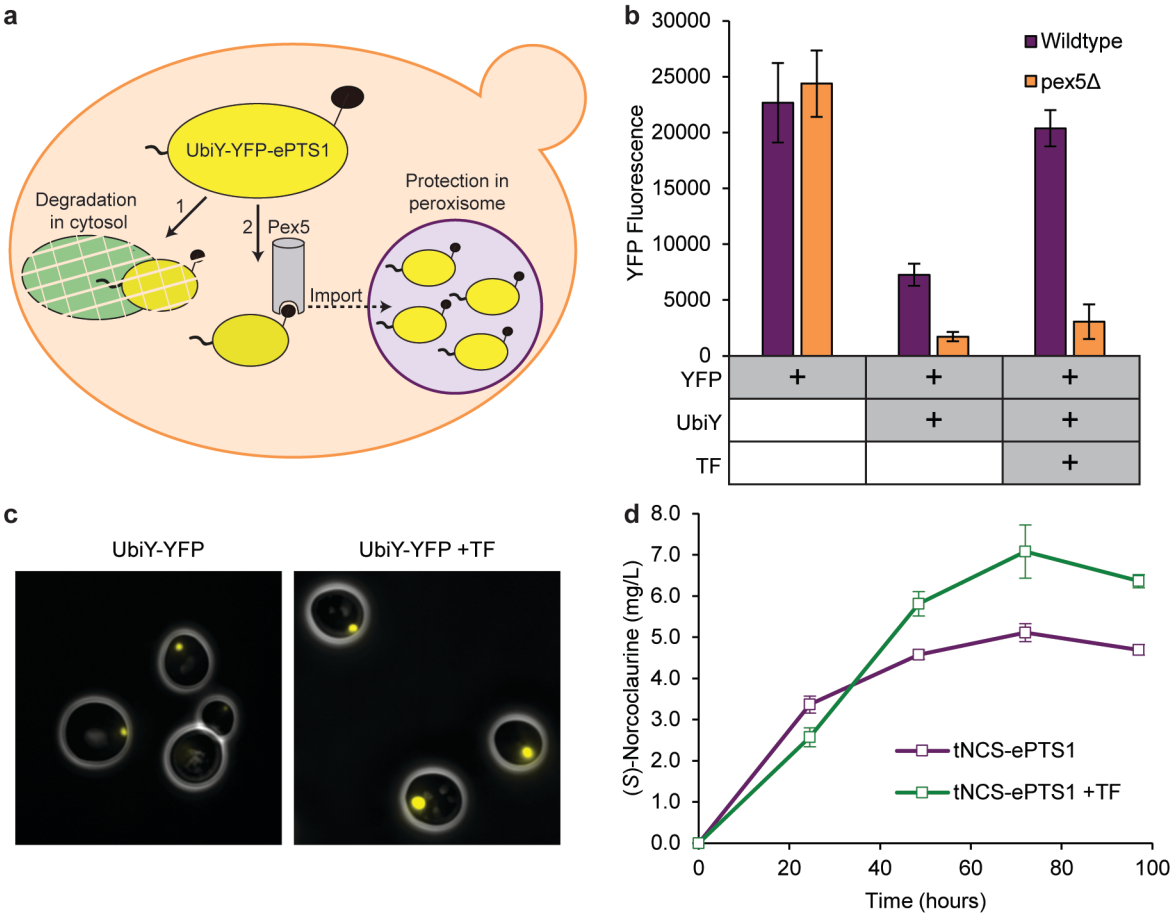

Figure 3-10. Genetic induction of peroxisome proliferation can address incomplete compartmentalization at very high expression levels of tNCS. (**a**) Degron-YFP assay for measuring peroxisomal compartmentalization. Residual UbiY-YFP-ePTS1 that is not imported to the peroxisome by Pex5p (path 2) is degraded in the cytosol by the proteasome (path 1). Changes in YFP signal are therefore indicative of changes in peroxisome import capacity. (**b**) Degron-YFP assay was used to assess transcription factor overexpression. Strains with UbiY-YFP-ePTS1 expressed in the cytosol (pex5Δ) have lower fluorescence than their corresponding peroxisomally-targeted strains (Wildtype) due to UbiY-YFP degradation by the proteasome. TF represents expression of engineered transcription factors ADR1c, OAF1c, and PIP2c. Error bars represent standard deviation of twelve biological replicates. (**c**) Microscopy of UbiY-YFP-ePTS1 cells shows larger peroxisomes when ADR1c, OAF1c, and PIP2c are expressed (+TF). Full images showing population variability are available in **Figure 3-13**. (**d**) (*S*)-Norcoclaurine production is improved upon expression of engineered transcription factors. Error bars represent standard deviation of eight biological replicates.

The degron-YFP assay functioned as expected, with degradation observed upon cytosolic expression and protection observed upon peroxisomal targeting. We demonstrated that fusion of the UbiY degron to YFP-ePTS1 resulted in cytosolic degradation by expressing this fusion in a pex5 knockout strain (pex5Δ), which prevents peroxisomal import (**Figure 3-10b**, second orange bar). Expression of this fusion protein, UbiY-YFP-ePTS1, in a

wildtype background strain containing Pex5p resulted in 4.2-fold higher YFP signal (**Figure 3-10b**, second purple bar), indicating protection from degradation due to peroxisomal import. Although considerable protection was achieved, this signal was 32% of the YFP signal measured for a strain containing YFP without the UbiY degron (**Figure 3-10b**, first purple bar), indicating that compartmentalization is not complete.

Expression of engineered transcription factors increased protection of cargo from degradation (**Figure 3-10b**) and resulted in visibly larger peroxisomes with increased fluorescence from importing UbiY degron-fused YFP (**Figure 3-10c**). The engineered transcription factors ADR1c, OAF1c, and PIP2c were first expressed in different combinations and assayed for UbiY-YFP-ePTS1 signal after growth for 48 hours in a 96-well culture block (**Figure 3-11**). The highest YFP signal, indicating improved protection from degradation, was observed upon expression of all three engineered transcription factors. We then investigated the dynamics of the system by directly culturing the triple-transcription factor strain (+TF), alongside controls, in a small-scale microwell plate (**Figure 3-12**). Strains with UbiY-YFP-ePTS1 expressed in the cytosol showed an increase in YFP signal over the first ~15 hours during the culture growth phase, and thereafter showed a drop in YFP signal as the rate of proteasomal degradation outpaced the rate of YFP synthesis, as expected. Strains with UbiY-YFP-ePTS1 targeted to the peroxisome exhibited protection from degradation by showing less YFP degradation after the growth phase, resulting in higher YFP signal at the endpoint relative to their cytosolic counterparts. Endpoint values from the timecourse experiment are depicted in **Figure 3-10b** and show that the triple-transcription factor combination (TF) resulted in 2.8-fold higher UbiY-YFP-ePTS1 fluorescence than without TF expression and 90% of the fluorescence compared to the no-degron strain. We then compared the wildtype background strain to the ADR1c/OAF1c/PIP2c expression strain, both expressing UbiY-YFP-ePTS1, by microscopy and found that transcription factor overexpression resulted in larger peroxisomes (**Figure 3-10c**). While there was cell-to-cell variability with regard to the presence and size of peroxisomes, they were routinely larger and brighter in the +TF strain (**Figure 3-13**). Thus, increased cargo capacity can be achieved in glucose media through the expression of constitutively-active versions of transcription factors involved in glucose derepression and oleate induction.

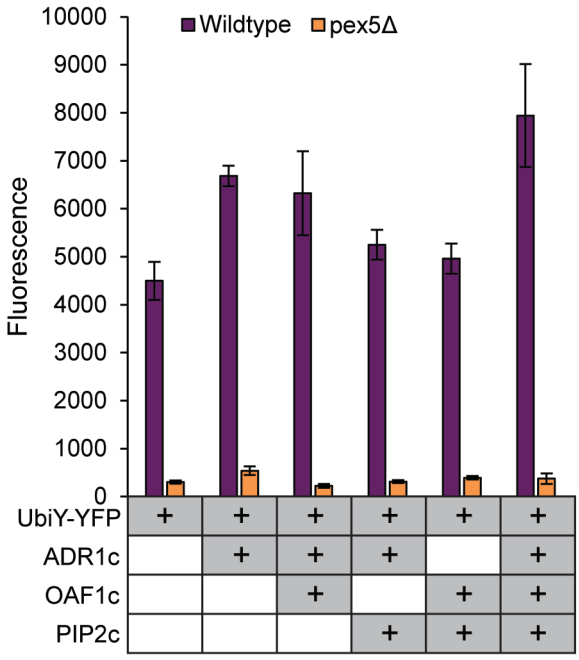

Figure 3-11. Expression of engineered transcription factors improves protection of peroxisomally-targeted UbiY-YFP-ePTS1. Yellow fluorescent protein (YFP) was expressed with an N-terminal degradation tag (UbiY) in the presence or absence of constitutively-active transcription factors ADR1c, OAF1c, PIP2c. Wildtype strains import UbiY-YFP-ePTS1 into the peroxisome whereas pex5Δ strains are import-deficient due to knockout of the cytosolic receptor protein Pex5p. Samples were taken from a 96-well culture block for measurement at 48 hours. Error bars represent standard deviation of at least five biological replicates.

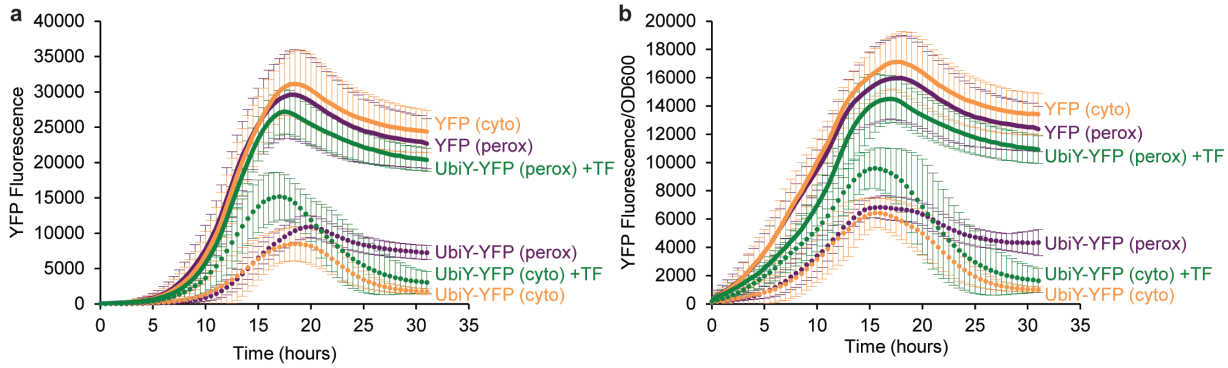

Figure 3-12. Dynamics of peroxisomal protection of UbiY-YFP-ePTS1 from degradation. (**a**) Fluorescence. (**b**) Fluorescence normalized by OD600. Yellow fluorescent protein (YFP) was expressed with an N-terminal degradation signal (UbiY) in the presence or absence of constitutively-active transcription factors ADR1c/OAF1c/PIP2c (+TF). All strains contain the peroxisomal targeting signal ePTS1 fused to YFP. Constructs transformed into a wildtype background strain will target (UbiY-)YFP-ePTS1 protein to the peroxisome (perox). Cytosolic expression of (UbiY-)YFP-ePTS1 (cyto) is achieved by use of a pex5Δ background strain, which is import-deficient due to knockout of the cytosolic receptor protein Pex5p. Error bars represent standard deviation of twelve biological replicates.

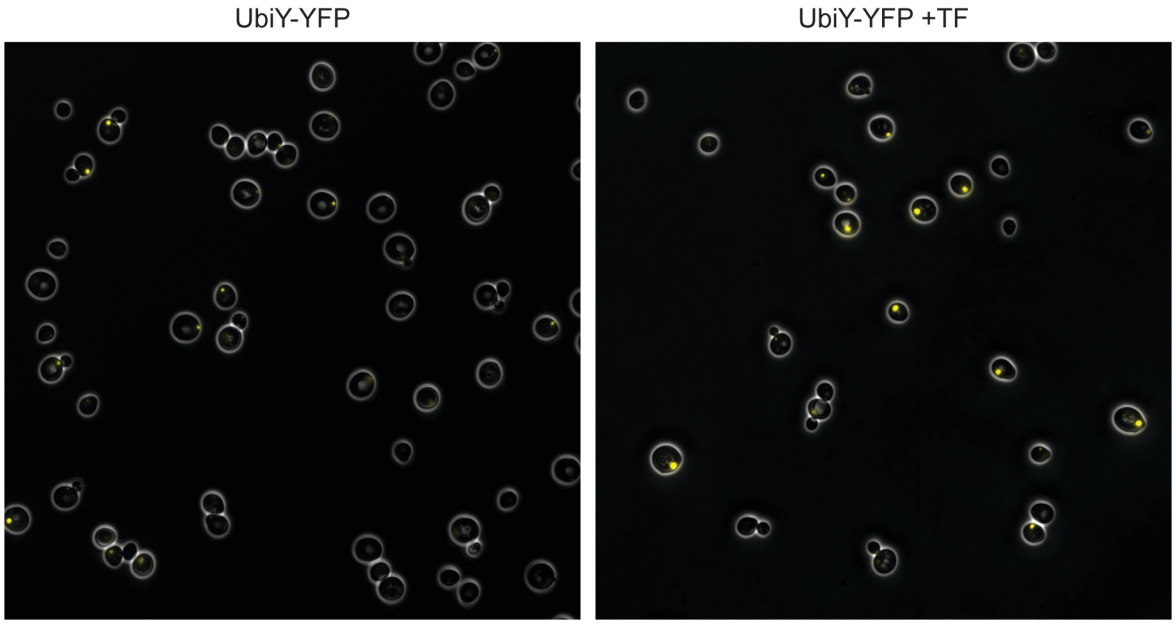

Figure 3-13. Expression of engineered transcription factors increases protection of peroxisomally-targeted UbiY-YFP-ePTS1 (zoomed-out version of Figure 3-10c). Fluorescence microscopy showing cells without (left) or with (right) expression of constitutively-active transcription factors ADR1c, OAF1c, PIP2c (+TF). Both strains contain YFP fused to the UbiY degradation signal on the N-terminus and the peroxisomal targeting signal ePTS1 on the C-terminus.

Improved capacity for UbiY-YFP-ePTS1 translated to a 36% improvement in (*S*)-norcoclaurine titer when tNCS is targeted to the peroxisome compared to peroxisome targeting without transcription factor overexpression. We built strains containing the high copy 2μ plasmid expressing peroxisome-targeted tNCS (pTDH3-tNCS-ePTS1), in either a wildtype strain background or a strain containing the best set of transcription factors overexpressed (ADR1c/OAF1c/PIP2c). Transcription factor overexpression resulted in a 36% increase in (*S*)-norcoclaurine titer compared to the wildtype strain without transcription factor overexpression (**Figure 3-10d**). Although we did not observe the expected increase in growth upon expression of constitutively active ADR1c/OAF1c/PIP2c (**Figure 3-14**), we also noted that transcription factor overexpression resulted in a decrease in growth even in the absence of toxic tNCS (**Figure 3-15**). Thus, one or more of the over 100 genes regulated by these transcription factors presents a burden or directly inhibits growth[127,128]. When normalized by OD, expression of the engineered transcription factors resulted in a 47% improvement in (*S*)-norcoclaurine production (**Figure 3-14**). Ultimately, the benefit of transcription factor overexpression on peroxisome size and compartmentalization capability outweighed the growth defect, resulting in a higher final titer of (*S*)-norcoclaurine.

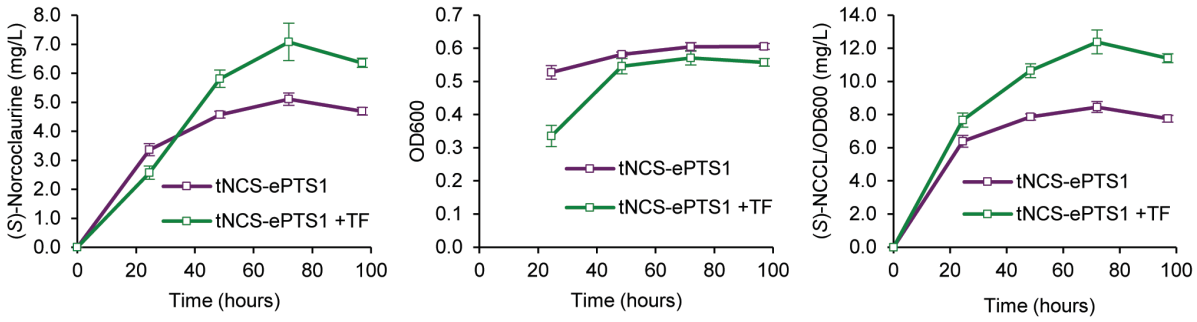

Figure 3-14. (*S*)-Norcoclaurine titer, OD600, and OD-normalized titer from transcription factor overexpression experiment. All strains contain the upstream BIA pathway plus 2μ pTDH3-tNCS-ePTS1. The +TF strain also contains ADR1c, OAF1c, and PIP2c. Error bars represent standard deviation of eight biological replicates.

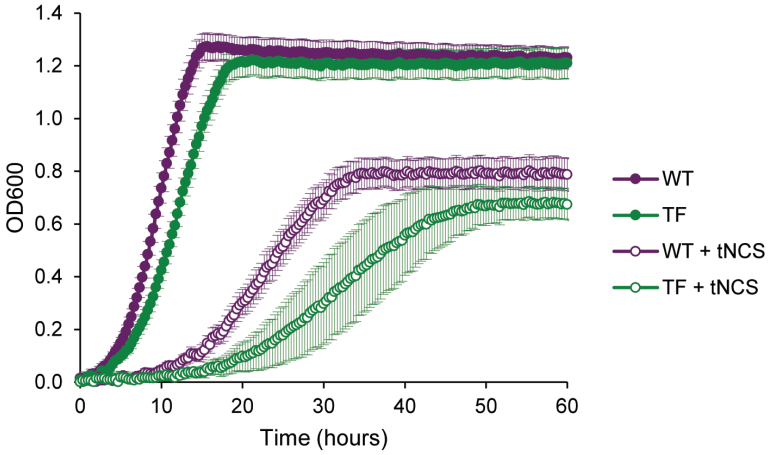

Figure 3-15. Expression of engineered transcription factors is linked to slower growth. All strains contain the upstream BIA pathway. Strains without transcription factor overexpression (WT) contain a LEU2 marker. Strains with transcription factor overexpression (TF) contain ADR1c, OAF1c, PIP2c, and a LEU2 marker. Error bars represent standard deviation of twelve biological replicates.

3.3. Discussion

Toxicity of heterologous proteins[129–135] and metabolites[4,136–141] is a significant problem in metabolic engineering. Toxicity manifests as substantial obstructions to large scale fermentation in terms of slower growth of cells and ultimately lower titer and productivity. Our group faced the challenge of needing to highly express tNCS enzyme in order to improve titer of BIAs while discovering that high expression of tNCS also caused cytotoxicity in *S. cerevisiae*. With regard to compartmentalization, this challenge required a specific solution, one in which the tNCS protein would be efficiently targeted and sequestered but retain access to its small molecule substrates and allow the (*S*)-

norcoclaurine product to exit to the cytosol where the upstream and downstream enzymes are localized. One approach could involve the use of a compartment that is not readily permeable to small molecules (e.g., vacuole[142]) and compartmentalization of the entire metabolic pathway. However, in addition to the requirement for high protein capacity that has not been demonstrated for most organelles, this approach would necessitate the incorporation of one or several transporters recognizing the enzyme's substrate(s) and, potentially, product at the organelle membrane.

Peroxisomal compartmentalization has the potential to be a generalizable strategy for expression of toxic proteins. As is the case for many engineered metabolic pathways that suffer from toxicity, the mechanism of tNCS toxicity is not known. The mechanisms causing toxicity can be difficult to elucidate. A common strategy for minimizing, or even overcoming, this undesired effect on the production host is to conduct adaptive laboratory evolution (ALE)[143]. ALE works best when the desired flux can be selected such that derived mutations for improved growth are not exclusive with desired pathway flux, and ALE can fail if growth is improved at the expense of product titer[144]. ALE often requires months of cell passaging to enable mutations to be acquired, especially when the acquisition of multiple mutations are required[143]. We conducted ALE on a strain expressing tNCS followed by a secondary screen of the fastest growing strains for (*S*)-norcoclaurine titer. The first type that we observed, a strain that downregulates or loses entirely the expression of tNCS, is detrimental to product formation. The second type that we observed was a strain that appeared to alleviate toxicity while producing high (*S*)-norcoclaurine titer, comparable to the titer from our 2μ plasmid-expressed tNCS-ePTS1 strain. Unfortunately, sequencing the genome of this adapted strain did not yield any decipherable mutations to explain how the toxicity was alleviated. Although frequently successful, ALE will not work for all toxic proteins. If the mechanism of toxicity is well understood, a more rational solution may be developed, such as a mutation to the protein to block undesired interactions, or a genomic modification (gene deletion or mutation) that reduces toxicity. Compartmentalization in the peroxisome is a considerably more rapid strategy to employ, requiring only the addition of the C-terminal ePTS1 tag and does not require understanding of the mechanism of toxicity other than it is due to the protein itself and not any metabolite product. Further, this strategy should generalize to all soluble proteins directly exerting toxicity (i.e. via an interaction with protein(s), lipid(s), carbohydrate(s), etc. accessible in the cytosol).

The peroxisome in *S. cerevisiae* has evolved for the compartmentalization of increased copies of enzymes required for the β-oxidation of long-chain fatty acids[111]. Examples in nature indicate that the peroxisome is an inherently flexible organelle and, therefore,

likely has the potential to be engineered as a synthetic compartment for desired applications. In addition to functioning as a catabolic compartment for the β-oxidation pathway, peroxisomes are used for unique biochemical reactions, such as penicillin biosynthesis[145] and generation of light in fireflies[146]. Moreover, peroxisome size, number, and morphology can be substantially altered in different organisms using a variety of substrates such as oleate[113], methanol[147,148], D-alanine[149], and butyrate[150] indicating that genetic circuits for peroxisome proliferation are prevalent across a broad range of eukaryotes. We pursued genetic reprogramming of peroxisome proliferation via constitutive expression of engineered transcription factors and demonstrated increased cargo capacity without the requirement for oleate. While this is an important step toward genetic control over peroxisome cargo capacity, expression of these constitutively-active transcription factors resulted in a decrease in growth even in the absence of toxic tNCS. This should not be too surprising given that approximately 100 downstream genes are regulated by these transcription factors and, accordingly, one or more are likely to have an impact on cell state/growth[127,128]. Future work will seek to identify the critical downstream targets of ADR1, OAF1, and PIP2 such that only those critical genes will be manipulated to control cargo capacity without impeding growth as was observed when the engineered transcription factors were overexpressed.

Thus, this work establishes a robust strategy for circumventing the growth defect resulting from the expression of a cytotoxic metabolic enzyme while enabling increased flux. Protection of heterologous cargo from the effects of the host cell, such as proteasome-based degradation, was also demonstrated. Accordingly, peroxisome compartmentalization offers the engineer bidirectional benefits: protection of the host cell from the heterologous protein as well as protection of the heterologous protein from the host cell. This work highlights the peroxisome as a versatile, engineerable organelle that can be utilized to address challenges in metabolic engineering.

3.4. Materials and Methods

Strains and growth media. The base *S. cerevisiae* strain for all experiments was BY4741 (MATa his3Δ1 leu2Δ0 met15Δ0 ura3Δ0). Base strain BY4741 and BY4741 pex5Δ were ordered from Open Biosystems—GE Dharmacon. Wildtype yeast cultures were grown in YPD (10 g/L Bacto yeast extract; 20 g/L Bacto peptone; 20 g/L glucose). Selection of auxotrophic markers (URA3, LEU2, HIS3) was performed in synthetic complete (SC) media (6.7 g/L Difco Yeast Nitrogen Base without amino acids (Spectrum Chemical); 2 g/L Drop-out Mix Synthetic minus appropriate amino acids, without Yeast Nitrogen Base (US Biological); 20 g/L glucose). All strains used in this work are listed in **Table 3-1**.

Oleate induction media was prepared as 6.7 g/L Difco Yeast Nitrogen Base without amino acids (Spectrum Chemical); 2 g/L Drop-out Mix Synthetic minus appropriate amino acids, without Yeast Nitrogen Base (US Biological), with the following variations (final concentrations described): 1) 2% glucose, 2) 10% glycerol, 0.1% oleic acid, 0.4% Tween80, 3) 0.5% glucose, 10% glycerol, 0.1% oleic acid, 0.4% Tween80.

Golden gate assembly reactions were transformed into chemically competent *Escherichia coli* prepared from strain TG1 (Lucigen). Transformed cells were selected on Lysogeny Broth containing the antibiotics chloramphenicol, ampicillin, or kanamycin.

Table 3-1. Yeast strains used in peroxisome chapter.

Strain #	**Strain Name**	**Strain Parent**	**Plasmid Used**	**Description**	**Yeast Marker**	**Used in Figure**
1	yWCD230	BY4741	pWCD1351	his3Δ		
2	yWCD231	BY4741 pex5Δ::KanMX	pWCD1351	his3Δ	KanMX	
3	yWCD745	BY4741	pWCD2249	pTDH3-CYP76AD1_W13L_F309L-tTDH1-pCCW12-DODC-tADH1-pPGK1-ARO4_FBR-tPGK1	URA3	
4	yPSG633	yWCD745	pPSG958	pTDH3-PsNCS-tENO2	URA3, LEU2	3-2
5	yPSG634	yWCD745	pPSG959	pTDH3-PsNCSΔC-tENO2	URA3, LEU2	3-2
6	yPSG635	yWCD745	pPSG960	pTDH3-TfNCS-tENO2	URA3, LEU2	3-2
7	yPSG636	yWCD745	pPSG961	pTDH3-TfNCSΔN1-tENO2	URA3, LEU2	3-2
8	yPSG637	yWCD745	pPSG962	pTDH3-TfNCSΔN2-tENO2	URA3, LEU2	3-2
9	yPSG638	yWCD745	pPSG963	pTDH3-TfNCSΔN1ΔC-tENO2	URA3, LEU2	3-2
10	yPSG639	yWCD745	pPSG964	pTDH3-TfNCSΔN2ΔC -tENO2	URA3, LEU2	3-2
11	yPSG627	yWCD745	pBSC009	pTDH3-CjNCS-tENO2	URA3, LEU2	3-2
12	yPSG628	yWCD745	pPSG325	pTDH3-CjNCSΔN1-tENO2	URA3, LEU2	3-2

13	yPSG629	yWCD745	pBSC011	pTDH3-CjNCSΔN2-tENO2	URA3, LEU2	3-2
14	yPSG408	yWCD231	pPSG465	pTDH3-CYP76AD5-tTDH1-pCCW12-DODC-tADH1-pPGK1-ARO4_FBR-tPGK1	URA3	
15	yPSG440	yPSG408	pPSG532	CEN6/ARS4	URA3, LEU2	3-1b, 3-1c, 3-1d
16	yPSG521	yPSG408	pPSG711	pREV1-tNCS-ePTS1-tENO2-CEN6/ARS4	URA3, LEU2	3-1b
17	yPSG520	yPSG408	pPSG710	pRNR2-tNCS-ePTS1-tENO2-CEN6/ARS4	URA3, LEU2	3-1b
18	yPSG519	yPSG408	pPSG709	pRPL18B-tNCS-ePTS1-tENO2-CEN6/ARS4	URA3, LEU2	3-1b, 3-1c
19	yPSG518	yPSG408	pPSG708	pTEF1-tNCS-ePTS1-tENO2-CEN6/ARS4	URA3, LEU2	3-1b
21	yPSG438	yPSG408	pPSG569	pTDH3-tNCS-ePTS1-tENO2-CEN6/ARS4	URA3, LEU2	3-1b, 3-1c, 3-1d
22	yPSG723	yWCD231	pPSG569	pTDH3-tNCS-ePTS1-tENO2-CEN6/ARS4	LEU2	3-1d
23	ySJD004	yWCD230	pSJD001	YBR197CΔ::pPAB1-Pex22(1-36)-mRuby2-tSSA1		
24	yPSG751	ySJD004	pPSG1066	pTDH3-tNCS-Venus-ePTS1-tENO2-CEN6/ARS4	LEU2	3-3b
25	yPSG306	yWCD230	pPSG465	pTDH3-CYP76AD5-tTDH1-pCCW12-DODC-tADH1-pPGK1-ARO4_FBR-tPGK1	URA3	
26	yPSG575	yPSG306	pPSG804, pPSG820	YDR514CΔ::pTDH3-VioA-tENO1-pTEF1-VioB-tPGK1	URA3	
27	yJAS816	yPSG575	pJAS1643	pTDH3-tNCS-VioE-ePTS1-tENO2-CEN6/ARS4	URA3, LEU2	3-3c, 3-3d, 3-3e, 3-4
28	yJAS817	yPSG575	pJAS1644	pTDH3-tNCS-VioE-dead_ePTS1-tENO2-CEN6/ARS4	URA3, LEU2	3-3c, 3-3d, 3-3e, 3-4
29	yJAS832	yPSG575	pJAS1668	pTDH3-VioE-ePTS1-tADH1-CEN6/ARS4	URA3, LEU2	3-3d
30	yJAS833	yPSG575	pJAS1669	pTDH3-VioE-dead_ePTS1-tADH1-CEN6/ARS4	URA3, LEU2	3-3d
31	yPSG718	yPSG306	pPSG1059	pTDH3-tNCS-ePTS1-tENO2-pTEF1-Ec_CYP80B1-tTDH1-pCCW12-Ps_6OMT-tPGK1-pPGK1-Ps_4'OMT2-tENO1-pTEF2-Ps_CNMT-tSSA1-CEN6/ARS4	URA3, LEU2	3-3g, 3-5

32	yPSG719	yPSG306	pPSG1060	pTDH3-tNCS-dead_ePTS1-tENO2-pTEF1-Ec_CYP80B1-tTDH1-pCCW12-Ps_6OMT-tPGK1-pPGK1-Ps_4'OMT2-tENO1-pTEF2-Ps_CNMT-tSSA1-CEN6/ARS4	URA3, LEU2	3-3g, 3-5
33	yPSG752	ySJD004	pPSG1067	pTDH3-tNCS-Venus-ePTS1-tENO2-2μ	LEU2	3-6a
34	yJAS971	yPSG575	pJAS1766	pTDH3-VioE-ePTS1-tENO2-2μ	URA3, LEU2	3-6c
35	yJAS972	yPSG575	pJAS1767	pTDH3-VioE-dead_ePTS1-tENO2-2μ	URA3, LEU2	3-6c
36	yJAS973	yPSG575	pJAS1769	pTDH3-tNCS-VioE-ePTS1-tENO2-2μ	URA3, LEU2	3-6b, 3-6c, 3-6d, 3-7, 3-9
37	yJAS974	yPSG575	pJAS1770	pTDH3-tNCS-VioE-dead_ePTS1-tENO2-2μ	URA3, LEU2	3-6b, 3-6c, 3-6d, 3-7
38	yPSG335	yWCD230	pJAS1052	pTDH3-VioA-tENO1-pTEF1-VioB-tPGK1	URA3	
39	yPSG666	yPSG335	pPSG1010	pTEF1-VioE-Venus-ePTS1-tENO2-CEN6/ARS4	URA3, LEU2	3-8
40	yJJB006	yWCD230	pJJB111	pTDH3-Venus-ePTS1-tTDH1	URA3	
41	yJJB012	yWCD231	pJJB111	pTDH3-Venus-ePTS1-tTDH1	URA3	
42	yJJB013	yWCD230	pJJB207	pTDH3-UbiY-Venus-ePTS1-tTDH1	URA3	
43	yJJB014	yWCD231	pJJB207	pTDH3-UbiY-Venus-ePTS1-tTDH1	URA3	
44	yPSG777	yJJB006	pPSG372	LEU2 marker	URA3, LEU2	3-10b, 3-12
45	yPSG778	yJJB012	pPSG372	LEU2 marker	URA3, LEU2	3-10b, 3-12
46	yJJB150	yJJB013	pPSG372	LEU2 marker	URA3, LEU2	3-10b, 3-10c, 3-11, 3-12, 3-13
47	yJJB151	yJJB014	pPSG372	LEU2 marker	URA3, LEU2	3-10b, 3-11, 3-12
48	yJJB154	yJJB013	pJJB306	pRPL18B-ADR1c-tPGK1	URA3, LEU2	3-11
49	yJJB157	yJJB014	pJJB306	pRPL18B-ADR1c-tPGK1	URA3, LEU2	3-11

50	yJJB064	yJJB013	pJJB175	pRPL18B-ADR1c-tPGK1-pRPL18B-OAF1c-tTDH2	URA3, LEU2	3-11
51	yJJB076	yJJB014	pJJB175	pRPL18B-ADR1c-tPGK1-pRPL18B-OAF1c-tTDH2	URA3, LEU2	3-11
52	yJJB061	yJJB013	pJJB172	pRPL18B-ADR1c-tPGK1-pRPL18B-PIP2c-tTEF1	URA3, LEU2	3-11
53	yJJB073	yJJB014	pJJB172	pRPL18B-ADR1c-tPGK1-pRPL18B-PIP2c-tTEF1	URA3, LEU2	3-11
54	yJJB069	yJJB013	pJJB180	pRPL18B-PIP2c-tTEF1-pRPL18B-OAF1c-tTDH2	URA3, LEU2	3-11
55	yJJB081	yJJB014	pJJB180	pRPL18B-PIP2c-tTEF1-pRPL18B-OAF1c-tTDH2	URA3, LEU2	3-11
56	yJJB059	yJJB013	pJJB170	pRPL18B-ADR1c-tPGK1-pRPL18B-PIP2c-tTEF1-pRPL18B-OAF1c-tTDH2	URA3, LEU2	3-10b, 3-10c, 3-11, 3-12, 3-13
57	yJJB071	yJJB014	pJJB170	pRPL18B-ADR1c-tPGK1-pRPL18B-PIP2c-tTEF1-pRPL18B-OAF1c-tTDH2	URA3, LEU2	3-10b, 3-11, 3-12
58	yPSG726	yPSG306	pPSG372	LEU2 marker	URA3, LEU2	3-15
59	yPSG727	yPSG306	pJJB170	pRPL18B-ADR1c-tPGK1-pRPL18B-PIP2c-tTEF1-pRPL18B-OAF1c-tTDH2	URA3, LEU2	3-15
60	yPSG738	yPSG726	pPSG830	pTDH3-tNCS-ePTS1-tENO2-2μ	URA3, LEU2, HIS3	3-10d, 3-14, 3-15
61	yPSG739	yPSG727	pPSG830	pTDH3-tNCS-ePTS1-tENO2-2μ	URA3, LEU2, HIS3	3-10d, 3-14, 3-15

Yeast strain construction. Yeast expression vectors were built using Golden Gate Assembly as described in the YTK system[57]. Integration into the yeast genome via homologous recombination at the URA3 or LEU2 locus was achieved by transformation of linearized plasmids (NotI digestion, NEB) whereas replicating CEN6/ARS4 or 2μ plasmids were transformed directly into yeast. All transformations were performed using a standard lithium acetate method[58] and cells were plated onto selective auxotrophic SC 2% glucose agar plates. All strains are described in **Table 3-1**. Replicate colonies were picked directly from this transformation plate for further analysis.

Chromosomal integrations of Pex22-RFP, VioA, and VioB were performed by co-transforming a CEN6/ARS4 CRISPR plasmid (containing Cas9, guide RNA for targeting

the appropriate locus, HIS3 auxotrophic marker) with linearized repair DNA designed to integrate the gene(s) of interest. Cells were plated on histidine dropout media, restreaked on histidine dropout media, then grown in non-selective media to remove the CRISPR plasmid. Chromosomal integration was confirmed by PCR and removal of CRISPR plasmid was confirmed by replica plating from non-selective media onto histidine dropout media (colony will not grow on histidine dropout media if CRISPR plasmid has been removed).

Growth curves in microwell plates. Single colonies were grown to saturation in SC 2% glucose media with auxotrophic selection at 30°C with shaking. Saturated cultures were then diluted 50-fold in fresh selective media and grown for 6-7 hours before a second dilution (10-fold) in 96-well Costar microplates (black, clear bottom) and sealed with breathe-easy film (Sigma). OD600 was measured at 30 minute intervals using a microplate reader (Tecan Spark), with continuous orbital shaking at 30°C in a humidity cassette. Variation between biological replicates was calculated as standard deviation of the average OD600 at each time point and represented as error bars in figures.

Fluorescence microscopy. For confirmation of protein localization, strains were grown to saturation in SC 2% glucose media with auxotrophic selection, diluted 50-fold into fresh selective media and grown for a further 6-8 hours. Cultures were resuspended in 1x PBS before spotting onto plain glass slides for imaging on a Zeiss Axio observer Z1 microscope with X-Cite Series 120 fluorescent lamp and Hamamatsu Orca-Flash 4.0 Digital Camera. All images were analyzed using Fiji software (http://fiji.sc.) or Zen Software (Zeiss). Fluorescent protein variants used in this study were the yellow fluorescent protein Venus and the red fluorescent protein mRuby2.

Spot assays for PDV production and PDV quantification. Agar plate spots for visualization of PDV production were generated by plating 5 µl of saturated culture on SC 2% glucose agar plates with appropriate auxotrophic selection. Plates were grown at 30°C and imaged at 24, 48 and 72 hours. For PDV quantification, strains were grown to saturation at 30°C with shaking in SC 2% glucose media with auxotrophic selection. Saturated cultures were then diluted 50-fold into fresh selective media and grown for a further 72 hours before PDV extraction was performed as previously described[92]. Relative PDV quantification was determined using bulk fluorescence measurements with 100 µl extracts on a microplate reader (Tecan Infinite M1000 Pro) at excitation 535/5 nm and emission 585/5 nm. PDV production can be estimated using fluorescence measurements at these wavelengths due to a linear correlation to extracts quantified by HPLC[92].

BIA production in 96-well culture blocks. (*S*)-Norcoclaurine production experiments for Figure 3-1b, Figure 3-10d, Figure 3-2, Figure 3-9, and Figure 3-14 were performed in 96-well culture blocks. Single colonies were grown to saturation at 30°C in selective media before 50-fold dilution into fresh selective media. For Figure 3-1b and Figure 3-2, cultures were grown for 72 hours after the 50-fold dilution. For Figure 3-9, cultures were grown for 160 hours after the 50-fold dilution. For Figure 3-10d and Figure 3-14, the inoculation culture was diluted 50-fold into a separate block for each timepoint. At each timepoint or at final harvest, samples were taken for measurement of OD600. The remaining culture was centrifuged at ~4000 g and the supernatant filtered with an Acroprep Advance 0.2 µl filter plate (Pall Corporation). Eight-point standard curves using (*S*)-norcoclaurine chemical standard (Bepharm) were generated as two-fold serial dilutions prepared in culture media and used to convert LC/MS peak area to concentration. Samples and standards were diluted in water prior to LC/MS analysis to achieve concentrations within the linear range of detection of the instrument. Data shown is the average (*S*)-norcoclaurine titer for three-to-eight biological replicates of each strain (as indicated in each figure legend) and error bars represent standard deviation of the average.

BIA production in shake flasks. Shake flask fermentation experiments were performed for (*S*)-norcoclaurine production with tNCS expressed at CEN6/ARS4 level (Figure 3-3e, Figure 3-4), (*S*)-reticuline production with tNCS at CEN6/ARS4 level (Figure 3-3g, Figure 3-5), and (*S*)-norcoclaurine with tNCS at 2µ level (Figure 3-6d, Figure 3-7). Single colonies were grown to saturation at 30°C in selective media. For Figure 3-3e and Figure 3-4, saturated cultures were diluted 500-fold into 50mL selective media in 250mL baffled shake flasks. For all other experiments, saturated cultures were diluted to a starting OD of 0.05 in 50mL selective media in 250mL baffled shake flasks. Shake flask cultures were grown at 30°C with shaking at 220 rpm in an Innova 44 incubator (Eppendorf). At each timepoint, samples were taken for measurement of OD600 and BIA production. BIA samples were processed as described above for LC/MS and compared to an (*S*)-norcoclaurine or (*S*)-reticuline (ChemCruz) standard curve for quantification.

Fluorescence measurements for degron-YFP assay. Single colonies were grown to saturation in SC 2% glucose media with auxotrophic selection at 30°C with shaking. Saturated cultures were then diluted 50-fold in fresh media to a final volume of 500 µL in Corning 96-well culture blocks (Catalog number 07-200-700) and incubated at 30°C with shaking at 750 rpm. To sample OD600 and YFP fluorescence, 100 µL was aliquoted into 96-well Costar microplates (black, clear bottom) and measured on a Tecan Infinite M1000 Pro plate reader. YFP fluorescence was measured using an excitation wavelength of 515 nm and emission wavelength of 528 nm (5 nm bandwidth for excitation and

emission). Variation between biological replicates was calculated as standard deviation of the average and represented as error bars in figures.

Measurement of the dynamics of degron-YFP was performed as above for growth curves in microwell plates, but included the measurement of YFP in addition to OD600 at every timepoint. YFP fluorescence was measured using an excitation wavelength of 513 nm (5 nm bandwidth) and an emission wavelength of 531 nm (7.5 nm bandwidth).

LC/MS analysis. Liquid chromatography/mass spectrometry (LC/MS) was performed using a 1260 Infinity LC System connected to a 6120 Quadrupole Mass Spectrometer (Agilent Technologies). All samples and standards were diluted in water prior to injection, to achieve linear calibration curves for (*S*)-norcoclaurine and (*S*)-reticuline with all samples falling within the bounds of the calibration curve. Ten microliters of each diluted sample were injected and sample separation was achieved using a Zorbax Eclipse Plus C18 guard column (4.6 cm×12.5 cm, 5 μm packing, Agilent Technologies) connected to a Zorbax Eclipse Plus C18 column (4.6 mm × 100 mm, 3.5 μm packing, Agilent Technologies) at ambient temperature using a 0.5 mL/min flow rate. Samples were eluted with a linear gradient from 100% water/0% acetonitrile plus 0.1% formic acid to 65% water/35% acetonitrile plus 0.1% formic acid over the course of 15 min. MS was conducted in atmospheric pressure ionization-positive electrospray (API-ES positive) mode at 100-V fragmentor voltage with ion detection set to targeted detection of (*S*)-norcoclaurine (272.1 m/z) and/or (*S*)-reticuline (330.2 m/z).

Chapter 4. Conclusion

Consumer demand for natural food dyes, flavors, and fragrances is growing[20]. Companies are shifting their processes and supply chains to meet this demand[20]. We have demonstrated the first microbial synthesis of the red dye betanin as well as several novel betalains, including the most red-shifted betalain reported to date. These yeast-derived colorants have the potential to supplement or replace synthetic food dyes derived from petrochemicals. In particular, betanin is already used as a food dye. With appropriate engineering and scale-up, our bioprocess may become cost-competitive with the current method of extraction from red beets.

New spatial and temporal control strategies will be important for future advancements in metabolic engineering and synthetic biology. Synthetic compartmentalization is likely to be one of these emerging strategies. We have demonstrated the use of the peroxisome to isolate a toxic enzyme while maintaining its catalytic function and access to its substrates. This engineered compartmentalization enabled improved host cell growth as well as higher titer of benzylisoquinoline alkaloids, which are an important family of medicines. In the future, the peroxisome could be used to produce other toxic proteins. Increasing peroxisome cargo capacity would be valuable for high level protein production. Toward this goal, we have begun to genetically engineer peroxisome proliferation and have started work on organisms such as *Ogataea polymorpha* which can be induced to have 80% of their cell volume taken up by peroxisomes[151]. Finally, we envision that long term research projects may attempt to convert the peroxisome into a compartment for selective post-translational modifications of proteins, or to create chemical environments in the peroxisome that are distinct from anywhere else in the cell to enable unique chemistries.

Next generation metabolic engineering will aim to deliver engineered cells as products themselves, in contrast to previous advances in which the commercial product is a protein or metabolite synthesized by the cell. In medicine, developments in cell therapy are already being realized, with two FDA-approved T-cell therapies[152], one FDA-approved oncolytic virus[153], and clinical trials underway for gut bacteria-based therapies[154–156]. In agriculture, cereal-associating microbes have been engineered to controllably fix nitrogen[157] and plants are being engineered directly using cutting edge tools based on CRISPR[158–162]. Finally, work is ongoing to create synthetic multicellular structures, cell pattern formation, and model organoids using engineered cell-to-cell communication, quorum sensing, chemical gradients, and engineered transcription factors[163–167]. Development of whole cell products with desired, user-defined

characteristics will require metabolic engineering in order to introduce novel biosynthetic pathways, control pathway dynamics and production levels, and manipulate cellular feedback in response to extracellular signals such as hormone levels in the human body or water content in soil. Our work toward understanding and control of complex, branched reaction pathways (such as the betalain biosynthesis pathway) and engineering of subcellular specialization (such as user-defined sequestration of a toxic enzyme within the peroxisome) fit into the broader metabolic engineering toolbox that will enable the biotechnological solutions of the future.

Chapter 5. References

1. EBRC Roadmap Working Group. Engineering biology: a research roadmap for the next-generation bioeconomy. (2019).
2. Murdock, D., Ensley, B. D., Serdar, C. & Thalen, M. Construction of Metabolic Operons Catalyzing the De Novo Biosynthesis of Indigo in Escherichia coli. *Nat. Biotechnol.* **11**, 381–386 (1993).
3. Ro, D. K. *et al.* Production of the antimalarial drug precursor artemisinic acid in engineered yeast. *Nature* **440**, 940–943 (2006).
4. Ajikumar, P. K. *et al.* Isoprenoid pathway optimization for Taxol precursor overproduction in Escherichia coli. *Science (80-.).* **330**, 70–74 (2010).
5. Galanie, S., Thodey, K., Trenchard, I. J., Interrante, M. F. & Smolke, C. D. Complete biosynthesis of opioids in yeast. *Science (80-.).* **349**, 1095–1100 (2015).
6. Luo, X. *et al.* Complete biosynthesis of cannabinoids and their unnatural analogues in yeast. *Nature* **567**, 123–126 (2019).
7. Keasling, J. D. Manufacturing Molecules Through Metabolic Engineering. *Science (80-.).* **330**, 1355–1358 (2010).
8. Xu, P., Bhan, N. & Koffas, M. A. G. Engineering plant metabolism into microbes: From systems biology to synthetic biology. *Curr. Opin. Biotechnol.* **24**, 291–299 (2013).
9. Li, Y. *et al.* Complete biosynthesis of noscapine and halogenated alkaloids in yeast. *Proc. Natl. Acad. Sci. U. S. A.* **115**, E3922–E3931 (2018).
10. Paddon, C. J. & Keasling, J. D. Semi-synthetic artemisinin: A model for the use of synthetic biology in pharmaceutical development. *Nat. Rev. Microbiol.* **12**, 355–367 (2014).
11. Denby, C. M. *et al.* Industrial brewing yeast engineered for the production of primary flavor determinants in hopped beer. *Nat. Commun.* **9**, 1–10 (2018).
12. Threadingham, D., Obrecht, W., Wieder, W., Wachholz, G. & Engehausen, R. Rubber, 3. Synthetic Rubbers, Introduction and Overview. *Ullmann's Encycl. Ind. Chem.* (2011). doi:10.1002/14356007.a23_239.pub5
13. Steingruber, E. Indigo and Indigo Colorants. *Ullmann's Encycl. Ind. Chem.* 55–63 (2012). doi:10.1002/14356007.a14
14. Brockington, S. F., Walker, R. H., Glover, B. J., Soltis, P. S. & Soltis, D. E. Complex pigment evolution in the Caryophyllales. *New Phytol.* **190**, 854–864 (2011).
15. Christinet, L., Burdet, F. & Zaiko, M. Characterization and functional identification of a novel plant 4, 5-extradiol dioxygenase involved in betalain pigment biosynthesis in *Portulaca grandiflora*. *Plant Physiol.* **134**, 265–274 (2004).
16. Schliemann, W., Kobayashi, N. & Strack, D. The Decisive Step in Betaxanthin

Biosynthesis Is a Spontaneous Reaction. *Plant Physiol.* **119**, 1217–1232 (1999).
17. Hammer, S. K. & Avalos, J. L. Harnessing yeast organelles for metabolic engineering. *Nat. Chem. Biol.* **13**, 823–832 (2017).
18. Shai, N. *et al.* Systematic mapping of contact sites reveals tethers and a function for the peroxisome-mitochondria contact. *Nat. Commun.* **9**, (2018).
19. Esatbeyoglu, T., Wagner, A. E., Schini-Kerth, V. B. & Rimbach, G. Betanin-A food colorant with biological activity. *Mol. Nutr. Food Res.* **59**, 36–47 (2015).
20. Downham, A. & Collins, P. Colouring our foods in the last and next millennium. *Int. J. Food Sci. Technol.* **35**, 5–22 (2000).
21. König, J. Food colour additives of synthetic origin. *Colour Addit. Foods Beverages* 36–60 (2015). doi:10.1016/B978-1-78242-011-8.00002-7
22. Marienhagen, J. & Bott, M. Metabolic engineering of microorganisms for the synthesis of plant natural products. *J. Biotechnol.* **163**, 166–178 (2013).
23. Neelwarne, B. *Red Beet Biotechnology*. *Red Beet Biotechnology* (2012). doi:10.1007/978-1-4614-3458-0
24. Khan, M. I. & Giridhar, P. Phytochemistry Plant betalains : Chemistry and biochemistry. *Phytochemistry* **117**, 267–295 (2015).
25. Hendry, G. A. F. & Houghton, J. D. *Natural Food Colorants*. *Natural Food Colorants* (1996). doi:10.1007/978-1-4615-2155-6
26. Frost & Sullivan. Strategic Analysis of the European Natural and Nature-identical Food Colours Markets. (2007). Available at: https://cds.frost.com/p/72699/#!/nts/c?Id=M0AD-01-00-00-00. (Accessed: 6th October 2017)
27. Sunnadeniya, R. *et al.* Tyrosine hydroxylation in betalain pigment biosynthesis is performed by cytochrome P450 enzymes in beets (Beta vulgaris). *PLoS One* **11**, 1–16 (2016).
28. Hatlestad, G. J. *et al.* The beet R locus encodes a new cytochrome P450 required for red betalain production. *Nat. Genet.* **44**, 816–820 (2012).
29. Sasaki, N. *et al.* Isolation and Characterization of cDNAs Encoding an Enzyme with Glucosyltransferase Activity for cyclo -DOPA from Four O ' clocks and Feather Cockscombs. *Plant Cell Physiol.* **46**, 666–670 (2005).
30. Vogt, T., Grimm, R. & Strack, D. Cloning and expression of a cDNA encoding betanidin 5-O-glucosyltransferase, a betanidin- and flavonoid- specific enzyme with high homology to inducible glucosyltransferases from the Solanaceae. *Plant J.* **19**, (1999).
31. Sepúlveda-Jiménez, G., Rueda-Benítez, P., Porta, H. & Rocha-Sosa, M. A red beet (Beta vulgaris) UDP-glucosyltransferase gene induced by wounding, bacterial infiltration and oxidative stress. *J. Exp. Bot.* **56**, 605–611 (2005).
32. Martins, N., Roriz, C. L., Morales, P., Barros, L. & Ferreira, I. C. F. R. Coloring

attributes of betalains: A key emphasis on stability and future applications. *Food Funct.* **8**, 1357–1372 (2017).
33. Gonçalves, L. C. P., Da Silva, S. M., DeRose, P. C., Ando, R. A. & Bastos, E. L. Beetroot-Pigment-Derived Colorimetric Sensor for Detection of Calcium Dipicolinate in Bacterial Spores. *PLoS One* **8**, 1–6 (2013).
34. Gonçalves, L. C. P. *et al.* A Nature-Inspired Betalainic Probe for Live-Cell Imaging of Plasmodium-Infected Erythrocytes. *PLoS One* **8**, (2013).
35. Khairy, M., Ismael, M., El-Khatib, R. M., Abdelnaeem, M. & Khalaf, M. Natural betanin dye extracted from bougainvillea flowers for the naked-eye detection of copper ions in water samples. *Anal. Methods* **8**, 4977–4982 (2016).
36. Zhang, D. *et al.* Betalain pigments for dye-sensitized solar cells. *J. Photochem. Photobiol. A Chem.* **195**, 72–80 (2008).
37. Gandía-Herrero, F., Escribano, J. & García-Carmona, F. Structural implications on color, fluorescence, and antiradical activity in betalains. *Planta* **232**, 449–460 (2010).
38. Gandía-Herrero, F., García-Carmona, F. & Escribano, J. Development of a Protocol for the Semi-synthesis and Purification of Betaxanthins. *Phytochem. Anal.* **17**, 262–269 (2006).
39. DeLoache, W. C. *et al.* An enzyme-coupled biosensor enables (S)-reticuline production in yeast from glucose. *Nat. Chem. Biol.* **11**, 465–471 (2015).
40. Polturak, G. *et al.* Elucidation of the first committed step in betalain biosynthesis enables the heterologous engineering of betalain pigments in plants. *New Phytol.* **210**, 269–283 (2016).
41. Herbach, K. M., Stintzing, F. C. & Carle, R. Stability and color changes of thermally treated betanin, phyllocactin, and hylocerenin solutions. *J. Agric. Food Chem.* **54**, 390–398 (2006).
42. Wybraniec, S. *et al.* Antioxidant activity of betanidin: Electrochemical study in aqueous media. *J. Agric. Food Chem.* **59**, 12163–12170 (2011).
43. von Elbe, J. H. & Attoe, E. L. Oxygen involvement in betanine degradation-Measurement of active oxygen species and oxidation reduction potentials. *Food Chem.* **16**, 49–67 (1985).
44. Heuer, S., Vogt, T., Biihm, H. & Strack, D. Partial purification and characterization of UDP-glucose:betanidin 5-0- and 6-O-glucosyltransferases from cell suspension cultures of Dorotheanthus bellidiformis. *Planta* **199**, 244–250 (1996).
45. Thimmaraju, R., Bhagyalakshmi, N., Narayan, M. S. & Ravishankar, G. A. Kinetics of pigment release from hairy root cultures of Beta vulgaris under the influence of pH, sonication, temperature and oxygen stress. *Process Biochem.* **38**, 1069–1076 (2003).
46. Sasaki, N. *et al.* Detection of DOPA 4,5-dioxygenase (DOD) activity using recombinant protein prepared from escherichia coli cells Harboring cDNA

encoding DOD from mirabilis jalapa. *Plant Cell Physiol.* **50**, 1012–1016 (2009).
47. Grewal, P. S., Modavi, C., Russ, Z. N., Harris, N. C. & Dueber, J. E. Bioproduction of a betalain color palette in Saccharomyces cerevisiae. *Metab. Eng.* **45**, 180–188 (2018).
48. Gold, N. D. *et al.* Metabolic engineering of a tyrosine-overproducing yeast platform using targeted metabolomics. *Microb. Cell Fact.* **14**, 73 (2015).
49. Wang, M., Lopez-Nieves, S., Goldman, I. L. & Maeda, H. A. Limited Tyrosine Utilization Explains Lower Betalain Contents in Yellow than in Red Table Beet Genotypes. *J. Agric. Food Chem.* **65**, 4305–4313 (2017).
50. Yonekura-Sakakibara, K., Nakayama, T., Yamazaki, M. & Saito, K. Modification and Stabilization of Anthocyanins. in *Anthocyanins* 169–190 (2009).
51. Cabanes, J., Gandía-Herrero, F., Escribano, J., García-Carmona, F. & Jimenez-Atienzar, M. One-Step Synthesis of Betalains Using a Novel Betalamic Acid Derivatized Support. *J. Agric. Food Chem.* **62**, 3776–3782 (2014).
52. Avent, J., Naik, N., Mabry, T. J. & Passineau, M. J. Systems and methods for indicating oxidation of consumer products. (2008).
53. Blanc, V. *et al.* Identification and analysis of genes from Streptomyces pristinaespiralis encoding enzymes involved in the biosynthesis of the 4-dimethylamino- L -phenylalanine precursor of pristinamycin I. *Mol. Microbiol.* **23**, 191–202 (1997).
54. Suvannasara, P. *et al.* Biobased Polyimides from 4-Aminocinnamic Acid Photodimer. *Macromolecules* **47**, 1586–1593 (2014).
55. Gonçalves, L. C. P. *et al.* A comparative study of the purification of betanin. *Food Chem.* **131**, 231–238 (2012).
56. Schwartz, S. J. & von Elbe, J. H. Quantitative Determination of Individual Betacyanin Pigments by High-Performance Liquid Chromatography. *J. Agric. Food Chem.* **28**, 540–543 (1980).
57. Lee, M. E., DeLoache, W. C., Cervantes, B. & Dueber, J. E. A Highly Characterized Yeast Toolkit for Modular, Multipart Assembly. *ACS Synth. Biol.* **4**, 975–986 (2015).
58. Gietz, R. D. & Schiestl, R. H. High-efficiency yeast transformation using the LiAc/SS carrier DNA/PEG method. *Nat. Protoc.* **2**, 31–34 (2007).
59. Li, F., Vijayasankaran, N., Shen, A., Kiss, R. & Amanullah, A. Cell culture processes for monoclonal antibody production. *MAbs* **2**, 466–479 (2010).
60. Meadows, A. L. *et al.* Rewriting yeast central carbon metabolism for industrial isoprenoid production. *Nature* **537**, 694–697 (2016).
61. Sauer, M. Industrial production of acetone and butanol by fermentation-100 years later. *FEMS Microbiol. Lett.* **363**, 1–4 (2016).
62. Eibl, R. *et al.* Plant cell culture technology in the cosmetics and food industries: current state and future trends. *Appl. Microbiol. Biotechnol.* **102**, 8661–8675 (2018).

63. Yeates, T. O., Thompson, M. C. & Bobik, T. A. The protein shells of bacterial microcompartment organelles. *Curr. Opin. Struct. Biol.* **21**, 223–231 (2011).
64. Giessen, T. W. *et al.* Large protein organelles form a new iron sequestration system with high storage capacity. *Elife* **8**, 1–23 (2019).
65. Hecht, K. A., O'Donnell, A. F. & Brodsky, J. L. The proteolytic landscape of the yeast vacuole. *Cell. Logist.* **4**, e28023 (2014).
66. Khalfan, W. A. & Klionsky, D. J. Molecular machinery required for autophagy and the cytoplasm to vacuole targeting (Cvt) pathway in S. cerevisiae. *Curr. Opin. Cell Biol.* **14**, 468–475 (2002).
67. van den Hazel, H. B., Kielland-Brandt, M. C. & Winther, J. R. Autoactivation of proteinase A initiates activation of yeast vacuolar zymogens. *Eur. J. Biochem.* **207**, 277–283 (1992).
68. Haanstra, J. R. *et al.* Compartmentation prevents a lethal turbo-explosion of glycolysis in trypanosomes. *Proc. Natl. Acad. Sci. U. S. A.* **105**, 17718–17723 (2008).
69. Bakker, B. M. *et al.* Compartmentation protects trypanosomes from the dangerous design of glycolysis. *Proc. Natl. Acad. Sci. U. S. A.* **97**, 1–6 (2000).
70. Awan, A. R. *et al.* Biosynthesis of the antibiotic nonribosomal peptide penicillin in baker's yeast. *Nat. Commun.* **8**, 1–8 (2017).
71. Lau, Y. H., Giessen, T. W., Altenburg, W. J. & Silver, P. A. Prokaryotic nanocompartments form synthetic organelles in a eukaryote. *Nat. Commun.* (2018). doi:10.1038/s41467-018-03768-x
72. Zhao, E. M. *et al.* Light-based control of metabolic flux through assembly of synthetic organelles. *Nat. Chem. Biol.* **15**, 589–597 (2019).
73. Gassler, T. *et al.* The industrial yeast Pichia pastoris is converted from a heterotroph into an autotroph capable of growth on CO2. *Nat. Biotechnol.* **38**, 210–216 (2020).
74. Liu, G. S. *et al.* The yeast peroxisome: A dynamic storage depot and subcellular factory for squalene overproduction. *Metab. Eng.* **57**, 151–161 (2020).
75. Farhi, M. *et al.* Harnessing yeast subcellular compartments for the production of plant terpenoids. *Metab. Eng.* **13**, 474–481 (2011).
76. Lv, X. *et al.* Dual regulation of cytoplasmic and mitochondrial acetyl-CoA utilization for improved isoprene production in Saccharomyces cerevisiae. *Nat. Commun.* **7**, (2016).
77. Avalos, J. L., Fink, G. R. & Stephanopoulos, G. Compartmentalization of metabolic pathways in yeast mitochondria improves the production of branched-chain alcohols. *Nat. Biotechnol.* **31**, 335–341 (2013).
78. Sheng, J., Stevens, J. & Feng, X. Pathway compartmentalization in peroxisome of saccharomyces cerevisiae to produce versatile medium chain fatty alcohols. *Sci. Rep.* **6**, 1–11 (2016).
79. Zhou, Y. J. *et al.* Harnessing Yeast Peroxisomes for Biosynthesis of Fatty-Acid-

Derived Biofuels and Chemicals with Relieved Side-Pathway Competition. *J. Am. Chem. Soc.* **138**, 15368–15377 (2016).
80. Bhataya, A., Schmidt-Dannert, C. & Lee, P. C. Metabolic engineering of Pichia pastoris X-33 for lycopene production. *Process Biochem.* **44**, 1095–1102 (2009).
81. Bayer, T. S. *et al.* Synthesis of methyl halides from biomass using engineered microbes. *J. Am. Chem. Soc.* **131**, 6508–6515 (2009).
82. Hossler, P., Khattak, S. F. & Li, Z. J. Optimal and consistent protein glycosylation in mammalian cell culture. *Glycobiology* **19**, 936–949 (2009).
83. Sigmund, F. *et al.* Bacterial encapsulins as orthogonal compartments for mammalian cell engineering. *Nat. Commun.* **9**, (2018).
84. Farhadi, A., Ho, G. H., Sawyer, D. P., Bourdeau, R. W. & Shapiro, M. G. Ultrasound imaging of gene expression in mammalian cells. *Science (80-.).* **365**, 1469–1475 (2019).
85. Hagel, J. M. & Facchini, P. J. Benzylisoquinoline alkaloid metabolism: A century of discovery and a brave new world. *Plant Cell Physiol.* **54**, 647–672 (2013).
86. Rueffer, M., El-Shagi, H., Nagakura, N. & Zenk, M. (S)-Norlaudanosoline synthase: the first enzyme in the benzylisoquinoline biosynthetic pathway. *FEBS Lett.* **129**, (1981).
87. Stadler, R., Kutchan, T. M. & Zenk, M. H. (S)-norcoclaurine is the central intermediate in benzylisoquinoline alkaloid biosynthesis. *Phytochemistry* **28**, 1083–1086 (1989).
88. Lee, E.-J. & Facchini, P. Norcoclaurine synthase is a member of the pathogenesis-related 10/Bet v1 protein family. *Plant Cell* **22**, 3489–3503 (2010).
89. Samanani, N. & Facchini, P. Isolation and partial characterization of norcoclaurine synthase, the first committed step in benzylisoquinoline alkaloid biosynthesis, from opium poppy. *Planta* **213**, 898–906 (2001).
90. Lichman, B. R. *et al.* Dopamine-first mechanism enables the rational engineering of the norcoclaurine synthase aldehyde activity profile. *FEBS J.* **282**, 1137–1151 (2015).
91. Purdue, P. E. & Lazarow, P. B. Peroxisome Biogenesis. *Annu. Rev. Cell Biol.* (2001).
92. DeLoache, W. C., Russ, Z. N. & Dueber, J. E. Towards repurposing the yeast peroxisome for compartmentalizing heterologous metabolic pathways. *Nat. Commun.* **7**, (2016).
93. Gould, S. J., Keller, G. A., Hosken, N., Wilkinson, J. & Subramani, S. A conserved tripeptide sorts proteins to peroxisomes. *J. Cell Biol.* **108**, 1657–1664 (1989).
94. Gould, S. J. *et al.* Peroxisomal protein import is conserved between yeast, plants, insects and mammals. *EMBO J.* **9**, 85–90 (1990).
95. Glover, J. R., Andrews, D. W., Subramani, S. & Rachubinski, R. A. Mutagenesis of the amino targeting signal of Saccharomyces cerevisiae 3- ketoacyl-CoA thiolase reveals conserved amino acids required for import into peroxisomes in vivo. *J. Biol.*

Chem. **269**, 7558–7563 (1994).
96. Kunze, M. *et al.* Structural requirements for interaction of peroxisomal targeting signal 2 and its receptor PEX7. *J. Biol. Chem.* **286**, 45048–45062 (2011).
97. Kohlwein, S. D., Veenhuis, M. & van der Klei, I. J. Lipid droplets and peroxisomes: Key players in cellular lipid homeostasis or a matter of fat-store'em up or burn'em down. *Genetics* **193**, 1–50 (2013).
98. Distel, B. & Kragt, A. *Purification of Yeast Peroxisomes*. *Yeast Protocols* **1**, (Humana Press, 2006).
99. Ehrenworth, A. M., Haines, M. A., Wong, A. & Peralta-Yahya, P. Quantifying the efficiency of Saccharomyces cerevisiae translocation tags. *Biotechnol. Bioeng.* **114**, 2628–2636 (2017).
100. Antonenkov, V. D., Sormunen, R. T. & Hiltunen, J. K. The rat liver peroxisomal membrane forms a permeability barrier for cofactors but not for small metabolites in vitro. *J. Cell Sci.* **117**, 5633–5642 (2004).
101. Samanani, N., Liscombe, D. K. & Facchini, P. J. Molecular cloning and characterization of norcoclaurine synthase, an catalyzing the first committed step in benzylisoquinoline alkaloid biosynthesis. *Plant J.* **40**, 302–314 (2004).
102. Nishihachijo, M. *et al.* Asymmetric synthesis of tetrahydroisoquinolines by enzymatic Pictet – Spengler reaction. *Biosci. Biotechnol. Biochem.* **78**, 701–707 (2014).
103. Letunic, I. & Bork, P. 20 years of the SMART protein domain annotation resource. *Nucleic Acids Res.* **46**, D493–D496 (2018).
104. Karim, A. S., Curran, K. A. & Alper, H. S. Characterization of plasmid burden and copy number in Saccharomyces cerevisiae for optimization of metabolic engineering applications. *FEMS Yeast Res.* **13**, 107–116 (2013).
105. Lee, M. E., Aswani, A., Han, A. S., Tomlin, C. J. & Dueber, J. E. Expression-level optimization of a multi-enzyme pathway in the absence of a high-throughput assay. *Nucleic Acids Res.* **41**, 10668–78 (2013).
106. Walton, P. A., Hill, P. E. & Subramani, S. Import of stably folded proteins into peroxisomes. *Mol. Biol. Cell* **6**, 675–683 (1995).
107. Antonenkov, V. D. & Hiltunen, J. K. Transfer of metabolites across the peroxisomal membrane. *Biochim. Biophys. Acta - Mol. Basis Dis.* **1822**, 1374–1386 (2012).
108. Halbach, A., Rucktächel, R., Rottensteiner, H. & Erdmann, R. The N-domain of Pex22p can functionally replace the Pex3p N-domain in targeting and peroxisome formation. *J. Biol. Chem.* **284**, 3906–3916 (2009).
109. Elgersma, Y. *et al.* Analysis of the carboxyl-terminal peroxisomal targeting signal 1 in a homologous context in Saccharomyces cerevisiae. *J. Biol. Chem.* **271**, 26375–26382 (1996).
110. Chan, K. M., Liu, Y. T., Ma, C. H., Jayaram, M. & Sau, S. The 2 micron plasmid of Saccharomyces cerevisiae: A miniaturized selfish genome with optimized

functional competence. *Plasmid* **70**, 2–17 (2013).
111. Kunau, W. H., Dommes, V. & Schulz, H. β-Oxidation of fatty acids in mitochondria, peroxisomes, and bacteria: A century of continued progress. *Prog. Lipid Res.* **34**, 267–342 (1995).
112. Yofe, I. *et al.* Pex35 is a regulator of peroxisome abundance. *J. Cell Sci.* **130**, 791–804 (2017).
113. Vizeacoumar, F., Torres-Guzman, J., Bouard, D., Aitchison, J. & Rachubinski, R. Pex30p, Pex31p, and Pex32p Form a Family of Peroxisomal Integral Membrane Proteins Regulating Peroxisome Size and Number in Saccharomyces cerevisiae. *Mol. Biol. Cell* **15**, 665–677 (2004).
114. Veenhuis, M., Mateblowski, M., Kunau, W. H. & Harder, W. Proliferation of microbodies in Saccharomyces cerevisiae. *Yeast* **3**, 77–84 (1987).
115. Grillitsch, K. *et al.* Lipid particles/droplets of the yeast Saccharomyces cerevisiae revisited: Lipidome meets Proteome. *Biochim. Biophys. Acta - Mol. Cell Biol. Lipids* **1811**, 1165–1176 (2011).
116. Zhang, J. W., Han, Y. & Lazarow, P. B. Novel peroxisome clustering mutants and peroxisome biogenesis mutants of Saccharomyces cerevisiae. *J. Cell Biol.* **123**, 1133–1147 (1993).
117. Swinnen, S. *et al.* Re-evaluation of glycerol utilization in Saccharomyces cerevisiae: Characterization of an isolate that grows on glycerol without supporting supplements. *Biotechnol. Biofuels* **6**, 1–12 (2013).
118. Simon, M., Adam, G., Rapatz, W., Spevak, W. & Ruis, H. The Saccharomyces cerevisiae ADR1 gene is a positive regulator of transcription of genes encoding peroxisomal proteins. *Mol. Cell. Biol.* **11**, 699–704 (1991).
119. Luo, Y., Karpichev, I. V., Kohanski, R. A. & Small, G. M. Purification, identification, and properties of a Saccharomyces cerevisiae oleate-activated upstream activating sequence-binding protein that is involved in the activation of POX1. *J. Biol. Chem.* **271**, 12068–12075 (1996).
120. Rottensteiner, H. *et al.* Pip2p: a transcriptional regulator of peroxisome proliferation in the yeast Saccharomyces cerevisiae. *EMBO J.* **15**, 2924–2934 (1996).
121. Young, E. T., Kacherovsky, N. & Van Riper, K. Snf1 protein kinase regulates Adr1 binding to chromatin but not transcription activation. *J. Biol. Chem.* **277**, 38095–38103 (2002).
122. Baumgartner, U., Hamilton, B., Piskacek, M., Ruis, H. & Rottensteiner, H. Functional Analysis of the Zn 2 Cys 6 Transcription Factors Oaf1p and Pip2p . *J. Biol. Chem.* **274**, 22208–22216 (1999).
123. Phelps, C. *et al.* Fungi and animals may share a common ancestors to nuclear receptors. *Proc. Natl. Acad. Sci. U. S. A.* **103**, 7077–7081 (2006).
124. Ratnakumar, S., Kacherovsky, N., Arms, E. & Young, E. T. Snf1 controls the activity

of Adr1 through dephosphorylation of Ser230. *Genetics* **182**, 735–745 (2009).
125. Ratnakumar, S. & Young, E. T. Snf1 dependence of peroxisomal gene expression is mediated by Adr1. *J. Biol. Chem.* **285**, 10703–10714 (2010).
126. Hackett, E. A., Esch, R. K., Maleri, S. & Errede, B. A family of destabilized cyan fluorescent proteins as transcriptional reporters in S. cerevisiae. *Yeast* **23**, 333–349 (2006).
127. Young, E. T., Dombek, K. M., Tachibana, C. & Ideker, T. Multiple pathways are co-regulated by the protein kinase Snf1 and the transcription factors Adr1 and Cat8. *J. Biol. Chem.* **278**, 26146–26158 (2003).
128. Trzcinska-Danielewicz, J., Ishikawa, T., Miciałkiewicz, A. & Fronk, J. Yeast transcription factor Oaf1 forms homodimer and induces some oleate-responsive genes in absence of Pip2. *Biochem. Biophys. Res. Commun.* **374**, 763–766 (2008).
129. Miroux, B. & Walker, J. E. Over-production of proteins in Escherichia coli: Mutant hosts that allow synthesis of some membrane proteins and globular proteins are high levels. *J. Membr. Biol.* **260**, 289–298 (1996).
130. Wagner, S. *et al.* Tuning Escherichia coli for membrane protein overexpression. *Proc. Natl. Acad. Sci. U. S. A.* **105**, 14371–14376 (2008).
131. Sletta, H. *et al.* Broad-host-range plasmid pJB658 can be used for industrial-level production of a secreted host-toxic single-chain antibody fragment in escherichia coli. *Appl. Environ. Microbiol.* **70**, 7033–7039 (2004).
132. Eguchi, Y. *et al.* Estimating the protein burden limit of yeast cells by measuring the expression limits of glycolytic proteins. *Elife* **7**, e34595 (2018).
133. Outeiro, T. F. & Lindquist, S. Yeast Cells Provide Insight into Alpha-Synuclein Biology and Pathobiology. *Science (80-.).* **302**, 1772–1775 (2003).
134. Ju, S. *et al.* A Yeast Model of FUS/TLS-Dependent Cytotoxicity. *PLoS Biol.* **9**, (2011).
135. Zha, H. *et al.* Structure-function comparisons of the proapoptotic protein Bax in yeast and mammalian cells. *Mol. Cell. Biol.* **16**, 6494–6508 (1996).
136. Vincent JJ Martin, Douglas J Pitera, Sydnor T Withers, Jack D Newman & Jay D Keasling. Engineering a mevalonate pathway in Escherichia coli for production of terpenoids. *Nat. Biotechnol.* **21**, 796–802 (2003).
137. Pitera, D. J., Paddon, C. J., Newman, J. D. & Keasling, J. D. Balancing a heterologous mevalonate pathway for improved isoprenoid production in Escherichia coli. *Metab. Eng.* **9**, 193–207 (2007).
138. Zhu, M. M., Skraly, F. A. & Cameron, D. C. Accumulation of methylglyoxal in anaerobically grown Escherichia coli and its detoxification by expression of the Pseudomonas putida glyoxalase I gene. *Metab. Eng.* **3**, 218–225 (2001).
139. Brennan, T. C. R., Turner, C. D., Krömer, J. O. & Nielsen, L. K. Alleviating monoterpene toxicity using a two-phase extractive fermentation for the bioproduction of jet fuel mixtures in Saccharomyces cerevisiae. *Biotechnol. Bioeng.*

109, 2513–2522 (2012).
140. Kildegaard, K. R. *et al.* Evolution reveals a glutathione-dependent mechanism of 3-hydroxypropionic acid tolerance. *Metab. Eng.* **26**, 57–66 (2014).
141. Brochado, A. R. *et al.* Improved vanillin production in baker's yeast through in silico design. *Microb. Cell Fact.* **9**, 1–15 (2010).
142. Li, S. C. & Kane, P. M. The yeast lysosome-like vacuole: Endpoint and crossroads. *Biochim. Biophys. Acta - Mol. Cell Res.* **1793**, 650–663 (2009).
143. Dragosits, M. & Mattanovich, D. Adaptive laboratory evolution - principles and applications for biotechnology. *Microb. Cell Fact.* **12**, 1–17 (2013).
144. Bentley, G. J. *et al.* Engineering glucose metabolism for enhanced muconic acid production in Pseudomonas putida KT2440. *Metab. Eng.* **59**, 64–75 (2020).
145. Meijer, W. H. *et al.* Peroxisomes are required for efficient penicillin biosynthesis in Penicillium chrysogenum. *Appl. Environ. Microbiol.* **76**, 5702–5709 (2010).
146. Subramani, S. Targeting of proteins into the peroxisomal matrix. *J. Membr. Biol.* **125**, 99–106 (1992).
147. Veenhuis, M., Keizer, I. & Harder, W. Characterization of peroxisomes in glucose-grown Hansenula polymorpha and their development after the transfer of cells into methanol-containing media. *Arch. Microbiol.* **120**, 167–175 (1979).
148. van der Klei, I. J., Yurimoto, H., Sakai, Y. & Veenhuis, M. The significance of peroxisomes in methanol metabolism in methylotrophic yeast. *Biochim. Biophys. Acta - Mol. Cell Res.* **1763**, 1453–1462 (2006).
149. Goodman, J. M., Trapp, S. B., Hwang, H. & Veenhuis, M. Peroxisomes induced in Candida boidinii by methanol, oleic acid and D-alanine vary in metabolic function but share common integral membrane proteins. *J. Cell Sci.* **97**, 193–204 (1990).
150. Weng, H., Endo, K., Li, J., Kito, N. & Iwai, N. Induction of peroxisomes by butyrate-producing probiotics. *PLoS One* **10**, 1–11 (2015).
151. Veenhuis, M., Dijken, J. P. V. & Harder, W. *The Significance of Peroxisomes in the Metabolism of One-Carbon Compounds in Yeasts*. *Advances in Microbial Physiology* **24**, (1983).
152. Calmes-Miller, J. FDA Approves Second CAR T-cell Therapy. *Cancer Discov.* 5–6 (2018). doi:10.1158/2159-8290.CD-NB2017-155
153. Eissa, I. R. *et al.* The current status and future prospects of oncolytic viruses in clinical trials against melanoma, glioma, pancreatic, and breast cancers. *Cancers (Basel).* **10**, (2018).
154. Orenstein, R. *et al.* Safety and Durability of RBX2660 (Microbiota Suspension) for Recurrent Clostridium difficile Infection: Results of the PUNCH CD Study. *Clin. Infect. Dis.* **62**, 596–602 (2016).
155. Isabella, V. M. *et al.* Development of a synthetic live bacterial therapeutic for the human metabolic disease phenylketonuria. *Nat. Biotechnol.* **36**, 857–867 (2018).

156. Bobilev, D. *et al.* VE303, A live biotherapeutic product for prevention of recurrent Clostridioides difficile (C. difficile) infection. Preliminary results of a Phase 1, open-label healthy volunteers study of oral VE303 after vancomycin. *Gastroenterology* **156**, S-899-S-900 (2019).
157. Ryu, M. H. *et al.* Control of nitrogen fixation in bacteria that associate with cereals. *Nat. Microbiol.* **5**, 314–330 (2020).
158. Li, J.-F. *et al.* Multiplex and homologous recombination-mediated genome editing in Arabidopsis and Nicotiana benthamiana using guide RNA and Cas9. *Nat. Biotechnol.* **31**, 688–691 (2013).
159. Nekrasov, V., Staskawicz, B., Weigel, D., Jones, J. D. G. & Kamoun, S. Targeted mutagenesis in the model plant Nicotiana benthamiana using Cas9 RNA-guided endonuclease. *Nat. Biotechnol.* **31**, 691–693 (2013).
160. Jiang, W. *et al.* Demonstration of CRISPR/Cas9/sgRNA-mediated targeted gene modification in Arabidopsis, tobacco, sorghum and rice. *Nucleic Acids Res.* **41**, 1–12 (2013).
161. Zong, Y. *et al.* Precise base editing in rice, wheat and maize with a Cas9-cytidine deaminase fusion. *Nat. Biotechnol.* **35**, 438–440 (2017).
162. Lu, Y. & Zhu, J. K. Precise Editing of a Target Base in the Rice Genome Using a Modified CRISPR/Cas9 System. *Mol. Plant* **10**, 523–525 (2017).
163. Toda, S., Blauch, L. R., Tang, S. K. Y., Morsut, L. & Lim, W. A. Programming self-organizing multicellular structures with synthetic cell-cell signaling. *Science (80-.).* **361**, 156–162 (2018).
164. Sekine, R., Shibata, T. & Ebisuya, M. Synthetic mammalian pattern formation driven by differential diffusivity of Nodal and Lefty. *Nat. Commun.* **9**, 1–11 (2018).
165. Dinh, C. V. & Prather, K. L. J. Development of an autonomous and bifunctional quorum-sensing circuit for metabolic flux control in engineered Escherichia coli. *Proc. Natl. Acad. Sci. U. S. A.* **116**, 25562–25568 (2019).
166. Kaminski, M. M. *et al.* Direct reprogramming of fibroblasts into renal tubular epithelial cells by defined transcription factors. *Nat. Cell Biol.* **18**, 1269–1280 (2016).
167. Guye, P. *et al.* Genetically engineering self-organization of human pluripotent stem cells into a liver bud-like tissue using Gata6. *Nat. Commun.* **7**, 1–12 (2016).